

Lakehead University

CFD Modeling of an Activated Sludge Bubble Column

Submitted by

Mohammad Gholamzadehdevin

A thesis submitted to the Faculty of Graduate Studies in partial
fulfillment of the requirements for degree of Master of Science
in
Environmental Engineering
Department of Engineering

Winter 2017
Thunder Bay, Ontario

Advisor: Dr. Leila Pakzad

Abstract:

CFD Modeling of an Activated Sludge Bubble Column

Mohammad Gholamzadehdevin

The bubble columns are widely used in different industries such as wastewater treatment, chemical, petrochemical, and biochemical. The current design of the bubble columns including but not limited to the geometry and dimensions of the column, the location, size, and type of the gas spargers, gas superficial velocity, and fluid rheology relies on the assumptions about the gas and liquid behavior and the mixing performance. The main objective of this study was to evaluate the effect of superficial gas velocity and sparger type on the liquid and gas phase flow patterns, gas hold up, and mixing time through computational fluid dynamic (CFD) modeling and simulation. The CFD model was simulated the multiphase flow based on the Eulerian-Eulerian approach and validated by experimental measurements. The standard k- ϵ model was employed to predict the turbulent flow and circulations of the liquid phase. The activated sludge as a shear thinning non-Newtonian fluid has been modeled as a power-law rheological model. The trends of the mixing process were calculated by using the species and transport model. The CFD model accurately predicted the flow pattern and mixing process. The results reveal that the increase of the superficial gas velocity increases the value of gas holdup. Moreover, the mixing time have been decreased by increasing the rate of superficial gas velocity. One of the most important results of this study highlighted the significant effect of the tracer injection location on the mixing time. The typical star shape sparger has also been modified in this study. The performance of the modified sparger was assessed and compared to the performance of the typical star shape in terms

of liquid and gas flow pattern and mixing time. The modified sparger exhibited better performance in sparging the gas through non-Newtonian activated sludge.

The validated CFD data was employed to investigate the effect of superficial gas velocity, type of gas sparger, and tracer injection location on the mixing time of the activated sludge bubble column.

A statistical-based experimental design with full factorial design method was applied to evaluate the individual and interactive effects of the design parameters.

Acknowledgements

I would like to express my sincere gratitude and appreciation on my supervisor Dr. Leila Pakzad for her kindly support during all times of this work, without her this work would not have been completed. Financial support from Natural Sciences and Engineering Research Council of Canada (NSERC) is gratefully acknowledged. I acknowledge the HPCVL (High Performance Computing Virtual Laboratory) organization for providing high speed calculation process during my research.

To Atieh,

For her love and support

Contents

Abstract:	i
Acknowledgements	iii
Chapter 3: CFD modeling of the activated sludge bubble column: axial velocity profile and mixing	vii
Chapter 3: CFD modeling of the activated sludge bubble column: axial velocity profile and mixing time	x
Chapter 1: Introduction	1
Chapter 2: Literature Review	4
2.1 Introduction	4
2.2 Bubble Column Reactor	5
2.3 Flow Regimes.....	10
2.4 Gas Sparger	16
2.5 Gas Holdup.....	18
2.6 Computational Fluid Dynamic (CFD)	19
2.7 Electrical Resistance Tomography (ERT) System.....	23
2.8 Knowledge Gap and Research Objectives	26
2.9 Notations	26
Chapter 3: CFD Modeling of the Activated Sludge Bubble Column: Axial Velocity Profile and Mixing	28
3.1 Introduction	28
3.2 CFD Model Development	33
3.3 Results and Discussion.....	44
3.3.1 Typical Star Shape.....	44
3.3.2 Modified Star Shape Gas Sparger	63
3.4 Conclusions	71
3.5 Notations	73
Chapter 4: Evaluation of the Effect of Sparger Type, Superficial Gas Velocity, and Tracer Injection Location on the Non-Newtonian Activated Sludge Bioreactor Mixing Performance	75
4.1 Introduction	75
4.2 CFD Model Development	78

4.3 Results and Discussion.....	83
4.4 Conclusions	105
4.5 Notations	106
Chapter 5: Overall Conclusions and Recommendations for Future Research.....	107
5.1 Conclusions	107
The CFD model with star shape gas sparger:	108
5.2 Recommendations for Future Research	110
References	111

List of Figures

Chapter 2: Literature Review

Figure 2.1: The design and geometry of (a) trickle bed reactor, (b) fluidized bed reactor, and (c) bubble column reactor.....	6
Figure 2.2: The rectangular bubble column reactor of experiment of Pflieger et al. (1999).....	8
Figure 2.3: Various gas-liquid flow regimes in vertical tubes; (a) bubbly, (b) Slug, (c) Churn, (d) Annular, and (e) Wispy-Annular.....	12
Figure 2.4: The relationship between vessel diameter, gas velocity and flow transition (source: Deckwer et al., 1980).....	13
Figure 2.5: The different types of bubbly flow in bubble column reactor (source: Kataoka et al., 2010).....	15
Figure 2.6: Schematic view of different types of spargers where: (a) sieve plate sparger, (b) multiple ring spargers, (c) spider, and (d) pipe sparger (source: Kulkarni et al., 2009).....	17
Figure 2.7: Block diagram of an ERT system with for measuring plane (source: Pakzad, 2007).....	25

Chapter 3: CFD modeling of the activated sludge bubble column: axial velocity profile and mixing

Figure 3.1: (a) the bubble column numerical grids, (b) the star shape sparger, (c) the modified star shape sparger (dimensions in m).....	34
Figure 3.2: CFD injection points and monitoring planes used for estimation of the mixing times. The Monitoring Plane (1): $z=0.585$ m, Monitoring Plane (2): $z=0.46$ m, Monitoring Plane (3): $z=0.41$ m, Monitoring Plane (4): $z=0.293$ m, Monitoring Plane (5): $z=0.205$ m, and Monitoring Plane (6): $z=0.117$ m.....	42
Figure 3.3: The diagram of non-dimensional tracer concentration as a function of time for activated sludge aerated at superficial gas velocity of 0.163 cm/s, while tracer was added at Injection Point (4).....	43

Figure 3.4: The comparison between CFD and experimental for: (a) mixing time, and (b) gas volume fraction.....	46
Figure 3.5: The comparison between CFD contour plots based on gas holdup and ERT tomograms based on conductivity for: (a) the CFD contour plot of gas holdup distribution at plane 6, (b) the ERT tomogram of conductivity at plane 6, (c) the CFD contour plot of gas holdup distribution at plane 3, and (d) the ERT tomogram of conductivity at plane 3.....	47
Figure 3.6: Mixing time as function of superficial gas velocity (cm/s) and tracer injection locations for star shape sparger.....	48
Figure 3.7: Liquid velocity (m/s) contour plots for start shape gas sparger at superficial gas velocities of: (a) 0.163 cm/s, (b) 0.326 cm/s, (c) 0.814 cm/s, and (d) 1.14 cm/s.....	50
Figure 3.8: Liquid velocity (m/s) vector plots for star shape gas sparger at superficial gas velocity of (a) 0.163 (cm/s) and (b) 1.14 cm/s.....	52
Figure 3.9: The radial distribution of air axial velocity (m/s) for star shape gas sparger superficial gas velocity of (a) 0.163, (b) 0.326, (c) 0.814, (d) 1.14 cm/s.....	54
Figure 3.10: The contour plots of distribution of axial gas velocity (m/s) at vertical XZ plane for superficial gas velocity of: (a) 0.163 cm/s, (b) 0.326 cm/s, (c) 0.814 cm/s, and (d) 1.14 cm/s....	57
Figure 3.11: The radial distribution of the axial velocity of the activated sludge for superficial gas velocity of (a) 0.163 cm/s, (b) 0.326 cm/s, (c) 0.814 cm/s, and (d) 1.14 cm/s.....	59
Figure 3.12: The radial distribution of secondary phase volume fraction for superficial gas velocity of (a) 0.163 cm/s, (b) 0.326 cm/s, (c) 0.814 cm/s, and (d) 1.14 cm/s.....	61
Figure 3.13: The radial distribution of the axial velocity of the activated sludge for superficial gas velocity of (a) 0.163 cm/s, (b) 0.326 cm/s, (c) 0.814 cm/s, and (d) 1.14 cm/s.....	64
Figure 3.14: The contours of volume fraction of the modified star shape sparger for superficial gas velocities of: (a) 0.163 cm/s, (b) 0.326 cm/s, (c) 0.814 cm/s, and (d) 1.14 cm/s.....	67
Figure 3.15: The comparison of the radial distribution of the gas holdup for the star shape sparger and the modified star shape at lines 1 and 3 for superficial gas velocity of 1.14 cm/s.....	69
Figure 3.16: The radial distribution of gas holdup for superficial gas velocity of (a) 0.163 cm/s and (b) 1.14 cm/s.....	70
Figure 3.17: The comparison of the star shape and the modified star shape gas sparger.....	71

Chapter 4: Evaluation of the effect of sparger type, superficial gas velocity, and tracer injection location on the non-Newtonian activated sludge bioreactor mixing performance

Figure 4.1: (a) the geometry of bubble column, (b) the isometric view of the star shape sparger, and (c) the isometric view of the modified sparger.....79

Figure 4.2: Effect of the grid numbers on radial gas holdup in case of superficial gas velocity of 0.814 cm/s at line 3.....81

Figure 4.3: The locations of tracer injection.....82

Figure 4.4: Main effect plots for mixing time (s) for all 3 variables90

Figure 4.5: The contours of species mass fraction for all location: (a) location 1, (b) location 2, (c) location 3, and (d) location 4 with superficial gas velocity of 0.163 cm/s.....91

Figure 4.6: Predicted values of mixing time (s) versus their experimental values.....96

Figure 4.7: The response surface is showing the mixing time as a function of two independent variables (the other variables were assumed at respective average level): (a) superficial gas velocity (X1) and gas sparger type (X3), (b) superficial gas velocity (X1) and tracer injection location (X2), (c) tracer injection location (X2) and gas sparger type (X3).....97

Figure 4.8: Mixing time as function of superficial gas velocity (cm/s) and tracer injection locations for modified star shape sparger.....100

Figure 4.9: Liquid velocity (m/s) vector plots at vertical YZ plane in case of superficial gas velocity of 1.14 cm/s for models with (a) typical gas sparger (b) modified gas sparger.....101

Figure 4.10: The contours of liquid pathline with color of gas holdup at XZ vertical plane in case of superficial gas velocity of 1.14 cm/s for models with (a) typical gas sparger (b) modified gas sparger.....102

Figure 4.11: The vertical contour (XZ plane) of apparent viscosity at superficial gas velocity of 1.14 cm/s for models with (a) typical (b) modified gas sparger.....104

Figure 4.12: The vertical contour (XZ plane) of liquid viscosity (m/s) at superficial gas velocity of 1.14 cm/s for models with (a) typical (b) modified gas sparger.....105

List of Tables

Chapter 2: Literature Review

Table 2.1: The review of previous researches measuring method, model geometry and flow regime.....	9
Table 2.2: Review of the experimental equations of gas holdup.....	18

Chapter 3: CFD modeling of the activated sludge bubble column: axial velocity profile and mixing time

Table 3.1: Review of interphase forces.....	38
---	----

Chapter 4: Evaluation of the effect of sparger type, superficial gas velocity, and tracer injection location on the non-Newtonian activated sludge bioreactor mixing performance

Table 4.1: Experimental range and levels of the independent variables.....	84
Table 4.2: Design matrix in coded units and the experimental responses.....	84
Table 4.3: ANOVA test for response function (mixing time).....	95

Chapter 1: Introduction

The bubble column reactor is used frequently in different industries, especially the wastewater treatment industry for aeration process of the activated sludge. Understanding the bubble column behavior, crucial to industrial scale-up, flow pattern, and mixing process remains complicated particularly in case of non-Newtonian fluids. The activated sludge is a liquid with non-Newtonian behavior and usually contains a certain amount of the suspended solid that is measured by Mixed Suspended Solid Liquor (MLSS) value. The working fluid of this study was an activated sludge with shear thinning behavior, that has low apparent viscosities at high shear rates and high viscosities in case of low shear rates. The value of fluid MLSS was 0.712 g/L in this study and the rheological properties was fitted with power-law model presented by Babaei et al. (2015) with regression coefficient of 0.99.

The semi-batch bubble column reactors usually consists of a vessel filled with liquid and an aeration system at the bottom of the vessel which can be a gas sparger, gas diffuser, etc. In case of the activated sludge bioreactors, the aeration is used to supply of oxygen to the biomass and to provide an efficient mixing process within bubble column (Braak et al., 2011). At the beginning of the process, the liquid phase is at rest then gas phase is introduced to the vessel region by gas sparger with a certain amount of gas flow rate. Understanding the flow behavior and mixing process of the non-Newtonian liquid in terms of aeration is one of the most important components of designing a bubble column reactor. The desired mixing can provide a good interaction among gas and liquid phases to improve the rate of chemical reactions and break down the sludge's microorganisms.

The quantity of gas holdup and the distribution profile of gas among the liquid phase are listed as critical hydrodynamic characteristics of the activated sludge process. The knowledge of the effect

of proper design, operational and environmental parameters on gas holdup and the distribution pattern of gas phase in activated sludge are necessary for an optimum design and operation. The rate of superficial gas velocity and type of the gas sparger are two most important parameters which can develop the quantity of gas holdup and mixing process. There are several experimental studies in the field of investigation of bubble column hydrodynamics and mixing process among literature (Babaei et al., 2015; Jin and Lant, 2004; Prakash et al., 2001; Fransolet et al., 2005; Jin et al., 2007; Chen et al., 1998). The mixing time is another important parameter to investigate the performance of the activated sludge bioreactor, which is a time required for mixing a small amount of tracer into the vessel to reach a specific level of homogeneity.

During past few years, a wide range of experimental investigations were done for activated sludge bioreactors with different geometries, aeration systems, and fluid rheology (Karpinska and Bridgeman, 2016). The experimental methods are not always easy task and they are cost effective. The investigation process of the activated sludge hydrodynamics and mixing made an attempt to use advanced Computational Fluid Dynamics (CFD). The use of CFD provides a wide range of details about the different parameters which are contributing in activated sludge process in a shorter time and lower costs. To use this approach, the results must be validated with specific amount of experimental measurements. As soon as the validated solution is achieved, the CFD model can provide a wide range of valuable details which are not possible to obtain experimentally.

There are various tomographic experimental methods to recognize the dynamic properties of activated sludge process such as acoustic (ultrasonic), electrical (Electrical Resistance Tomography), and electromagnetic (X-ray). The Electrical Resistance Tomography (ERT) represents valuable information about the process which can be used to validate the CFD model (Bolton et al., 2004).

The mixing time value depends on many different process variables such as superficial gas velocity, type of gas sparger, fluid rheology, geometry of vessel, and tracer injection location (Babaei et al., 2015, McClure et al., 2015, Li et al., 2016). In this regard, the full factorial design method was used by employing the trial version of JMP software from Statistical Analysis System (SAS). The full factorial design method provides an ability to measure the interactions among a group of variables with different levels at the same time and predict all possible experiments with contributed variables (Capetillo and Ibarra, 2017).

Chapter two presents a brief literature review about the fundamentals of bubble column design such as bubble column geometry, gas-liquid flow regimes, bubble size theory, gas sparger, gas holdup, superficial gas velocity, and mixing process.

Chapter three is concerned with a brief introduction, the detailed CFD model development, results and discussion and conclusions regarding the study of the axial velocity profile of gas and liquid phase, hydrodynamics, and mixing time.

Chapter four provides valuable information about the evaluation of the effect of variables in mixing time with statistical analysis. This chapter also consists of an introduction, the brief CFD model development, experimental design, results and discussion, and conclusions. And finally chapter five summarizes the overall conclusions of present study and provide recommendations for future work.

Chapter 2: Literature Review

2.1 Introduction

The activated sludge process is a biological process consists of bacteria which is used for treating the sewage and industrial wastewater using aeration. Usually, it is using for secondary treatment in wastewater treatment plants. The activated sludge process was developed in United Kingdom in 1900s. This process is a kind of suspended growth methods that is based on the presence of the bacteria, fungi, and protozoa among the sludge floc which provides a complete mineralization of wastewater during the operation (Sahinkaya and Dilek, 2005). The high performance of activated sludge bioreactors usually depends on their efficient agitation process and hydrodynamic conditions (Jin et al., 2006; Le Moullec et al., 2011).

There are several studies in the field of activated sludge hydrodynamic investigation in the literature (Rubio et al., 2001; Ndinisa et al., 2006; Vermande et al., 2007; Babaei et al., 2015). The main obstacle among these studies is the limitation of the activated sludge concentration. In some cases, the opacity of the activated sludge avoids some measuring methods such as Particle Image Velocimetry, Laser Doppler Anemometry, and high-speed photography (Naessens et al., 2012). To overcome this drawback, surrogates usually are used to simulate the hydrodynamics conditions, but they are not precise enough to predict the complex flow behavior of the non-Newtonian sludge. The Electrical Resistance Tomography (ERT) provides a wide range of applications to measure the non-Newtonian fluids characteristics with up to 15 g/L Mixed Suspended Solid Liquor (MLSS) concentration.

A study on gas phase characterization and mixing performance of activated sludge bioreactor was performed by Babaei et al. (2015). This experimental study has been investigated the aeration

process of a cylindrical bioreactor to peruse gas phase characteristics and mixing time. Moreover, they worked on Dynamic Gas Disengagement technique to measure the bubbles residence time. They used Electrical Resistance Tomography (ERT) measurement technique to monitor the rate of conductivity in 6 horizontal planes in different distances from sparger at the bottom of the vessel.

This chapter attempts to present a complete literature review of gas-liquid multiphase flow, bubble column reactors, and CFD modeling. In this regard, a set of information about chemical and bubble column reactors, the gas-liquid multiphase flow regimes, gas sparger, gas holdup, mixing time and a brief introduction about ERT system are presented in this chapter.

2.2 Bubble Column Reactor

Generally, there are three main types of chemical reactors that have a wide range of application in industries as follows: **(i)** the trickle bed reactor (fixed or packed bed), **(ii)** fluidized bed reactor, and **(iii)** bubble column reactor (Kantarci et al. 2005). As can be seen in **Figure 2.1**, the design of three different kinds of bubble column reactors is presented.

The trickle bed reactor usually consists of two or three phases. Typically in operation process of this type of reactors, the liquid phase is moving downward through the packed bed of solid particles and gas phase is moving downward or upward and usually is used for performing catalytic reactions. The fluidized bed reactor is a kind of reactor device that is able to provide a range of multiphase chemical reactions. General process in this type of reactor consists of a gas or liquid phase is passing through a suspended solid material. There is a wide range of applications of fluidized bed reactors in oil and petrochemical industries.

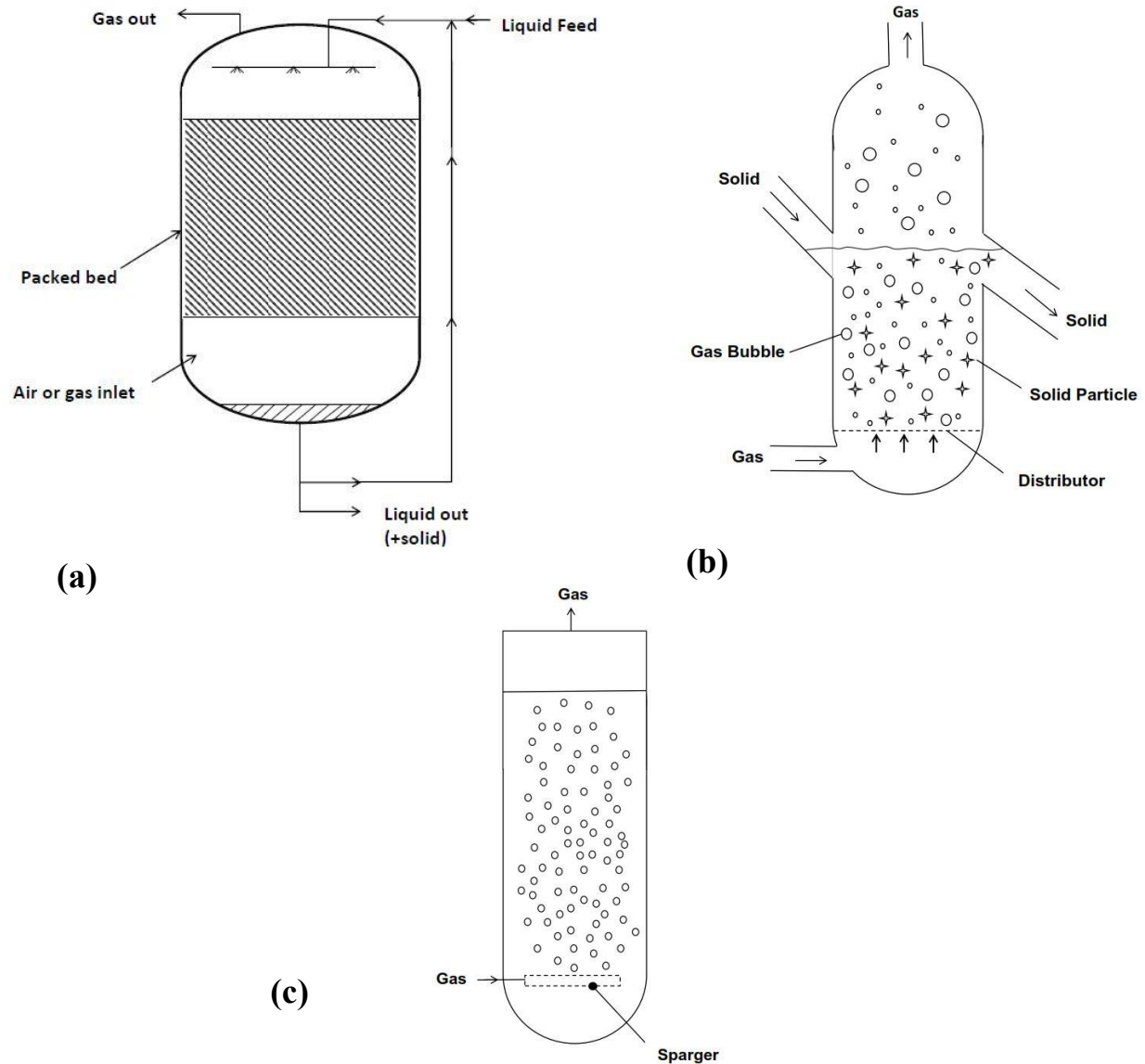


Figure 2.1: The design and geometry of (a) trickle bed reactor, (b) fluidized bed reactor, and (c) bubble column reactor (source: Baron et al., 1996).

The bubble column reactor is widely used in chemical, petrochemical, biochemical and metallurgical industries. The most important applications of bubble column are: (1) oxidation, (2) wastewater treatment, (3) column flotation, (4) hydrogenation, (5) ozonolysis, and (6) alkylation (Yang et al., 2001; Wu et al., 2002).

Generally, bubble column consists of a rectangular or cylindrical process vessel and an aeration system at the bottom of process vessel for injecting the gas phase. The process vessel can be filled with a primary phase of liquid or multiphase mixture of liquid and solid. The bubble column reactor is much more popular among three types of mentioned chemical reactors because of their wide range of applications and cost efficiency.

In some industries such as wastewater treatment and chemical, the bubble column is using as a bioreactor to break down or utilize the microorganisms for production of valuable products such as enzymes, proteins and antibiotics (Kantarci et al., 2005). In a study of Arcuri et al. (1986) the *Streptomyces cattleya* was used to investigate the process of production of thienamycin by bubble column bioreactor.

There is a wide range of effective parameters in design of bubble column reactor which are playing a significant role in operation optimization. Some of these parameters are the gas-liquid interfacial area, the axial solids dispersion coefficient, gas and liquid axial dispersion coefficient, sauter mean bubble diameter, heat and mass transfer coefficient, gas holdup, and physical and chemical properties of liquid area (Kantarci et al., 2005).

The aforementioned effective parameters are measured and controled in experiments by different equipment to monitor the operation conditions. There are some more important measuring tools such as rotameter for controlling the gas inflow rate, thermometer to control the temperature during operation, thermocouple for non-constant temperature operations, manometer to control pressure distribution, and heat flux sensor to control heat transfer along the vessel (Kantarci et al., 2005).

The geometry of bubble column`s vessel is one of the most important terms in design of this kind of reactors. There are two typical geometries with cylindrical cross section (Sanyal et al., 1999;

Ranade and Tayalia, 2001; Ekambara and Joshi, 2003a, b; Dhotre and Joshi, 2004; Babaei et al., 2015) and rectangular cross section (Lin et al., 1996; Mudde et al., 1997; Delnoij et al., 1997; Sokolichin et al., 1997; Pflieger et al., 1999; Pan et al. 1999 and 2000; Mudde and Simonin, 1999; and Sokolichin and Eigenberger, 1999). **Table 2.1** shows some details about the studies with different bubble column geometries and flow regimes.

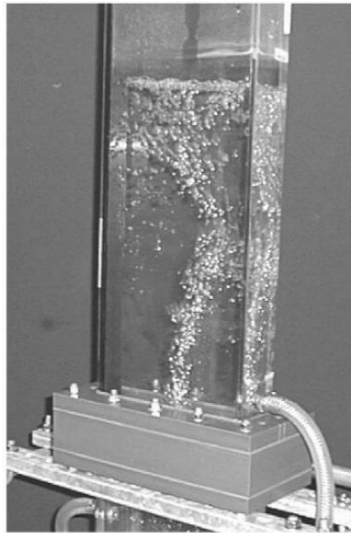


Figure 2.2: The rectangular bubble column reactor of experiment of Pflieger et al. (1999).

In design of the reactor's vessel, the aspect ratio is so important to predict the multiphase flow regime which will be created along the vessel. The aspect ratio is a ratio of height to diameter of the bubble column vessel. Generally, the value of aspect ratio must be 5 at least (Degaleesan et al., 2001), but in case of biochemical bubble column reactors aspect ratio is between 2 and 5. The reactors with larger diameter and height contain larger amount of gas throughput and gas holdup.

Figure 2.2 shows the rectangular bubble column geometry which was used by Pflieger et al. (1999).

Table 2.1: The review of previous researches measuring method, model geometry and flow regime.

Aim	Reference	Measuring Method	Dimension	Geometry	Flow Regime
Quantifying the macroscopic hydrodynamic characteristics of various scale bubble columns. Investigation flow characteristics such as averaged velocity profiles and Reynolds stress profiles	Lin et al., 1996	Flow visualization and a particle image velocimetry (PIV) system.	2D	Rectangular bubble column	Dispersed and coalesced bubble regimes.
Investigation of gas-liquid multiphase bubble's motion with Eulerian-lagrangian model	Mudde et al., 1997	PIV	2D	Rectangular bubble column	Bubbly flow
Investigating a transient two-dimensional axisymmetric model with various setups	Delnoij et al., 1997	Numerical modeling by computer code, called LeBuc.	2D	Rectangular bubble column	Dispersed bubbly regime.
simulate transient fluid dynamics and mixing in shallow bubble columns and effect of sparger design on bubble column characteristics	Sanyal et al., 1999	Computer Automated Radioactive Particle Tracking (CARPT), Computed Tomography (CT), and numerical modeling by Computational Fluid Dynamic	2D	Cylindrical reactor	Bubbly flow and churn turbulent flow.
Dynamic numerical simulation of gas-liquid two-phase flow and comparison between Eulerian-Eulerian and Eulerian-Lagrangian methods	Ranade and Tayalia, 2001	Modeling by Computational Fluid Dynamic (CFD)	2D and 3D	Cylindrical and rectangular bubble column	Dispersed bubbly regime.
	Sokolichin et al., 1997	Total Variation Diminution (TVD) and UPWIND discretization	2D and 3D	Rectangular bubble column	–

Continued

Aim	Reference	Measuring Method	Dimension	Geometry	Flow Regime
Investigation of the hydrodynamic of two-phase gas-liquid flow in a laboratory scale bubble column. Study hydrodynamics, gas phase characteristics, Dynamic gas disengagement (DGD) technique, and mixing time	Pfleger et al., 1999	Modeling by Computational Fluid Dynamic (CFD)	3D	Rectangular bubble column	Bubbly flow
Investigation of gas-liquid model to predict flow pattern, pressure drop and heat transfer Coefficient.	Babaei et al., 2015	Electrical Resistance Tomography (ERT) system	–	Cylindrical bioreactor	Bubbly flow
Numerical simulations of a bubble plume in a bubble column	Dhotre and Joshi, 2004	Modeling by Computational Fluid Dynamic (CFD)	2D	Cylindrical bubble column reactor	–
Investigation of applicability of standard k-ε model for bubble column by numerical modeling	Mudde and Simonin, 1999	Numerical simulation using ASTRID code	2D and 3D	Rectangular flat bubble column	Dispersed bubbly flow
	Sokolichin and Eigenberger, 1999	Total Variation Diminution (TVD)	2D and 3D	Rectangular bubble column	Bubbly flow

2.3 Flow Regimes

There is a general explanation for gas-liquid flows and usually discussed as a motion of gas bubbles among liquid phase (Clayton et al., 2005). There are various publications released by scientists and theoreticians in the field of fluid dynamics and particularly multiphase flow (Karpinska et al. 2016; Ekambara et al. 2005; Babaei et al., 2015; Li et al., 2016). The measurement techniques of single and multiphase flow were growing rapidly from a simple pitot tube to complex laser techniques (Clayton et al., 2005).

There are two common types of gas-liquid flow operations in bubble column reactors (Kantarci et al., 2005). The first one is continuous operation where both of the phases are moving along the column (i.e. pipe) and in second one the liquid phase is stagnant and the gas phase is introducing to vessel at the bottom (i.e. semi-batch bubble column operation).

In general, gas-liquid flows are classified to five different regimes as follows: **(1)** bubbly flow, **(2)** churn-turbulent flow, **(3)** slug flow, **(4)** annular flow, and **(5)** wispy-annular flow (Clayton et al., 2005). **Figure 2.3** shows different types of gas-liquid flow regimes in vertical tubes and indicates the shape of bubbles in each type. One of the most popular flow regimes in the environmental related industries is bubbly flow as can be seen in **Figure 2.3 (a)**. The most important application of bubbly flow in industry is the high interaction among gas bubbles and liquid phase. Moreover, the motion of the gas phase creates a turbulent liquid flow field which is affecting the mixing process. In the case of semi-batch operations, bubbly flow, churn-turbulent, and slug flow are more common flow regimes (Hyndman et al., 1997).

The bubble column multiphase flow regime is directly related to superficial gas velocity. In this regard, scientists found a linear relation between these two parameters (Kawagoe et al., 1976). Generally, superficial gas velocity of 5 cm/s and lesser is creating bubbly flow in semi-batch reactors (Hills, 1974; Fan 1989) and batch reactors with greater superficial gas velocity value than 5 cm/s are experiencing the churn-turbulent flow.

Moreover, there is a relationship among superficial gas velocity, bubble column vessel diameter and type of multiphase flow. According to **Figure 2.4**, there is a homogenous bubbly flow for the vessel diameter of 0.025 to 1 m and superficial gas velocity of less than 0.02 m/s. The increase of

superficial gas velocity causes flow transition to slug flow for bubble columns with smaller diameters and churn-turbulent flow for vessels with larger diameters (Deckwer et al., 1980).

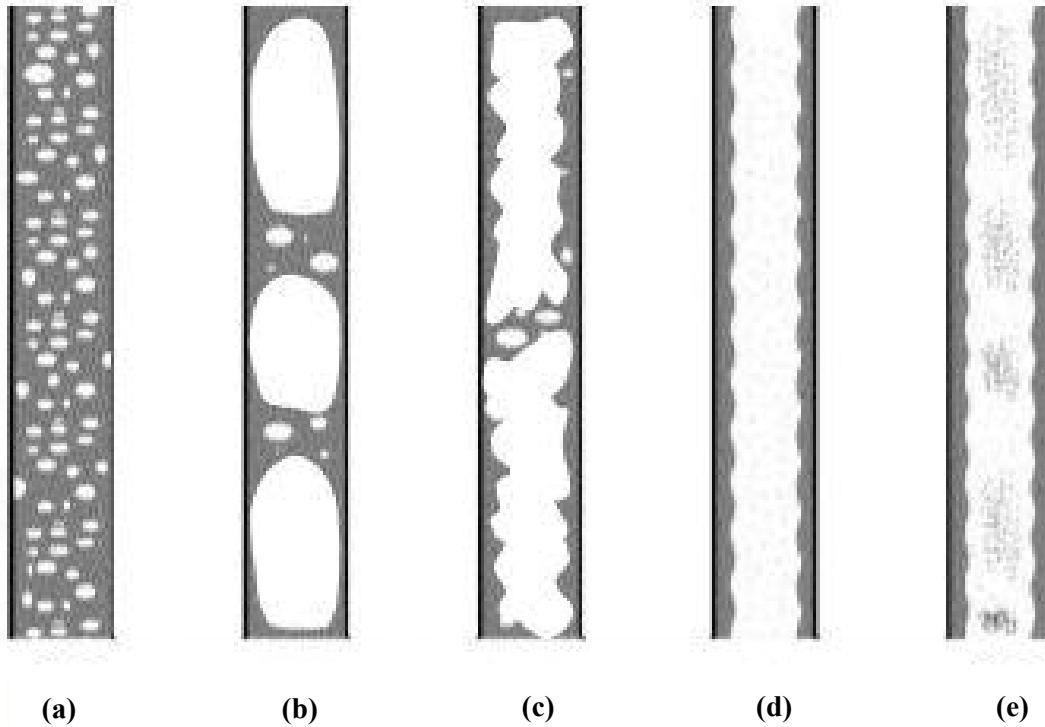


Figure 2.3: Various gas-liquid flow regimes in vertical tubes; **(a)** Bubbly, **(b)** Slug, **(c)** Churn, **(d)** Annular, and **(e)** Wispy-Annular (source: Ghajar, 2005).

The slug flow is one of the typical gas-liquid flow patterns for vertical tubes. Generally, this type of flow appears in small and medium size tubes (Fabre et al., 2010). As can be seen in **Figure 2.3 (b)**, the bubble distribution of slug flow is unique that provides a different multiphase zone in compare with the other types of flow patterns. Fundamentally, the slug flow defines as the upward flow of bullet-shaped Taylor bubbles of gas while surrounded by the liquid slugs. These slugs spread in whole volume of the pipe and sometimes include a small amount of bubble dispersion.

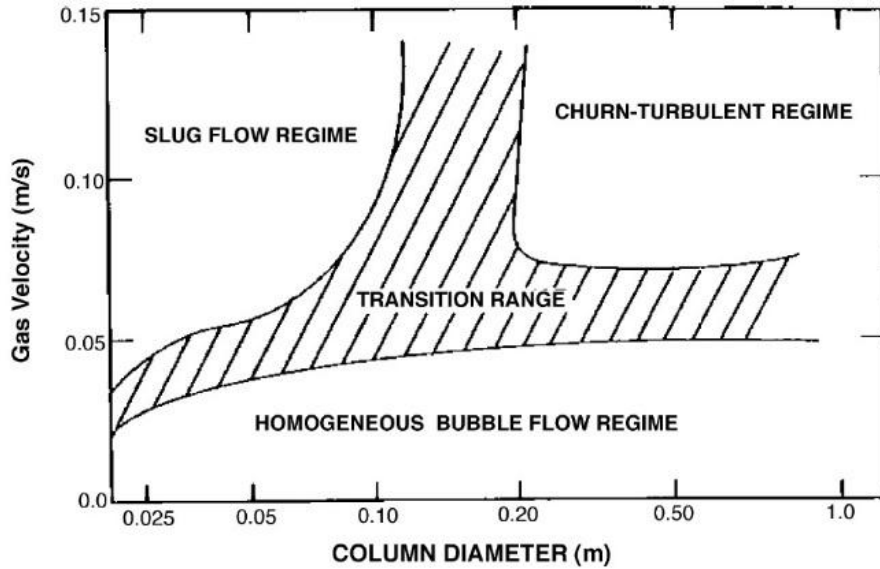


Figure 2.4: The relationship between vessel diameter, gas velocity and flow transition (source: Deckwer et al., 1980).

As can be seen in **Figure 2.3 (c)**, the Churn-turbulent flow is the other type of gas-liquid multiphase flow that is a flow regime with high level of agitation. In this type of flow, adequate amount of gas bubbles interact each other. Due to this interaction, the bubble coalescence will be occurred and larger offbeat bubbles with unique shapes and behaviors will be produced in the system. The churn-turbulent flow usually appears in vertical and near vertical tubes. There are some limitations for using churn-turbulent flow regime in operation. It is not easy to have this type of flow regime in reality, because it transits to slug or annular flow pattern during operation. Moreover, in case of bubble columns that both gas and liquid phase are dynamic, there is a limitation for liquid velocity to generate churn flow.

The annular flow is the other type of gas-liquid flow regime for vertical tubes (**Figure 2.3 (d)**). Generally, this type of flow appears at high rates of vapor mass fraction. The annular flow provides a range of industrial applications with high values of mass flux which is usually more than 1000

$\text{kg/m}^2 \cdot \text{s}$ (Hawkes et al., 2000). One of the prominent features of annular flow is that the liquid film flows on the wall of the channel and the gas phase flows among the central column. In some cases, liquid entrained as a droplet into the central gas flow that is called annular-dispersed flow. The main difference of pure annular flow and annular-dispersed flow is the fraction of entrained liquid droplets which is nearly zero for pure annular flow regime. Frequently, the pure annular flow and annular-dispersed flow are both named as annular flow.

The wispy-annular flow was found by Bennett et al. in 1965 as a new gas-liquid flow regime (**Figure 2.3 (e)**). Their work illustrated the presence of an amount of entrained droplets to the central column of the channel that is surrounded by a liquid film, while the velocity of droplets was more than the liquid film. Actually, the main reported characteristics are same for wispy annular and annular flow regime, but there are some specific features for wispy-annular flow regime as follows:

1. The pressure fluctuation is high (Baker, 1966).
2. There is a significant gas entrainment into the liquid film in this regime (Bennett et al., 1965).
3. The increase of liquid concentration is increasing the oxygen mass transfer coefficient and affects the deposition rate (Govan, 1990).

In case of the annular flow regime, the increase of liquid mass flux causes the liquid film flow to reach a constant value with a certain amount of entrained liquid into the central gas phase as droplets (Hawkes et al., 2000).

As mentioned above, the bubbly flow is one of the gas-liquid multiphase flow regimes in bubble column reactor. In bubbly flow the bubbles are dispersed into the liquid phase. In this type of flow

regime, bubbles try to flow into the liquid to produce the interface area between gas and liquid and create complex interaction of two phases. Due to type of interactions between bubbles and interactions among bubbles and liquid phase, bubbly flow is divided into four main flow patterns (as shown in **Figure 2.5**) as follows: (1) ideally-separated bubble flow, (2) interacting bubble flow, (3) churn-turbulent flow, and (4) clustered bubble flow (Kataoka et al., 2010).

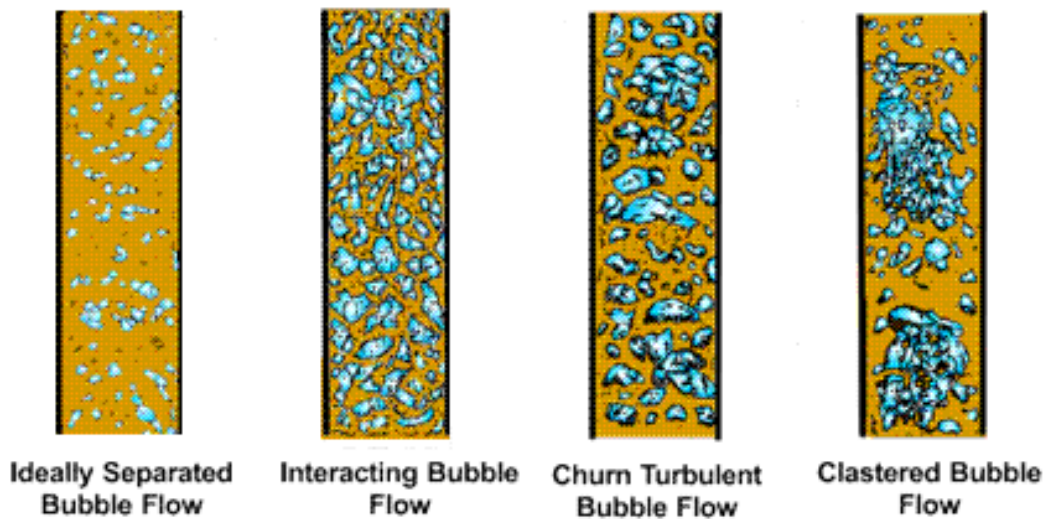


Figure 2.5: The different types of bubbly flow in bubble column reactor (source: Kataoka et al., 2010).

There is no direct or indirect interaction between bubbles in ideally-separated bubble flow pattern and each bubble is going through liquid phase such a single bubble. On the other hand in case of interacting bubble flow pattern, there are larger bubbles in compare with the ideally-dispersed flow that interact each other directly and indirectly. The increase of gas phase flow rate will be increase the amount of bubbles in the bubble column then bubble's coalescence will be happene to create new type of bubbles which are named as cap bubbles (Kataoka et al., 2010) and the flow pattern turns to churn turbulent bubble flow. This type of flow consists of cap bubbles and some small

bubbles. The churn turbulent flow is highly agitated which this prominent feature is related to the interaction of bubbles and turbulent flow.

In case of the clustered bubble flow, some large bubbles combine each other and create the cluster of bubbles then flow through the liquid phase such as a single gas slug. There are two issues will be happened for bubble clusters, in the first case they combine with some other small bubbles to make a larger gas slug after a certain travel, while in second case they divide to a group of small bubbles. In fact, this type of bubble flow can easily transit to other types of bubbly flow patterns or slug flow regime (Wallis, 1969).

2.4 Gas Sparger

There are different types of gas spargers to inject the gas phase in to the volume of the vessel. Generally the gas spargers are divided to two main types of plate and pipe spargers. The sieve spargers are the most popular type of plate gas spargers. As can be seen in **Figure 2.6**, the type of pipe gas spargers consists of straight pipe, single ring spargers, multiple ring spargers, and spider sparger (Kulkarni et al., 2009). In design process of a bubble column reactor, choosing an appropriate sparger is so important to increase the performance of aeration. The bubble column diameter is a critical parameter in determination of a proper gas sparger. Generally, the plate spargers are using for small diameters and pipe spargers are applying in vessels with large diameter. The flow type of bubbles in bubble column is strongly related to the uniformity and non-uniformity of gas injection pattern. The uniform gas injection causes the increase of fractional gas holdup, effective interfacial area, mixing time, and volumetric mass transfer coefficient. On the other hand, the non-uniformity causes a higher pressure drop, and increase the possibility of clogging some holes.

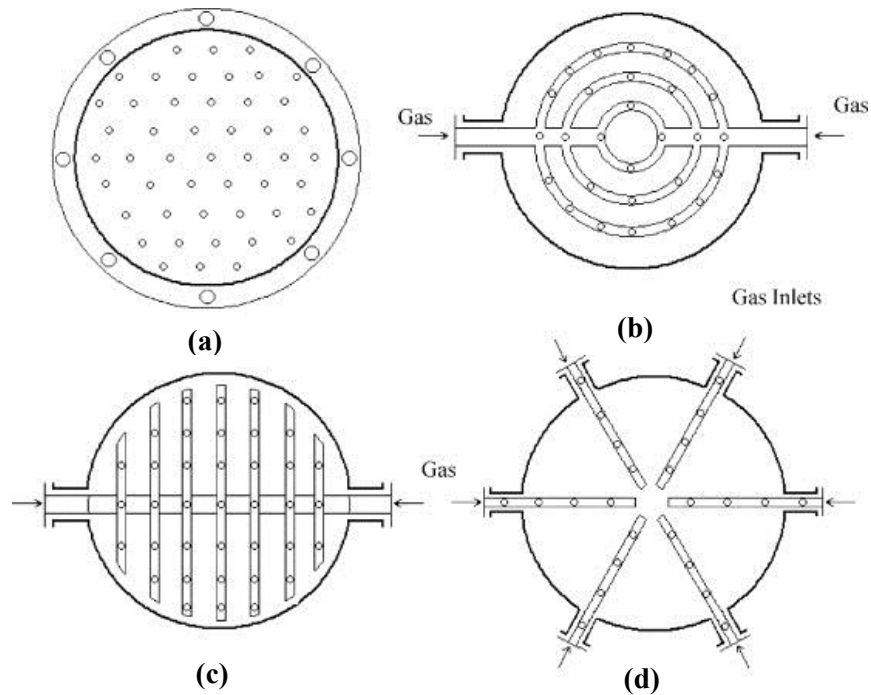


Figure 2.6: Schematic view of different types of spargers where: **(a)** sieve plate sparger, **(b)** multiple ring spargers, **(c)** spider, and **(d)** pipe sparger (source: Kulkarni et al., 2009).

In general, the non-uniformity of the pipe spargers has two main reasons. The first reason is the friction between fluid and vessel's wall which causes the pressure drop and the second one is the decrease of the gas momentum by decreasing the gas phase flow rate. In fact, the internal gas flow of sparger is unpredictable, complicated and completely depends on the geometry of sparger.

In case of gas-liquid multiphase reactors, the gas sparger is strongly affecting the distribution of bubbles among the vessel. Ranade and Tayalia (2001) investigated the effect of design of sparger on hydrodynamics of bubble column by using Eulerian-Eulerian approach. They studied the effect of two ring gas sparger on the mixing characteristics and hydrodynamics of a cylindrical bubble column reactor.

The gas sparger has a significant effect on the bubbles distribution in the bubble column. In case of bubble columns with lower aspect ratio, the effect of gas sparger on the process performance is

more decisive (Haque et al., 1986; Grevskott et al., 1996; Lin et al., 1998; Delnoij et al., 1999; Ranade et al., 2001; Joshi, 2001; and Kulkarni, 2010).

2.5 Gas Holdup

One of the most important parameters in study of bubble column reactor hydrodynamic is gas holdup. Gas holdup is a ratio between gas phase volume and total volume of the liquid. The gas holdup is a dimensionless parameter that is defined as gas volume fraction. The residence time of bubbles in the vessel during operation is directly related to the distribution of gas holdup. The profile of gas holdup distribution is one of the basic topics that is investigated in multiphase flow studies. In this regard, Table 2.2 shows the literature review of some researches that have been derived equations to measure gas holdup.

Table 2.2: Review of the experimental equations of gas holdup.

Researcher(s)	Equation
Joshi and Sharma, 1979	$\varepsilon_g = \frac{V_g}{0.3 + 2V_g}$
Reilley et al., 1986	$\varepsilon_g = 0.009 + 296V_g^{0.44}\rho_l^{-0.98}\sigma_l^{-0.16}\rho_g^{0.19}$
Godbole et al., 1982	$\varepsilon_g = 0.239V_g^{0.634}d_B^{-0.5}$
Hughmark, 1967	$\varepsilon_g = \frac{1}{2 + (0.35/V_g)(\rho_l\sigma/72)^{1/3}}$
Zou et al., 1988	$\varepsilon_g = 0.17283\left(\frac{\mu_1^4 g}{\rho_l \sigma_l^3}\right)^{-0.15}\left(\frac{V_l \mu_l}{\sigma_l}\right)^{0.58}\left(\frac{P + P_V}{P}\right)^{1.61}$
Sada et al., 1984	$\frac{\varepsilon_g}{(1 - \varepsilon_g)^3} = 0.019V_\infty^{1/16}v_s^{-0.125}V_\infty^{-0.16}V_g$
Kawase et al., 1992	$\frac{\varepsilon_g}{1 + \varepsilon_g} = 0.0625\left(\frac{V_g}{v_l g}\right)^{1/4}$

where V is velocity, d is diameter, ρ is density, σ is the width of radial basis function (RBF) kernel, $\sigma =$ width of radial basis function (RBF) kernel, and σ_l is the liquid phase surface tension.

The gas holdup distribution in bioreactors usually is not homogenous in the whole volume of the vessel (Sieblist and Lubbert, 2010; Joshi et al., 1998). The mixing process of the liquid phase in bioreactors is strongly influenced by the gas phase dispersion. In this case of semi-batch bioreactors, the gas phase is dispersed by gas sparger at the bottom of the vessel. The gas inflow rate is really important to form an initial profile of gas holdup. The increase of the gas flow rate provides the larger amount of bubbles that can produce more shear rate to overcome the liquid resistance and reduce the apparent viscosity. Since the bubbles rise in bubble column, radial dispersion causes a gas holdup distribution with wider range in the vessel cross section (Sieblist and Lubbert, 2010). The gas holdup profile forces stagnant liquid to move upward among the gas holdup profile and downward flow near the wall of the vessel.

2.6 Computational Fluid Dynamic (CFD)

The Computational Fluid Dynamics (CFD) provides a general method to predict the sludge flow field during an aeration process in wastewater treatment system. The application of CFD modeling in the wastewater treatment industry has been developed the performance of this process (Essemiani et al., 2004). There are different studies in the field of ASP such as investigation of mixing efficiency and properties of flow by Le Moullec et al. (2008), study on agitator position in case of the minimum velocity to avoid sludge settling and optimization of oxygen transfer (Glover et al., 2006), and exploring the Gas-liquid behavior in the bioreactors (Cockx et al., 2001).

Lei and Ni (2014) simulated a solid-liquid-gas mixture model in a Carrousel oxidation ditch that was aerated and agitated by means of mechanical aerators and mixers, respectively. Carrousel is a

multichannel oxidation ditch which in this research contains horizontal rotors for aeration and submerged mixers for agitation. In this study, multiphase flow was modeled by Mixture method and oxygen mass transfer, carbon oxidation, nitrification, and de-nitrification were investigated. One of the most important parts of this study was simulation of sludge sedimentation which was simulated by species and transport technique to show physical kinematics of sludge sedimentations.

Xei et al. (2014) modeled a full-scale Carrousel ditch equipped with surface aerators and submerged impellers with only 5 to 8 percent error in compare with the experimental data. They worked on the mixing time and suspended solid distribution in their study. Moreover, the optimization of the oxidation process and sedimentation velocity of solid phase was investigated in their work.

Through CFD simulation, Le Moullec et al. (2011) performed a study on activated sludge channel pilot plant. They worked on the investigation of oxygen, COD, NO_3 , and NH_4 concentration profiles with three different approaches as follows: (1) a systematic approach, (2) CFD, and (3) compartmental modeling. However, they found no reasonable results in compare with experimental data for case of ammonium. Their analysis illustrated the significant effect of the applied kinetics model in the simulation of the activated sludge. Their CFD model was developed by fluent in three dimensional formats with turbulence standard k- ϵ model and Eulerian-Eulerian approach.

Samstag et al. (2012) simulated a three dimensional jet aeration system for a sequencing batch reactor to predict mixing performance. This reactor was part of the Blacks Ford Regional Water Reclamation Facility of the JEA utility in Jacksonville, Florida. The duty of this reactor was to

monitor the solid phase characteristics in aerated and un-aerated pumped mixing cases. They developed the 3D model based on the mixture multiphase model and used the standard k- ϵ model to predict the turbulent flow. They found out that the CFD model using no density coupling was significantly over-predicted the degree of mixing in compare with the model using density-coupled model.

Karspinka et al. (2015) compared different methods of turbulence simulation through CFD modeling. They designed an oxidation ditch to evaluate the performance of the hydrojets. They compared different types of turbulence models as follows: Reynolds averaged Navier–Stokes simulations (RANS) and unsteady RANS with the standard k- ϵ model, and large eddy simulation with the Smagorinsky subgrid scale model. They have been investigated the bubble's residence time distribution (RTD) and hydrodynamics.

The k- ϵ model is the most popular model for simulating the multiphase turbulence, due to its accuracy and simplicity (Ekambara et al., 2005). Borchers et al. (1999) simulated a flat bubble column to investigate the performance of standard k- ϵ model in turbulence modelling. Their study justified that standard k- ϵ model is able to simulate the 3D turbulent flow with a good agreement with experimental data. In the other study, Lain et al. (2002) used this turbulence model to simulate a time transient turbulent flow. Their model was successfully validated with the mean and fluctuated velocities of experimental results.

However, none of these studies achieved a good result for simulating turbulent flow in whole of the column. The main reason of this error is the difference among the turbulence models and the real turbulent flow.

Ekambara et al. (2005) used CFD method to predict the bubble column reactor flow field of gas-liquid multiphase flow in 2D, and 3D $k-\epsilon$ models. They focused on cylindrical bubble columns because of the important role of this type of bubble column reactors in the industry. All of the simulated models achieved good agreement with the experimental data, but due to the presence of eddies, the 3D model predicted more accurate results. Moreover, they tried to predict axial dispersion coefficient in 2D, and 3D dimensions. In this attempt, only 3D model achieved results with a good agreement with the experimental data in compare with 2D models.

The bubble size distribution is one of the important parameters about modeling the cylindrical bubble columns. There are various studies performed in the field of bubble size distribution and its effect on bubble column behavior (Lain et al., 1999; Krishna et al., 1999, 2000). Lain et al. (1999) studied the effect of bubble size distribution numerically and experimentally in multiphase gas-liquid flow and reported the significant effect of bubble size on the gas phase axial velocity.

Generally, the bubbles have been divided into two main classes of small bubbles and large bubbles. This concept is called two-bubble class (Krishna et al., 1999 and 2000; Van Baten and Krishna, 2001; Krishna and Van Baten, 2001). However, the interaction between these two classes is a main claim among scientists in this field. In two bubble class method, both classes are treated separately. As a result, the flow field of bubble column will be divided to three independent phases, i.e., liquid phase, small bubble phase, and large bubble phase. According to Krishna et al. (1999, 2000, 2001, and 2003) studies, the 2D axisymmetric simulations cannot predict accurate radial gas hold-up distribution due to axisymmetric imposition. The 3D simulation method was a spot light of gas holdup simulations and achieved valuable results in this field.

The comparison between 2D axisymmetric and 3D simulations showed that the concept of two-bubble classes is helpful to provide more accurate simulation, but it is not enough to simulate the gas holdup (Krishna et al., 2000).

The single-bubble and two-bubble class models have been compared in literature more often by assuming linear dependent gas flow conversion (Ghasemi et al., 2009; Hooshyar et al., 2009; Papari et al., 2012; Shah et al., 1985). Shah et al. (1985) reported that the method of two-bubble class provided basically different prediction in compare with the outcome of the single-bubble class model, while there are some other studies which do not agree with this claim and justify the similarity of the results of these two bubble size models (Ghasemi et al., 2009; Hooshyar et al., 2009). Actually, the substantial difference among single-bubble and two-bubble class models is related to the sub-models applied for the hydrodynamics, mass transfer, and reaction kinetics such as gas concentration (Jiang et al., 2015). There are two basic reasons for the difference between the bubble size class models in bubble column simulation, first one is related to the gas holdup and hydrodynamic model and second one is rate-limiting regime. Totally in both models, the large bubbles effect is dominant in compare with small bubbles. Consequently, the two-bubble class can be simplified to single-bubble class.

2.7 Electrical Resistance Tomography (ERT) System

The main topic of this study was simulating a cylindrical bubble column and investigating the hydrodynamics and gas characteristics. In this regard, the mentioned bubble column was simulated and validated based on the experimental work of Babaei et al. (2015). The ERT system did not use in any sections of current study, but all of the experimental data of Babaei et al. (2015) was

presented by ERT system. This section is presented to provide a brief introduction about the experimental method that was provided for the validation data of this study.

In the field of gas-liquid multiphase flow investigation, the concentration profile is the most important parameter to predict the flow field. In this regard, various methods are used to measure the gas phase concentration profile in agitated tanks to find out the multiphase flow characteristics. There are some scientists that used non-intrusive methods (i.e., x-ray) to investigate solid or gas phase concentration profile through the liquid (Montante et al., 2001; Shamlou and Koutsakos, 1989). Despite of the advantages of non-intrusive method such as providing a flow pattern without any disturbances, it is not able to measure the opaque systems.

The ERT system contains a wide range of applications in industry. This system provides ability to investigate the optically inaccessible cases such as the medical diagnosis. The scientists use this tool to recognize the diseases such as tumors, monitor and investigate industrial reactors and detect probable leaks in buried pipe lines underground. Generally, there two main categories for the studies in the field of ERT system. The first group of studies are working on the development of software and hardware of system (Mann et al., 1997; Stanley et al., 2002) and the second group are using different applications of ERT system in their specific criteria (Babaei et al., 2015; Pakzad, 2007). The ERT system is one of the powerful tools for flow visualization in the world. This system provides some particular features such as the ability of measuring flow characteristics globally and locally, the ability of measurement in both transparent and opaque fluids, and the ability of high speed data collection (Babaei et al. 2015).

As can be seen in **Figure 2.7**, an ERT system consists of three main components as follows: a sensor system, a Data Acquisition System (DAS), and a personal computer. All of these

components attempt to monitor the operation by contributing measurement tools and computer programs.

One of the important and sensitive parts of the ERT system is sensors which has effective role in gathering accurate data. Generally, sensors that include multiple electrodes are installed equispatially around a process vessel of case study and collecting data in different horizontal planes. The block diagram of **Figure 2.7** shows an ERT system with four monitoring planes. The operation of the ERT system starts from monitoring the electrical conductivity by sensors, then the collected data sends to the DAS for analysis and at the last step the computer shows the conductivity distribution tomograms in monitoring planes.

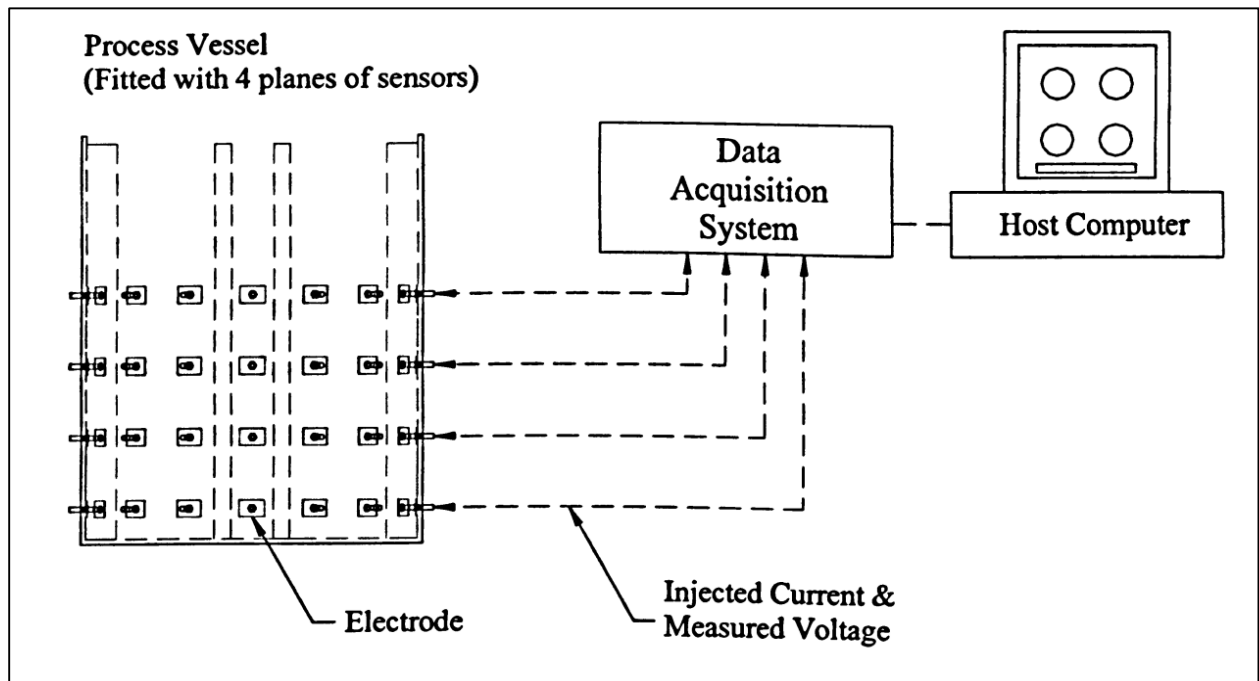


Figure 2.7: Block diagram of an ERT system with for measuring plane (source: Pakzad, 2007).

The conductivity is a rare data which is exported from ERT. In the next step the conductivity can change to concentration by using proper equations.

2.8 Knowledge Gap and Research Objectives

The importance of the activated sludge bubble column and especially the mixing process of this kind of bioreactors is illustrated during this chapter. There are some fundamental issues in the field of non-Newtonian fluid investigation which are still not well understood such as trends of mixing during the process, the gas holdup and liquid velocity distribution during operation, and the effect of superficial gas velocity on mixing process (Li et al., 2016). The experimental studies could not provide detailed information about the sludge behavior and the mixing time because of the optical inaccessibility of the non-Newtonian sludge. The only device which can measure the sludge flow behavior is the ERT system, but it is not able to provide the precise sludge flow pattern and mixing trends.

The objective of this study is to investigate the effect of superficial gas velocity, type of gas sparger, and tracer injection location on the flow behavior and mixing process using CFD. The mixing process and hydrodynamics is studied experimentally by Babaei et al. (2015) and the CFD modeling results will be validated. Then, the liquid and gas phase flow pattern, trends of mixing process, mixing time and the effect of gas sparger modification is determined by CFD simulations.

2.9 Notations

The following symbols are used in this chapter:

CFD = computational fluid dynamics

d = diameter, m

DAS = data acquisition system

ERT = electrical resistance tomography

g = gravity, m/s^2

K = turbulent kinetic energy, m^2/s^2

T = temperature, K or $^{\circ}\text{C}$

V = velocity, m/s

Greek letters

ε = gas holdup, non-dimensional

μ = turbulent viscosity, $\text{Pa}\cdot\text{s}$

ρ = density, $\text{kg}\cdot\text{m}^{-3}$

σ = width of radial basis function (RBF) kernel

σ_l = liquid phase surface tension (N/m)

Indices

g = gas phase

l = liquid phase

s = solid phase

B = bubble

Chapter 3: CFD Modeling of the Activated Sludge Bubble Column: Axial Velocity Profile and Mixing

3.1 Introduction

The activated sludge process (ASP) was developed by Ardern and Lockett (1914) and was so named because the process is able to produce an activated mass of microorganisms stabilizing a waste aerobically. There are different types of the original process however fundamentally they are all similar in operation (Metcalf and Eddy Inc., 1995). The ASP is a biological method of wastewater treatment technique in which a mixture of wastewater and biological sludge (microorganisms) is agitated and aerated. The biological solids are subsequently separated from the treated wastewater and recycled back to the aeration process as needed (Davis and Cornwell, 1991). In the large wastewater treatment plants the aerobic degradations often take place in channels or closed-loop reactors (Degre'mont, 1991).

The design and optimization of ASP requires knowledge of multiphase mixing methods and bubbles behavior in gas-liquid system. In these types of bioreactors, there are two basic concepts affecting the mixture's hydrodynamics: **(1)** rate of superficial gas velocity in an aeration system; **(2)** the rheological properties of the activated sludge (Babaei et al., 2015). The current design of the wastewater treatment systems included but are not limited to design of spargers, bubble size's distribution, and column structures relies on the assumptions about the gas and liquid behavior and the mixing performance. However the inflowing superficial gas velocity in the process bubble column has significant effect on the bubble size distribution and also on the shape of the bubbles (Karpinska Portela, 2013). On the other hand, the significant effect of different bubble sizes on superficial gas velocity, and thus gas holdup and liquid velocity profile have been observed

(Fayolle et al., 2006). Among available aerated bioreactors, bubble columns have attracted a lot of attentions due to their simple geometry and consequently low power consumption, high rate of heat and mass transfer, and high rate of gas-liquid mixing (Kantarci et al., 2005).

Bubble column generally consists of a rectangular or a cylindrical process vessel equipped with a gas sparger. Bubble columns are widely used in wastewater treatment plants, chemical, petrochemical, biochemical, and metallurgical industries. The most important applications of bubble columns are oxidation, wastewater treatment, column flotation, and hydrogenation (Yang et al., 2001; Wu et al., 2002). There are some chemical applications for bubble columns such as Fischer-Tropsch process that is a process of production of transportation fuels with indirect coal liquefaction, synthesis process of methanol, and other synthetic fuels (Kantarci et al., 2005; Degaleesan et al., 2001).

During past 30 years, many studies have been done on the bubble columns because of its high capacity for development and optimizations. Optimal bubble column can be determined on the basis of the different aspects such as mixing process, column's design, and phases' characteristics. Among the above mentioned aspects, design of a bubble column is a challenging task since several parameters are included such as specific gas-liquid interfacial area (Sada et al., 1987), the coefficient of axial solids dispersion (Kojima et al., 1986), gas and liquid axial dispersion coefficient (Moustiri et al., 2001), Sauter mean bubble diameter (Daly et al., 1992; Babaei et al., 2015), heat and mass transfer coefficient (Deckwer et al., 1980; Ozturk et al., 1987), bubble size distribution (Lain et al., 1999; Krishna et al., 1999, 2000), gas holdup, superficial gas velocity (Hills, 1974; Fan 1989; Babaei et al., 2015), gas-liquid flow regime (Clayton et al., 2005; Kawagoe et al., 1976), and physical and chemical properties of the process liquid (Kantarci et al., 2005). In this regard, recent studies are categorized into the five main topics: (a) gas holdup investigations

(Babaei et al., 2015; Wang et al., 2003; Kumar et al., 2012; Shimizu et al., 2000), (b) study of bubble properties (Lain et al., 1999; Ghasemi et al., 2009; Hooshyar et al., 2009; Lapin et al., 2002), (c) study on flow regime changes and CFD simulations (Ekambara et al., 2005; Lain et al., 2002; Dhotre et al., 2004; Thorat and Joshi, 2004), (d) investigations of mass transfer (Vandu and Krishna, 2004; Krishna and Van Baten, 2003; Maalej et al., 2003), and (e) investigations of heat transfer (Li and Prakash, 2002; Chen et al., 2003; Lin and Wang, 2001).

In order to evaluate the effect of the design parameters on the performance of the bubble column a number of experimental techniques can be employed such as conductivity probe (Al-Oufi et al., 2011), particle image velocimetry (Chen et al., 1999), optical fiber (Gheni wt al., 2016), electrical resistance tomography (Babaei et al., 2015), and ultrasonic methods (Han et al., 2008). However these experimental techniques are costly and time consuming especially for activated sludge in the tall bubble columns. To overcome the difficulties of experimental techniques, computational fluid dynamics (CFD) modeling and simulations can be applied to understand the complex flow behavior between gas and liquid.

There is a significant improvement in CFD applications in the field of wastewater treatment simulations especially in design of screens, grit chambers, and process columns (Karspinka and Bridgeman, 2016). Certainly, the most challenging part in CFD modeling of the activated sludge bubble columns is the simulation of the multiphase flow. The recent CFD modeling shows higher potential in compared with the old methods of modeling applied in the wastewater treatment processes. CFD is applied to design new activated sludge bubble columns and also it is employed to optimize the performance of existing systems and to assess the effectiveness of current operations.

There are several studies performed on the ASP applying CFD modeling and simulations such as predicting the gas dispersion flow pattern as a result of different gas and liquid flow rates in both bench scale and industrial size reactors, evaluating the mixing efficiency and properties of gas-liquid flow (Le Moullec et al., 2008), assessing the effect of gas velocity on the rate of oxygen mass transfer (Abusam et al., 2002), and molding the aeration basin to characterize the gas phase (Glover et al., 2006).

One of the most important factors affected the flow regime of gas-liquid multiphase flow is superficial gas velocity ($v_{s,gas}$) which is the velocity of gas if it flows into the pipe with no liquid in. The real definition of superficial gas velocity is the total gas throughput (q_{gas} in m^3/s at operating temperature and pressure) divided by the total cross sectional area of the pipe as shown in Equations **(3.1)** (Corneliussen et al., 2005). Also there is a same concept for liquid velocity.

$$v_{s,gas} = \frac{Q_{gas}}{A} \quad (3.1)$$

and for multiphase mixture velocity we have Equation **(3.2)** which is the sum of the $v_{s,gas}$ and $v_{s,liquid}$.

$$v_m = v_{s,gas} + v_{s,liquid} \quad (3.2)$$

However, in order to apply Equation **(3.2)**, both phases must be homogeneous and a slip free multiphase flow exist (Corneliussen et al., 2005).

Cockx et al. (2001) investigated the relation between global mass transfer and the liquid flow generated by mechanical mixers. In this case, the gas-liquid interaction was occurred while the liquid flew horizontally and the plume of gas flew vertically. Their CFD simulation illustrated that the circulation of the liquid phase increased the mass transfer rate by only less than 10 percent. Fayolle et al. (2007) investigated different setups of the developed numerical tool to predict the

oxygen mass transfer of a pilot and full-scale oxidation ditches. Gresch et al. (2011) studied two different air diffusers in terms of the flow field, efficiency, and performance of convectional activated sludge tank.

Karspinka et al. (2015) modeled an oxidation ditch and compared different types of turbulence models such as Reynolds averaged Navier–Stokes simulations (RANS) and unsteady RANS with the standard k- ϵ model, and large eddy simulation with the Smagorinsky subgrid scale model. They also investigated the residence time distribution (RTD) and hydrodynamic behavior of the process and the results illustrated the importance of turbulence models selected.

In order to show the mixing time sensitive parameters, McClure et al. (2015) investigated the effect of superficial gas velocity and location of tracer injection on the mixing time of the bubble column filled with water by applying both experimental and numerical approaches. It was found that in the range of 0.07 to 0.29 m/s of superficial velocity, no significant change has been observed in mixing time predictions, however such parameters as the location of the tracer injection and the measurement points showed significant impacts on the mixing time values.

Despite the importance of the bubble columns, the CFD approach has not been entirely assessed in this field. Recently Babaei et al. (2015) performed a study on the performance of the mixing and aeration processes of an activated sludge bioreactor. Applying electrical resistance tomography (ERT) they studied **(a)** the characteristics of the gas phase and the performance of the mixing process of a bubble column after shutting off the gas flow based on the dynamic gas disengagement (DGD) technique, **(b)** the effects of the superficial gas velocity and fluid mixed liquor suspended solid (MLSS) on the liquid flow field, **(c)** the average bubble rise velocity, **(d)** the sauter mean bubble diameter, and **(e)** the mixing time measurements. However the authors did

not assess the mixing flow pattern and the velocity profile existing in the bubble column due to the lack of required experimental tools. In this chapter, the investigation of the gas phase behavior in an aerated bubble column filled with the activated sludge and its effects on the liquid phase velocity using the CFD modeling and simulations approach are presented. The effect of the superficial gas velocity on the gas axial velocity profile, overall gas holdup, and mixing time has been fully evaluated.

In this Chapter, first CFD model development will be presented and then the model will be validated with the experimental data available in the literature, and then results will be shown with the adequate discussion. Finally the concluding remarks from this study will be presented.

3.2 CFD Model Development

Computational Fluid Dynamics (CFD) is a multitasking tool to study complex flows such as multiphase flow in the bubble column. As can be seen in **Figure 3.1(a)**, geometry consists of a cylindrical tank with diameter of 0.248 m and height of 1.000 m. Liquid height was 0.82 m providing a liquid volume of 0.396 m³. The bubble column was equipped with a sparger at the bottom of the vessel. The star shape gas sparger as can be seen in **Figure 3.1(b)** consists of six arms of 0.078 m long with 4 holes of 1 mm diameter on each arm. **Figure 3.1(c)** shows a novel sparger which is a modified star shape sparger. As presented in this figure, the modified sparger contains 7 holes with diameter of 1.852 mm that 6 of them located at the end of each arms and one of them is at the middle of the sparger.

A pre-processor, ANSYS Design Modeller (version 17.1) platform was used to generate the unstructured tetrahedral mesh as can be seen in **Figure 3.1(a)**. For capturing the gas characteristics at the main part of the vessel, a size function was employed to generate very refined mesh in central

area of the column. The grid independency analyses have been done and the final three-dimensional model had 749,125 cells in its mesh network.

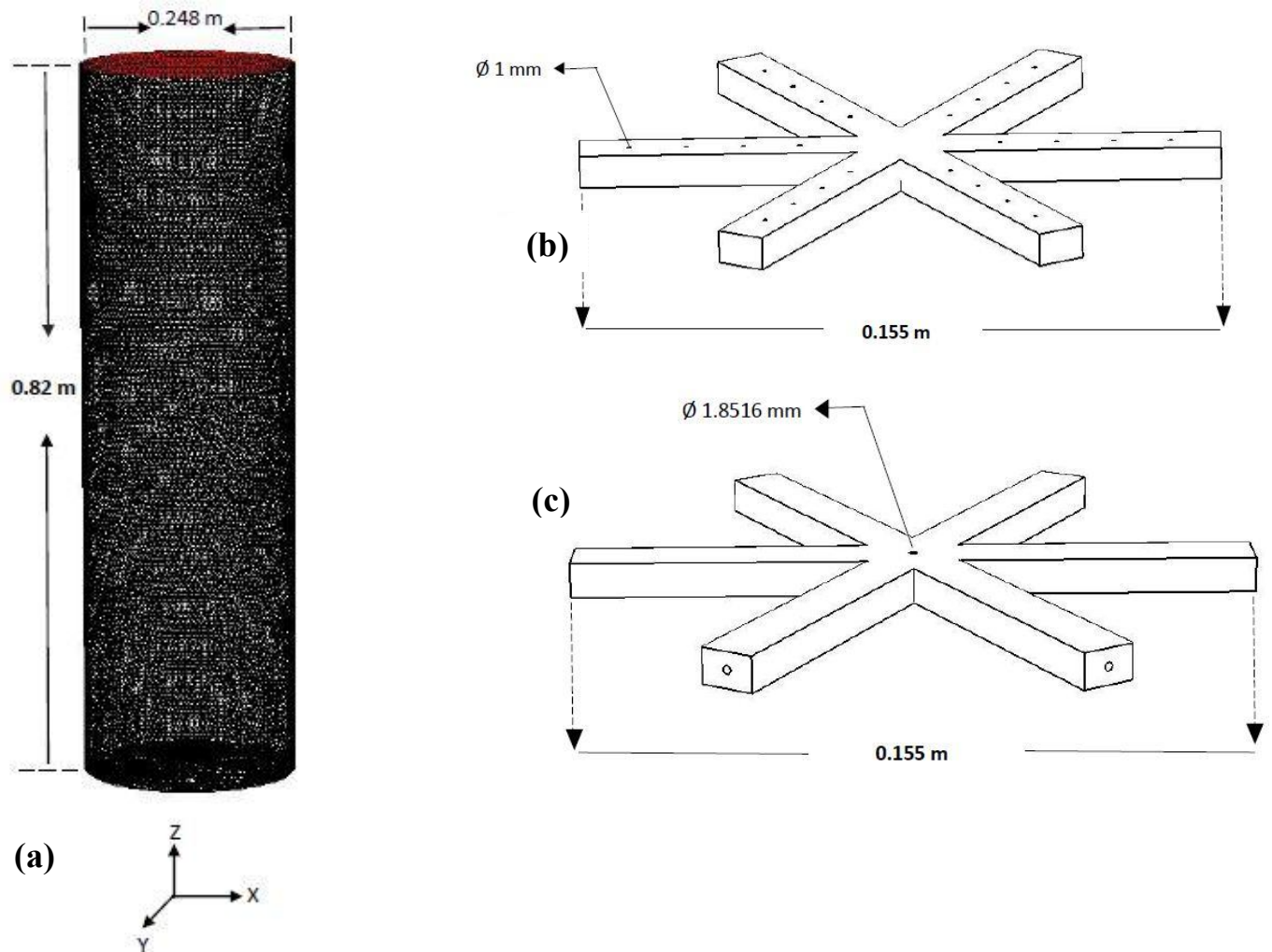


Figure 3.1: (a) the bubble column numerical grids, (b) the star shape sparger, and (c) the modified star shape sparger (dimensions in m and mm).

The Eulerian approach has been applied to model the multiphase flow inside the bubble column. Sokolichin et al. (1997) compared the Eulerian and Lagrangian flow models. They found that there is no difference between results of two approaches when appropriate discretization has been applied. This important result has been also justified by Sokolichin and Eigenberger (1999) and

Ekambara et al. (2005). The conservation laws in the Eulerian approach are the base of fluid dynamic principal equations such as conservations of the mass, momentum, and energy (Blazek, 2005). Since the operating conditions in this study occur in an isothermal environment, the flow field can be described by just considering the mass conservation equations (i.e. the continuity and momentum equations).

There are two basic equations of mass balance and momentum balance obtained for each control volume of mesh network as follows:

$$\frac{\partial(\rho_{\kappa} \alpha_{\kappa})}{\partial t} + \nabla(\rho_{\kappa} \alpha_{\kappa} \mathbf{u}_{\kappa}) = 0 \quad (3.3)$$

$$\frac{\partial(\rho_{\kappa} \alpha_{\kappa} \mathbf{u}_{\kappa})}{\partial t} + \nabla(\alpha_{\kappa} \rho_{\kappa} \mathbf{u}_{\kappa} \mathbf{u}_{\kappa}) = -\alpha_{\kappa} \cdot \nabla(P_{\kappa}) + \nabla(\alpha_{\kappa} \tau_{\kappa}) + \alpha_{\kappa} \rho_{\kappa} \mathbf{g} + \mathbf{M}_K \quad (3.4)$$

where k refers to the phase, $\mathbf{u} = (u, v, w)$ is the velocity of phase k, α is the volume fraction, ρ is the density, P is pressure, M consists of the interphase forces, and τ_{κ} is stress tensors. For phase k the stress tensor τ_{κ} is equal to:

$$\tau_{\kappa} = \mu(\nabla \mathbf{u}_{\kappa} + (\nabla \mathbf{u}_{\kappa})^T - \frac{2}{3} I(\nabla \cdot \mathbf{u}_{\kappa})) \quad (3.5)$$

where μ is the turbulent viscosity. In this case, the standard k- ϵ was used for turbulence modeling and turbulent viscosity is calculated by the following equation:

$$\mu = \rho C_{\mu} \frac{k^2}{\epsilon} \quad (3.6)$$

where C_{μ} is a constant parameter and equal to 0.09, k is the turbulent kinetic energy and ϵ is the turbulent energy dissipation. There are several studies have been reported on the turbulence closures (Shives et al., 2016; Amoudry, 2014). The complex approaches such as large eddy simulation-LES (Deen et al., 2001) and direct numerical simulation-DNS (Bunner and

Tryggvason, 1998 and 1999; Esmaeeli and Tryggvason, 1998 and 1999) have also been evaluated however refined large number of the grids and extensive computational time are essential for getting accurate results with these complex methods (Karpinska and Bridgeman, 2016).

The k-ε model is the most applicable and validated turbulence model applied in CFD simulations (Ekambara et al., 2005). The k-ε model has been applied for modeling of the confined flow where the shear stress is an important component (Fathi et al., 2012; Ranade, 2002). However the k-ε model has some limitations in modeling of the unconfined flows such as external aerodynamics applications. The other method is Reynolds stress models (RSM) which is mostly applied for modeling of non-circular ducts and curved flows. By using RSM not only the time of simulation is increased due to some more additional equations in comparison with the k-ε model, but also the convergence rate is reduced (Karpinska and Bridgeman, 2016; Launder et al., 1975) Borchers et al. (1999) modeled a flat bubble column to investigate the applicability of standard k-ε model and found that the use of 3D turbulent simulations provides virtuous results. Lain et al. (2002) also used k-ε model for modeling of the cylindrical bubble column. They validated their numerical results with the experimental ones in terms of the mean and fluctuated velocities of gas. The following equations are used to calculate K and ε.

$$\frac{\partial \alpha_L \rho_L K_L}{\partial t} + \nabla(\alpha_L \rho_L K_L \mathbf{u}_L) = \nabla \left(\alpha_L \frac{\mu}{\partial_k} \nabla K_L \right) + \alpha_L G_{k,L} - \alpha_L \rho_L \varepsilon_L \quad (3.7)$$

$$\frac{\partial \alpha_L \rho_L \varepsilon_L}{\partial t} + \nabla(\alpha_L \rho_L \varepsilon_L \mathbf{u}_L) = \nabla \left(\alpha_L \frac{\mu}{\partial_\varepsilon} \nabla \varepsilon_L \right) + \alpha_L \frac{\varepsilon_L}{K_L} (C_{\varepsilon 1} G_{k,L} - G_{\varepsilon 2} \rho_L \varepsilon_L) \quad (3.8)$$

where the constant values are described as follows: $C_{\varepsilon 1} = 1.44$, $G_{\varepsilon 2} = 1.92$, $\sigma_k = 1.0$, and $\sigma_\varepsilon = 1.3$. The term G in above equation is the production of turbulent kinetic energy that is calculated as follows:

$$G = \tau_L : \nabla \mathbf{u}_L \quad (3.9)$$

The term M_K in **Equation (3.4)** is describing the external forces for phase k and representing as follows:

$$M_K = M_{D,K} + M_{L,K} + M_{VM,K} \quad (3.10)$$

where the right hand side parameters are presenting external forces of drag, lift and virtual mass for phase k. The drag force $M_{D,L}$ is defined as **Equation (3.11)**.

$$M_{D,L} = \frac{3}{4} \alpha_G \rho_L \frac{C_D}{d_B} (u_G - u_L) |u_G - u_L| \quad (3.11)$$

The drag simulation for spherical and non-spherical particles is different. Generally, in case of non-spherical particles the drag curve must be obtained from experiments (Ranade, 2002). The Schiller and Naumann (1933) employed an approach to model spherical particles or fluid droplets which are sufficiently small. The Schiller and Naumann approach is valid if the particle deformation would be negligible (Loth, 2008). There are several studies employed Schiller and Naumann approach to simulate the drag multiphase interaction in the bubble column modeling (Laborde-Boutet et al., 2009; Chen et al., 2004; Larachi et al., 2003). The drag function C_D in this study was defined according to Schiller and Naumann model (Schiller and Naumann, 1933; Ishii and Zuber, 1979) as follows:

$$C_D = \frac{24(1 + 0.15Re^{0.687})}{Re} \quad Re \leq 1000 \quad (3.12)$$

$$C_D = 0.44 \quad Re > 1000$$

The effect of virtual mass force was neglected in this study, since it did not show any significant effect on the results. Hunt et al. (1987) studied the relation between the efficiency of the virtual mass force and bubble column diameter. They found out that for bubble columns with diameter bigger than 0.15 m, the effect of virtual mass force is negligible. Moreover, there are several studies which also neglected the effect of virtual mass force (Fletcher et al., 2016; Deen et al., 2001; Sokolichin and Eigenberger, 1994; Ranade and Tayalia, 2001; and Pfleger et al., 1999). In the

present study the lift force was also neglected since in comparison with the drag force, it has no significant impact on the simulation results (Sokolichin and Eigenberger, 1999; Delnoij, 1997). However, in such studies as Deen et al. (2001) and Lakehal et al. (2002), the lift force has been considered as a constant value for the lift coefficient. **Table 3.1** reviews the studies on the interphase forces.

Table 3.1: Review of interphase forces.

Reference	Geometry	Operating Details	Turbulence Model	Drag
Mudde and Simonin, 1999	Rectangular (Becker et al.): Width = 0.5 m; length = 0.08 m; Height = 1.5 m. Sparger: $d_o = 0.04$ m (100 mm from the left wall)	Semi batch, $V_G = 0.0011$ m/s	Standard k- ϵ , low Reynolds number k- ϵ	(a)
Pfleger et al., 1999	Rectangular Width = 0.2 m; length = 0.05 m; Height = 0.45 m. Sparger: set of 8 holes in rectangular configuration:(1) 1 set located in the center, (2) 1 set located off center, (3) 3 sets located centrally	Semi batch, $V_G = 0.0013$ m/s	Standard k- ϵ	$C_d = 0.66$
Deen et al., 2000	Rectangular Width = 0.15 m, length = 0.15 m, Height = 1.0 m. Sparger: perforated plate $d_o = 0.001$ m, 49 holes	Semi batch, $V_G = 0.005$ m/s	Standard k- ϵ	(b)
Deen et al., 2001	Rectangular Width = 0.15 m, length = 0.15 m, Height = 1.0 m. Sparger: perforated plate $d_o = 0.001$ m, 49 holes	Semi batch, $V_G = 0.005$ m/s	Standard k- ϵ , LES $C_s = 0.10$	(b)
<i>Continued</i>				

Reference	Geometry	Operating Details	Turbulence Model	Drag
Pfleger and Becker, 2001	Cylindrical Diameter = 0.288 m, Height = 2.6 m. Sparger: (1) perforated plate ($d_o = 0.0007$ m, 21 holes) (2) ring ($d_o = 0.0007$ m, 20 holes)	Semi batch, $V_G = 0.0015$, 0.005, 0.01, and 0.02 m/s	Standard k- ϵ	$C_d = 0.44$
Ranade and Tayalia, 2001	Cylindrical Diameter = 1 m, Height = 2 m. Sparger: (1) single ring (ring diameter = 0.45 m), (2) double ring (ring diameter = 0.45, 0.78 m)	Semi batch, $V_G = 0.01$, 0.02, and 0.03 m/s	Standard k- ϵ	(d)
Buwa and Ranade, 2002	Rectangular Width = 0.2 m, Diameter = 0.05 m, Height = 1.2 m. Sparger: (1) sintered sparger, (2) four multipoint ones having 8 holes ($d_o = 0.0008$ – 0.002 m)	Semi batch, $V_G = 0.0016$ – 0.0083 m/s	Standard k- ϵ	(e)
Lakehal et al., 2002	Convergent channel is divided at bottom with a splitter plate, and each side is supplied independently with mixture of bubbles ($d_B = 3$ mm) and water. Width = 0.30 m, Height = 0.60 m, Diameter = 0.04 m	Inlet 0.22 m/s on one side, 0.54 m/s in other side.	LES models. (a) $C_s = 0.12$, (b) DSM Model	(b)
Bove et al., 2004	Rectangular Width = 0.15 m, Diameter = 0.15 m, Height = 1.0 m. Sparger: perforated plate, $d_o = 0.001$ m, 49 holes	Semi batch, $V_G = 0.005$ m/s	VLES $C_s = 0.12$	(b), (f)
Bombardelli et al., 2006	Rectangular Width = 0.5 m, Diameter = 0.15 m, Height = 0.08 m	Semi batch, $V_G = 0.0016$ m/s	LES-NWM in a mixture model framework	Force get cancelled under the assumption of dilute plume hypothesis and use of mixture equation

In this table a, b, c, d, e, f, and g are drag formulas as follows:

$$(a) \quad C_D = \frac{24}{Re} (1 + 0.15Re^{0.687}) \mathcal{E}_t^{-1.7}, \text{ if } Re < 1000$$

$$(b) \quad C_D = \frac{2}{3} E_o^{0.5}; \text{ (Ishii and Zuber, 1979).}$$

$$(c) \quad C_D = \frac{4}{3} \frac{\rho_L - \rho_G}{\rho_L} g d_B \frac{1}{V_b^2}; \text{ where } V_b \text{ is a rise velocity.}$$

$$(d) \quad M_{D,L} = -5 \times 10^4 \mathcal{E}_G \mathcal{E}_L (u_G - u_L)$$

$$(e) \quad C_D = \max \left\{ \frac{24}{Re} (1 + 0.15Re^{0.687}), \frac{8}{3} \left(\frac{E_o}{E_o + 4} \right) \right\}; \text{ (Tsuchiya et al., 1997).}$$

$$(f) \quad C_D = \frac{4}{3} \frac{\rho_L - \rho_G}{\rho_L} g d_B \frac{1}{V_T^2}; \text{ where } V_T \text{ is the terminal rise velocity (Tomiyama et al., 2014).}$$

$$(g) \quad C_D = \frac{\rho_L - \rho_G}{V_s} g$$

In this study, the non-Newtonian sludge was modeled based on the non-Newtonian power-law model which is described as follows:

$$\eta = K \dot{\gamma}^{n-1} e^{T_0/T} \quad (3.13)$$

where k is the consistency index and n is the flow behavior index. As reported by Babaei et al. (2015) the k and n for the sludge are equal to 0.00528 pa.sⁿ and 0.6887.

The generalized Reynolds number for the non-Newtonian fluids is described as follows (Wu and Chen, 2008):

$$Re_g = \frac{\rho U_\infty^{2-n} D^n}{K(0.75 + 0.25/n)^n 8^{n-1}} \quad (3.14)$$

In order to calculate mixing time, after the flow field had been calculated, the homogenization of the injected tracer was simulated using ‘‘Species and Transport Model’’ (Pakzad et al., 2008) using

Equation (3.15):

$$\frac{\partial}{\partial t} (\rho w) + \nabla \cdot (\rho \bar{v} w) = \nabla \cdot \rho D_m \nabla \phi \quad (3.15)$$

where the w is the local mass fraction of the tracer, \bar{v} is the mean velocity vector, ρ is the fluid density, and D_m is the molecular diffusivity of the tracer in the mixture (Pakzad et al., 2013).

The tracer fluid properties were set same as bulk fluid as an activated sludge with MLSS of 0.712 reported by Babaie et al. (2015). In order to evaluate the effect of the injection's location on mixing time, four different locations for injection have been considered. These locations as shown in **Figure 3.2** are as: **(a)** Injection Point (1): middle of top of the column with $x=0$, $y=0$, and $z=0.82$ m (same as Babaei et al., 2015), **(b)** Injection Point (2): the middle of the liquid height with $x=0$, $y=0$, and $z=0.41$ m, **(c)** Injection Point (3): $x=0$, $y=0$, and $z=0.117$ m, and **(d)** Injection Point (4): the corner bottom of the vessel with $x=0.097$, $y=0$, and $z=0.027$ cm. The tracer was added into the bubble column from either above mentioned locations. This figure also shows six monitoring planes which were considered in order to calculate mixing time. The monitoring lines located at $X= -0.124$ to 0.124 m and the axial distance of the monitoring lines 1 to 6 from bottom of the vessel are $Z= 0.585$, 0.46 , 0.41 , 0.293 , 0.205 , and 0.117 m which are exactly same as the monitoring planes 1 to 6 and the non-dimensional distance (H/D) for planes and lines 1 to 6 are equal to 2.358, 1.855, 1.653, 1.181, 0.826, and 0.471.

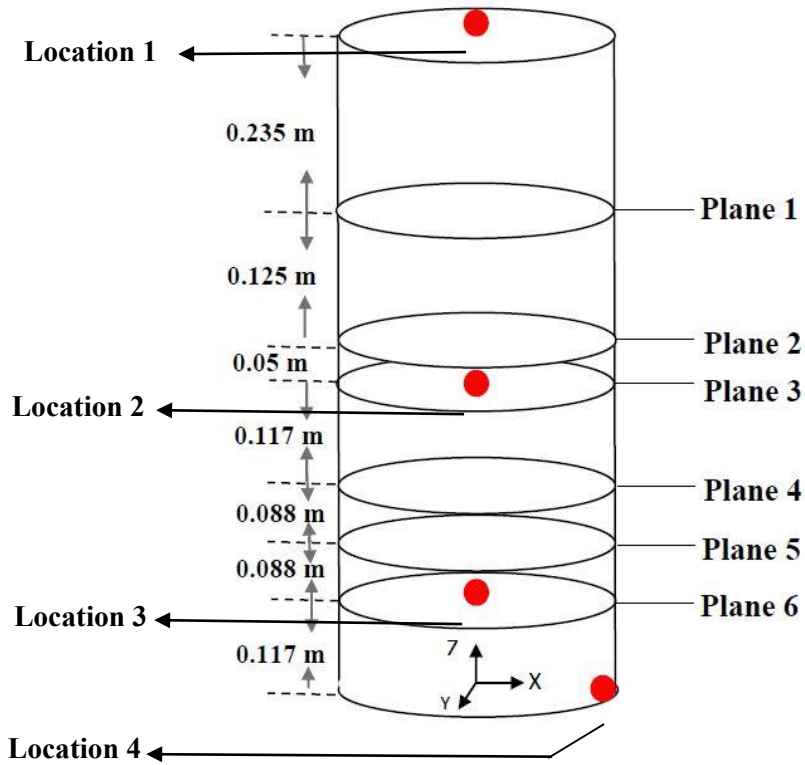


Figure 3.2: CFD injection points and monitoring planes used for estimation of the mixing times. The Monitoring Plane (1): $z=0.585$ m, Monitoring Plane (2): $z=0.46$ m, Monitoring Plane (3): $z=0.41$ m, Monitoring Plane (4): $z=0.293$ m, Monitoring Plane (5): $z=0.205$ m, and Monitoring Plane (6): $z=0.117$ m

Figure 3.3 shows the non-dimensional tracer concentration at 6 planes for case of 0.163 cm/s superficial gas velocity while the tracer was injected at location (4). As can be seen, the tracer was touched plane 6 at first place and then goes for planes 5 to 1. The tracer concentration for all planes reached equal value of 1 at 95.92 s.

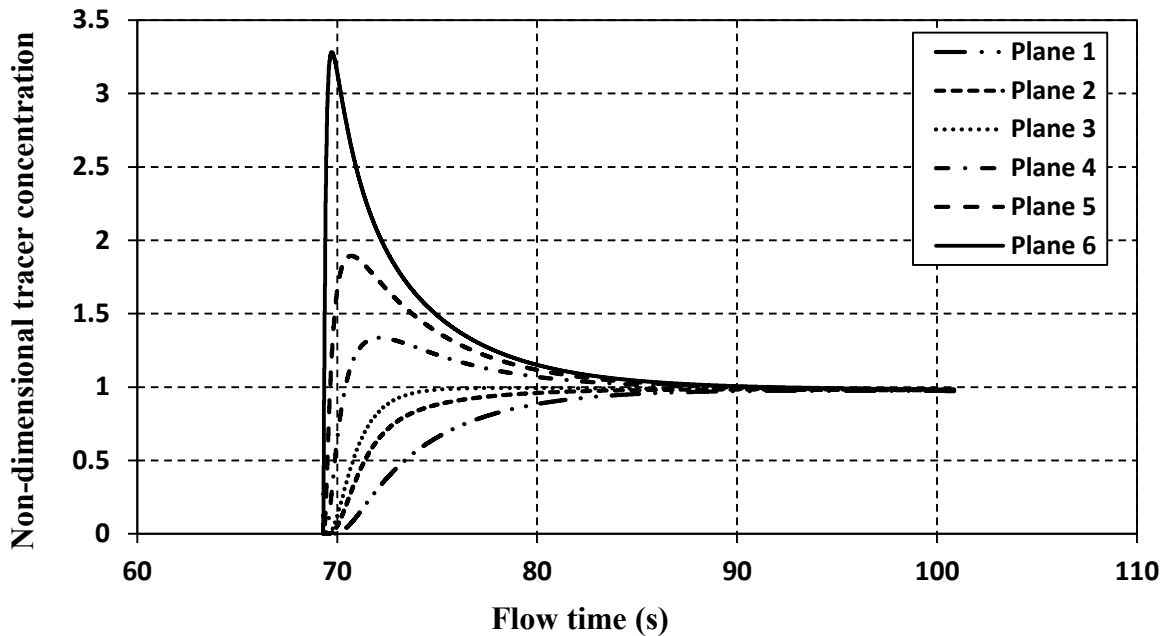


Figure 3.3: The diagram of non-dimensional tracer concentration as a function of time for activated sludge aerated at superficial gas velocity of 0.163 cm/s, while tracer was added at Injection Point (4).

ANSYS/Fluent package (version 17.1) was applied to simulate this model and solve transport equations for unsteady-state condition which all equations were integrated using control volume method. The phase coupled SIMPLE algorithm was used to solve velocity-pressure coupling. For calculating the face fluxes in the momentum and phase transport equations, the first-order upwind discretization scheme was employed. In order to simulate the flow of the gas phase, the velocity-inlet boundary condition was used for the sparger holes and the boundary condition of the pressure-outlet was used for the outlet of the vessel at top of the column. Moreover, the cylinder and sparger body was simulated by wall boundary condition. The initial value of all velocity components of the model was set to zero that means bubble column initially was at rest. The range of superficial gas velocity during simulation was 0.081 to 1.303cm/s. All of the equations during simulation process were solved simultaneously in unsteady state mode with two step sizes of 0.001, 0.01s. In

order to choose the appropriate time step, the value of liquid axial velocity was monitored at planes 3 and 6 for both cases. The simulations with time steps of 0.01 and 0.001s provided same trends of liquid axial velocity at steady-state mode. Therefore, the case with time step of 0.01s was selected because of the lower calculation process time. By monitoring the residuals for all aforementioned equations, the convergence of calculations was checked. Simulations were considered converged when the scaled residuals dropped below 10^{-5} . The simulations were carried out using Supercomputing facilities of HPCVL (High Performance Computing Virtual Laboratory). Each simulation was run in parallel with 24 dual cores Dell PowerEdge R410 Server with 2 sockets with a 6-core Intel® Xeon® processor (Intel x5675) running at 3.1 GHz. In this method of calculations, the grid was partitioned to 24 parts and one CPU was used to calculate for each partition. The convergence for each unsteady state model was achieved after about 72 hours.

3.3 Results and Discussion

3.3.1 Typical Star Shape

The effects of the superficial gas velocity, the location of tracer injection, and sparger's type on the mixing time and both phase's velocity profile have been investigated through CFD modeling and simulation. In order to validate the CFD model, the volume fraction of secondary phase (air) and mixing time for different gas superficial velocities were compared with the experimental data reported by Babaei et al. (2015). **Figures 3.4 (a) and (b)** show that the comparisons between experimental data and 3D CFD predictions for the mixing time and overall gas holdup, respectively showed good agreement with the maximum deviation of 5.5%. Moreover, **Figure 3.5** illustrated the good agreement among the CFD contour plots of gas holdup distribution and electrical conductivity tomograms at horizontal planes 3 and 6. As can be seen, the width of the predicted

bubble distribution for both figures are nearly the same and also the bubbles stray from the center of the column to the same radial direction.

Mixing time is a key factor to determine the effectiveness of a mixing process. One of the important parameters affecting mixing time in bubble column is the superficial gas velocity. **Figure 3.6** shows the mixing times for five different superficial gas velocities, i.e. $v_{s,gas} = 0.081, 0.163, 0.326, 0.652, 0.814, \text{ and } 1.14 \text{ cm/s}$. As can be seen in this figure, regardless of injection's location, the mixing time decreased by increasing the superficial gas velocity and was proportional to $12.117v_{s,gas}^{-0.426}$ until it reached almost a plateau. This figure also demonstrates that the location of tracer injection has considerable effect on the mixing time at the equal superficial gas velocity.

Figure 3.6 illustrates that injection point (2) (middle of the tank) for injection of tracer was the most effective location in reducing the mixing time regardless of the superficial gas velocity. In compared to injection points (2) and (3), injection point (1) located on the liquid surface was the second most effective release position in terms of mixing time in spite of its farthest distance from the gas sparger located at the bottom of the tank. However longest mixing times were achieved when the tracer was released from injection point (4). The injection point (4) was located at the bottom of the vessel in the corner at the path of downward flow in the circulation loop. In fact, the liquid circulations of bubble column is due to the radial velocity profile of the gas holdup, where the radial gas holdup and liquid velocity profile are linked up together (Wu and Al-Dahhan, 2001).

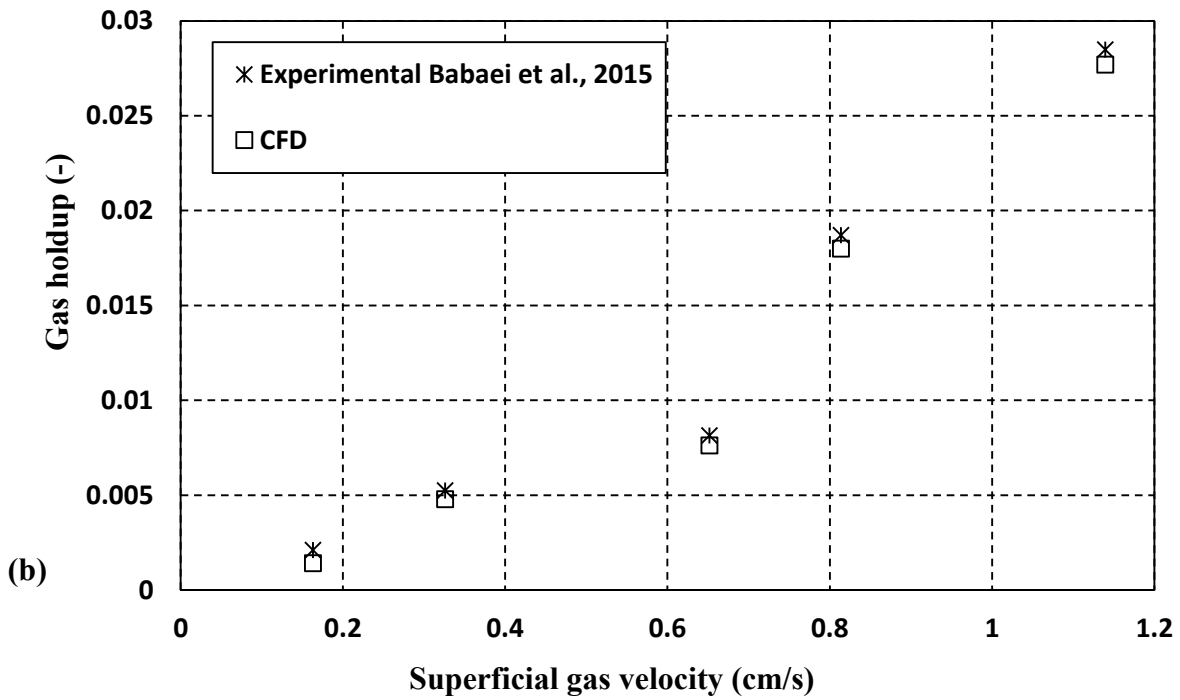
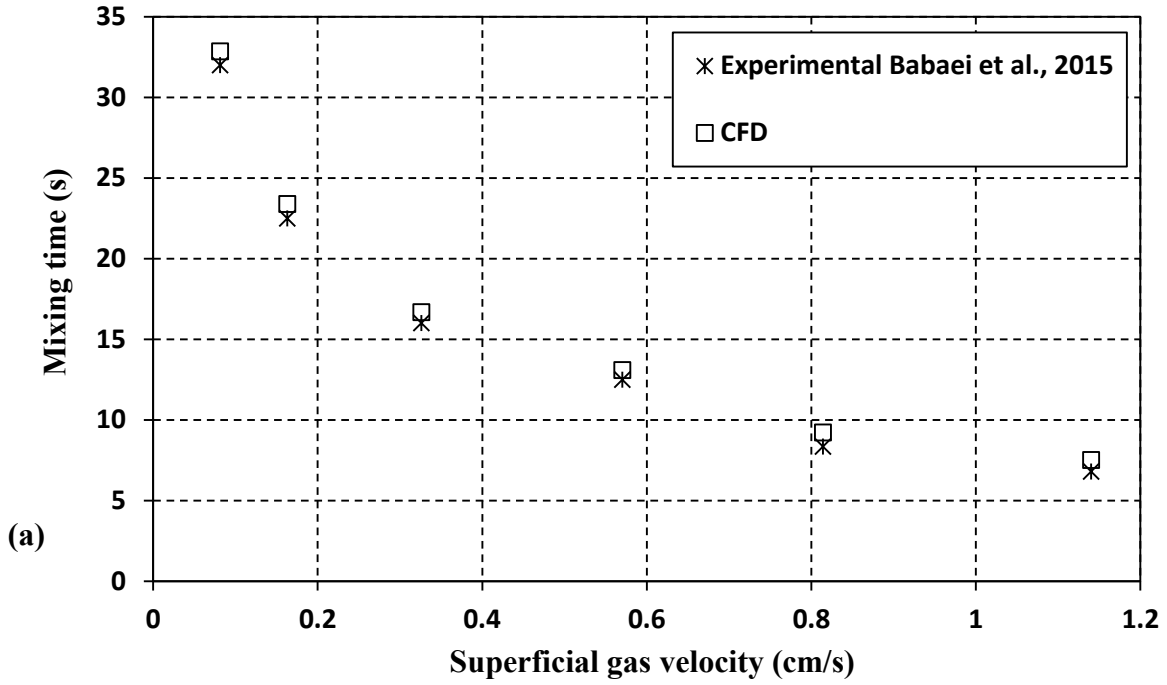


Figure 3.4: Mixing time as function of superficial gas velocity (cm/s) and tracer injection locations for star shape sparger.

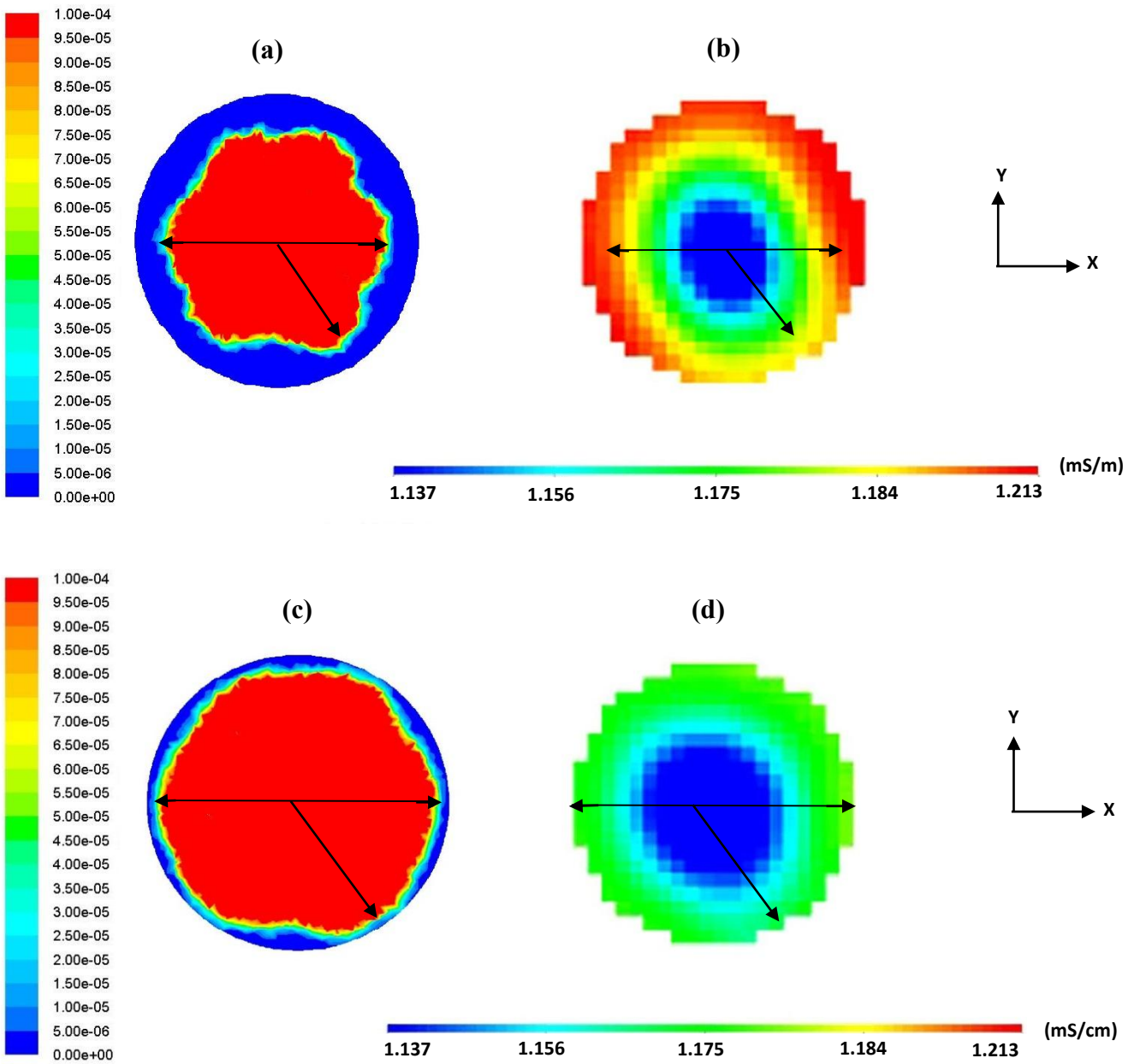


Figure 3.5: The comparison between CFD contour plots based on gas holdup and ERT tomograms based on conductivity (mS/cm) for: **(a)** the CFD contour plot of gas holdup distribution at plane 6, **(b)** the ERT tomogram of conductivity at plane 6, **(c)** the CFD contour plot of gas holdup distribution at plane 3, and **(d)** the ERT tomogram of conductivity at plane 3.

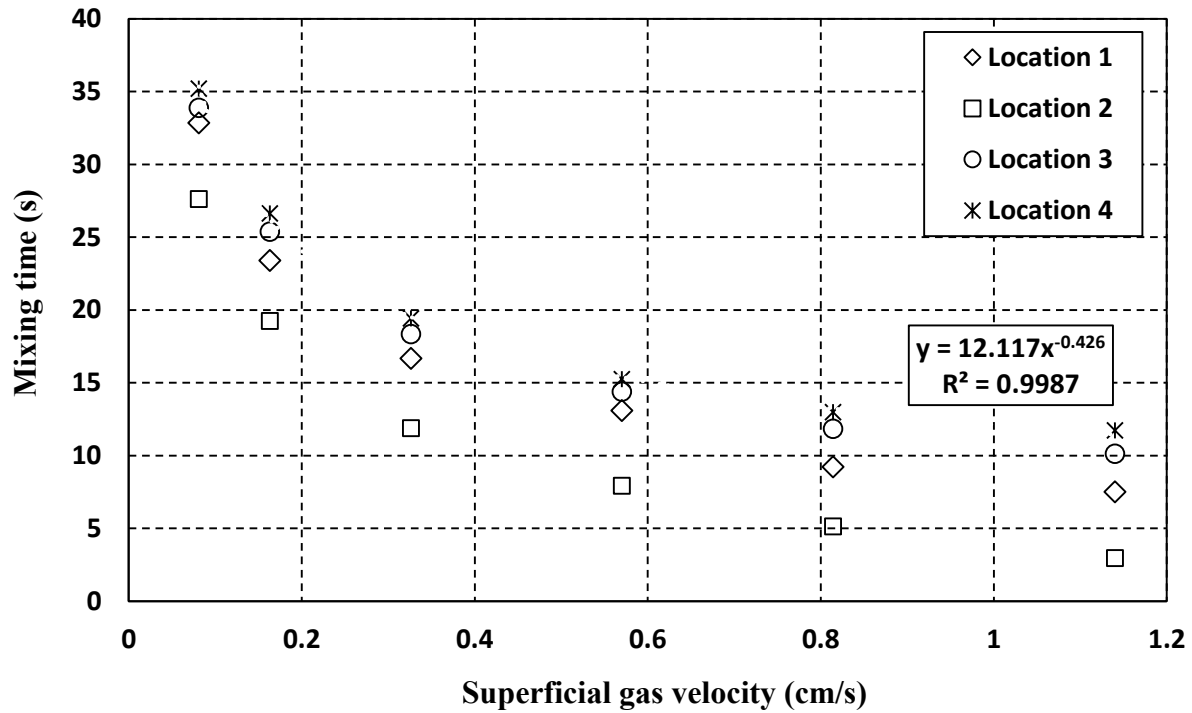
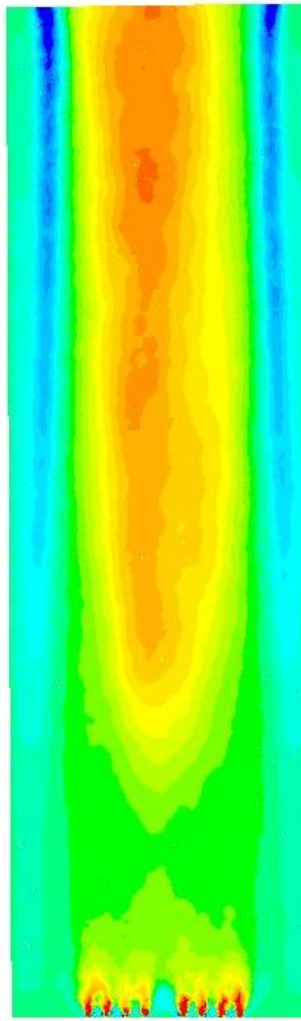
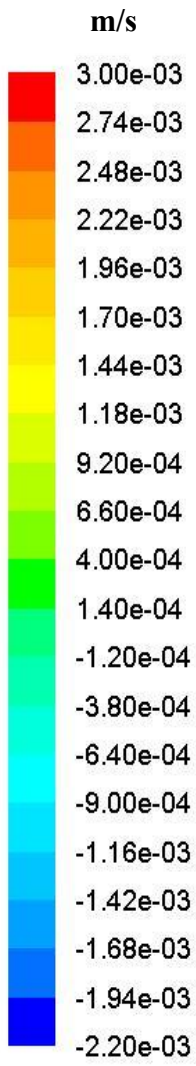


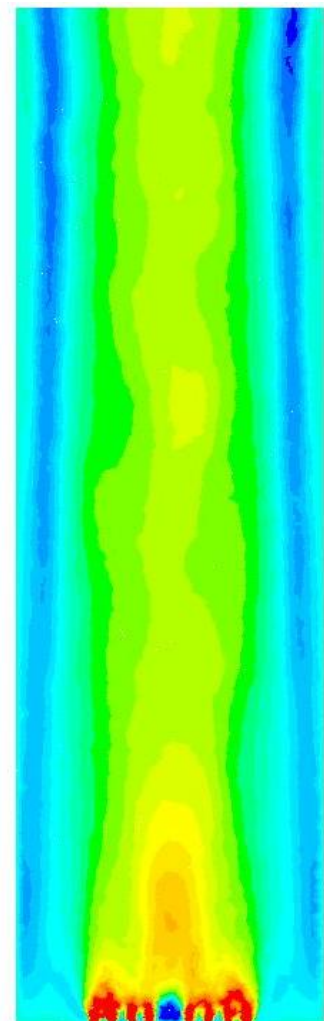
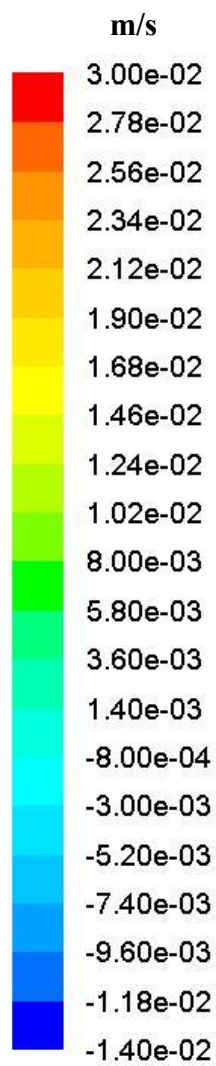
Figure 3.6: Mixing time as function of superficial gas velocity (cm/s) and tracer injection locations for star shape sparger.

Figure 3.7 shows contour plots of liquid velocity flow field on a vertical cross-section plane at the middle of the column. As can be seen in this figure there is a dominant upward flow field in the middle of the column which is surrounded by the downward (negative velocity) flow close to the column wall. These contours confirm the presence of a circulation flow inside column due to the air flow. Similar results have been reported by Borchers et al. (1999) for a rectangular bubble column with a frit sparger at the bottom of the column. As expected by increasing the superficial gas velocity, the upward-downward motion within the column was enhanced. In fact the superficial gas velocity had a significant effect on the liquid flow field and consequently on the air-sludge mixing performance.

In order to analyze the behavior of the axial-flow circulation pattern, **Figure 3.8** shows the velocity vector plots in the vertical cross-section planes. It can be seen that the sparger discharged the fluid upward and the fluid flow then returned towards the sparger through recirculation loop. Therefore the axial circulation loops consists of two parts, i.e. upward and downward flow. This Figure shows that as the superficial gas velocity increased the main upward liquid flow enhanced while the small eddies decreased. Therefore the downward flow was a little thinner when the superficial gas velocities were decreased and amount of small eddies were increased. The above-mentioned behavior observed in this figure was due to this fact that by increasing the velocity of gas the larger upward force was generated to overcome the downward force (i.e. drag force and gravity) and fluid apparent viscosity in the column as reported by Chakraborty et al. (2009). On the other hand sparger created higher shear in the middle of the column in compared with region close to the column wall. As mentioned earlier in this paper activated sludge showed shear thinning rheological behaviour, therefore the apparent viscosity in middle and lower heights of the tank was less than close to the wall and higher axial positions.

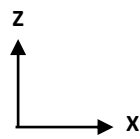


(a)



(b)

Continued...



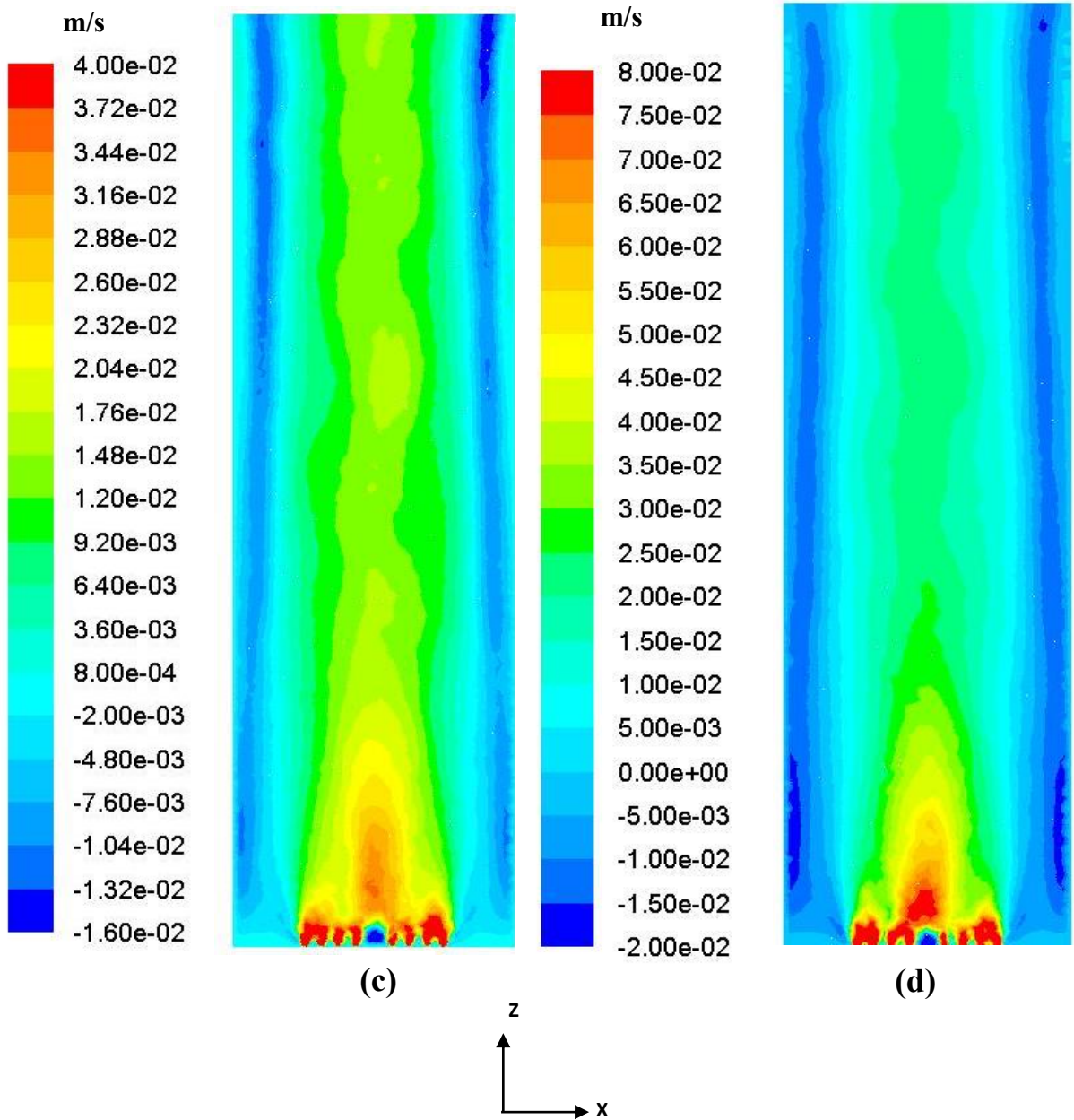
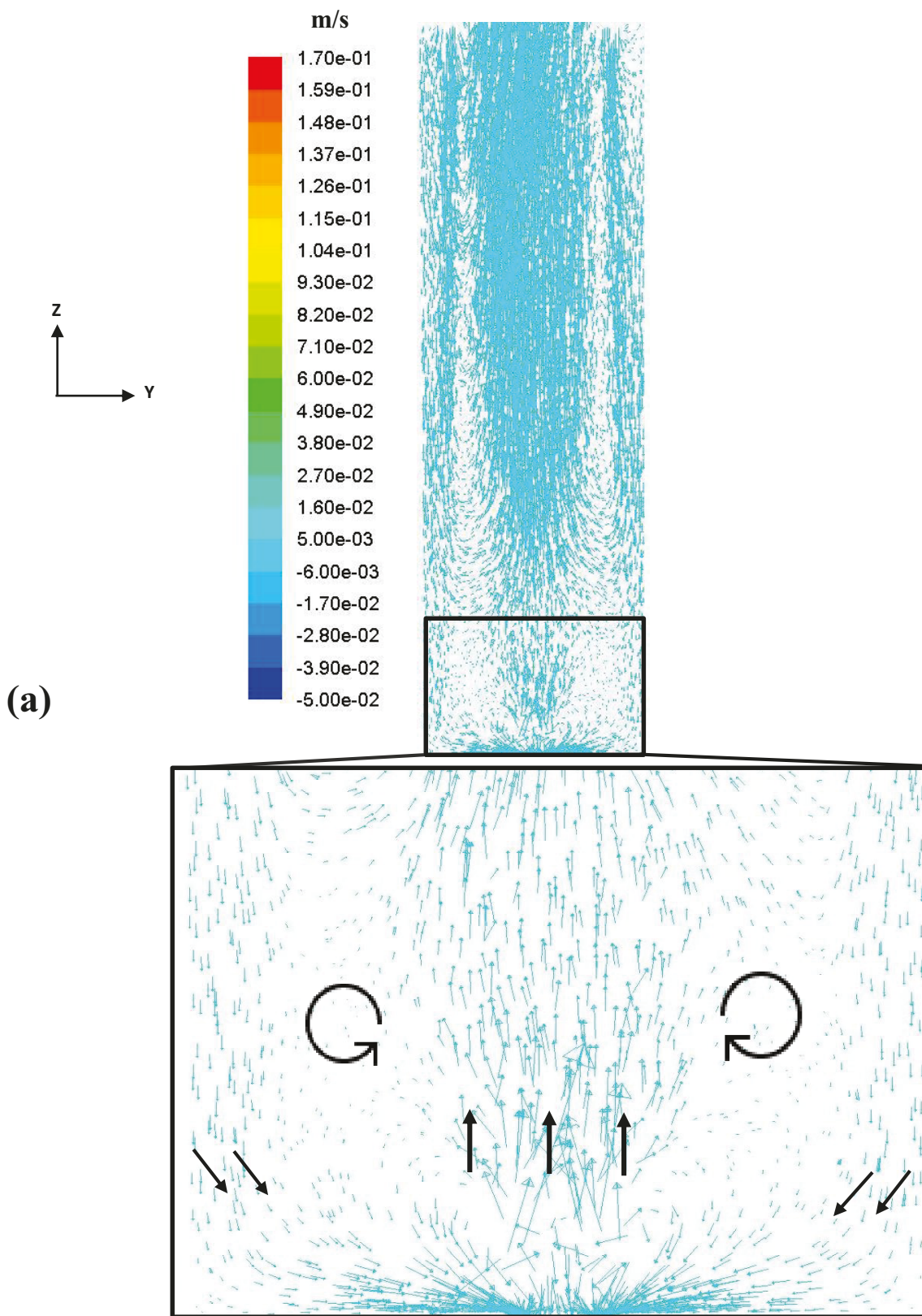


Figure 3.7: Liquid velocity (m/s) contour plots for star shape gas sparger at XZ vertical plane for superficial gas velocities of: **(a)** 0.163 cm/s, **(b)** 0.326 cm/s, **(c)** 0.814 cm/s, and **(d)** 1.14 cm/s.



Continued...

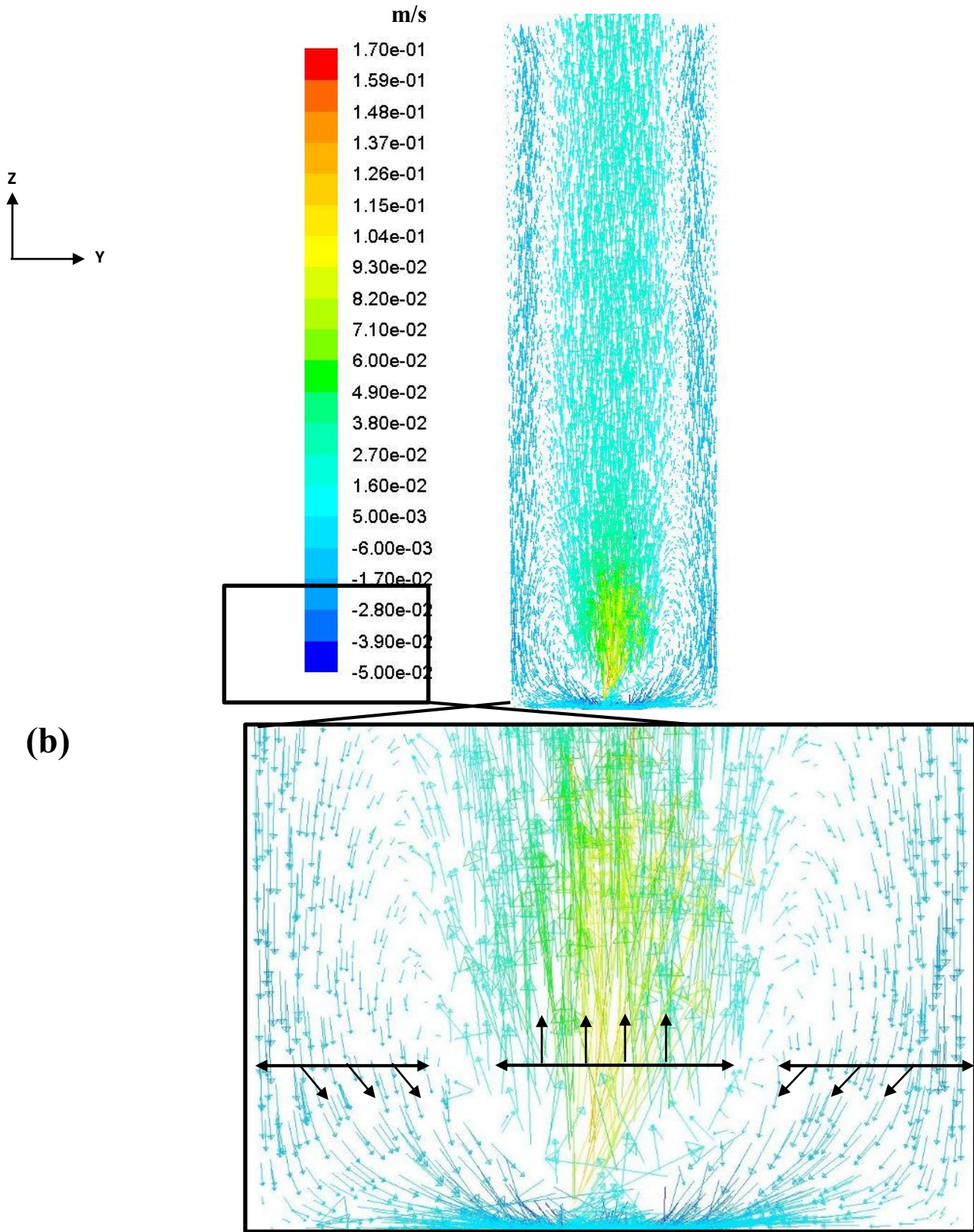
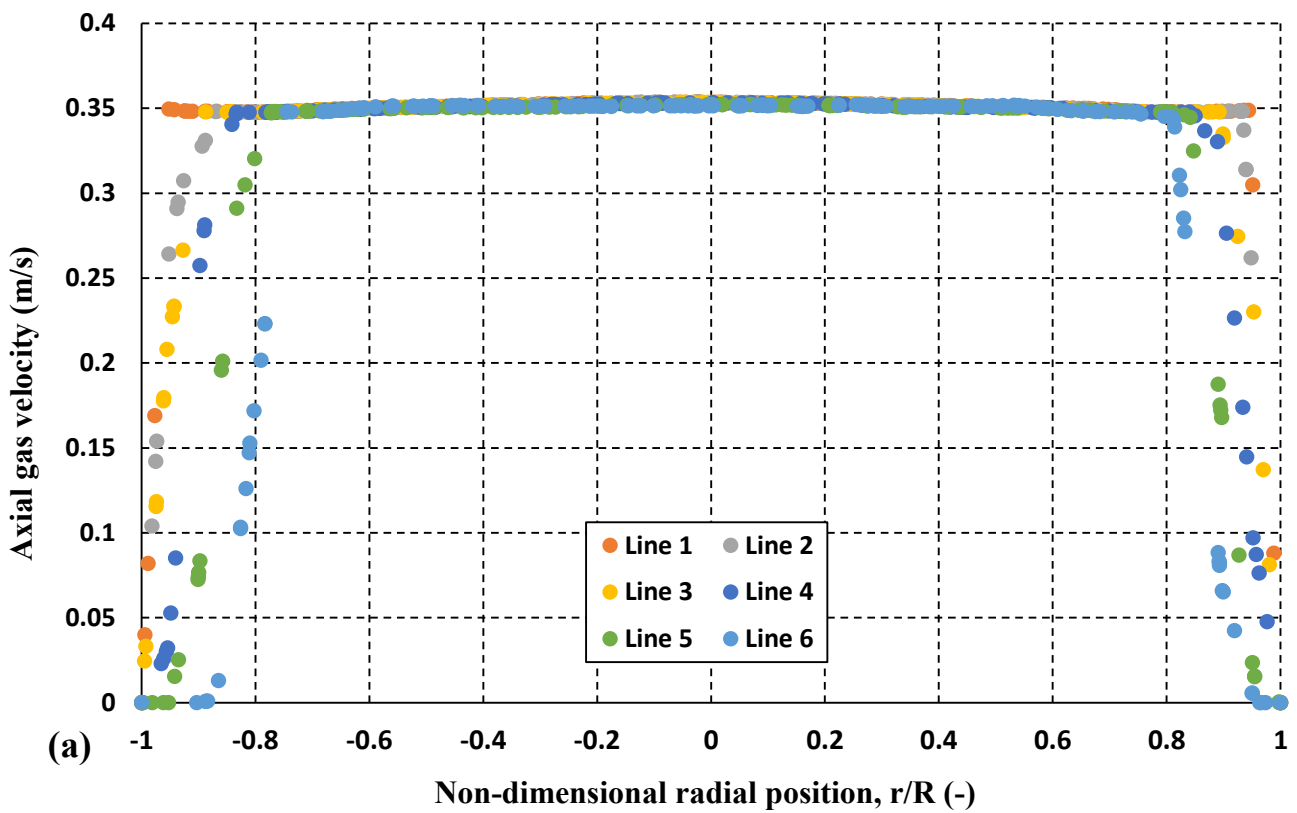


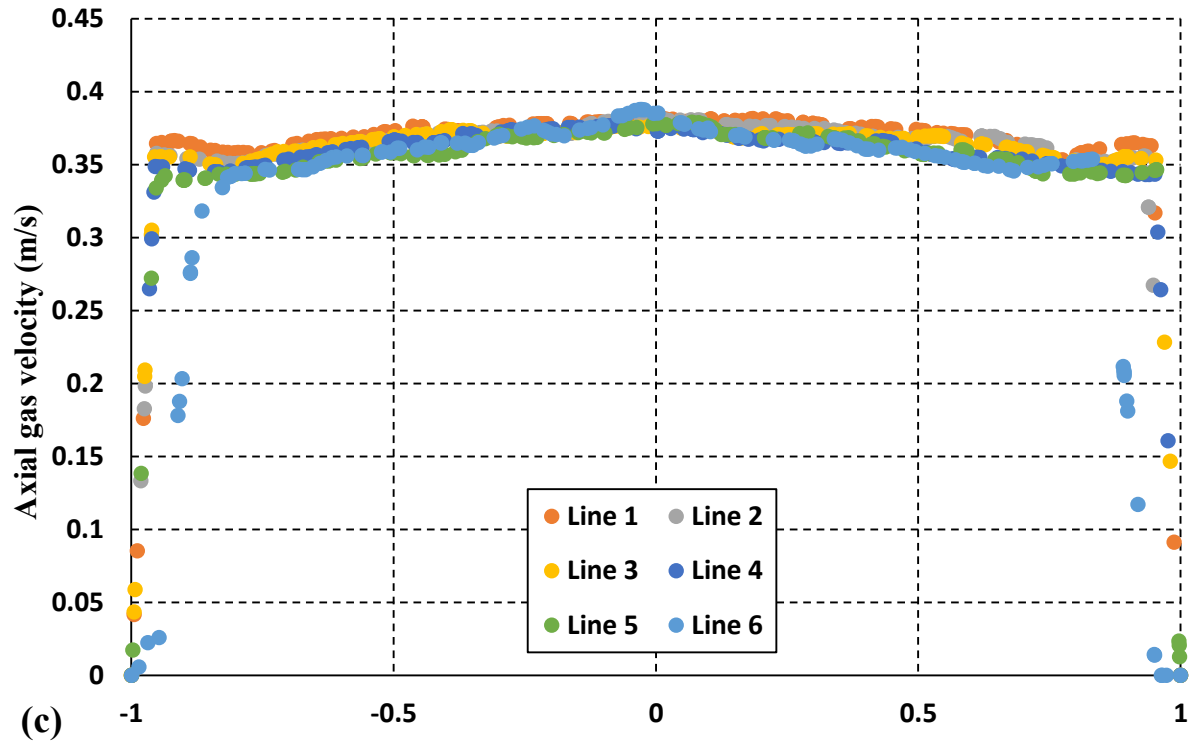
Figure 3.8: Liquid velocity (m/s) vector plots for star shape gas sparger at YZ vertical plane for superficial gas velocity of (a) 0.163 (cm/s), and (b) 1.14 cm/s.

In order to analyze the performance of the sparger, **Figure 3.9** presents the axial air velocity distribution on the radial position in middle of the tank in different vertical distances when superficial gas velocities varied between 0.163 to 1.14 cm/s. The character of the axial air velocity distribution was similar for both cases in this way that as distance from sparger increased the axial air velocity rapidly increased attaining its maximum positive value (terminal velocity), indicating upward flow in the middle of the column and then started to decrease to zero as it reached the column wall. The positive value of the axial air velocity indicates the existence of upward flow upstream in the middle of the tank.



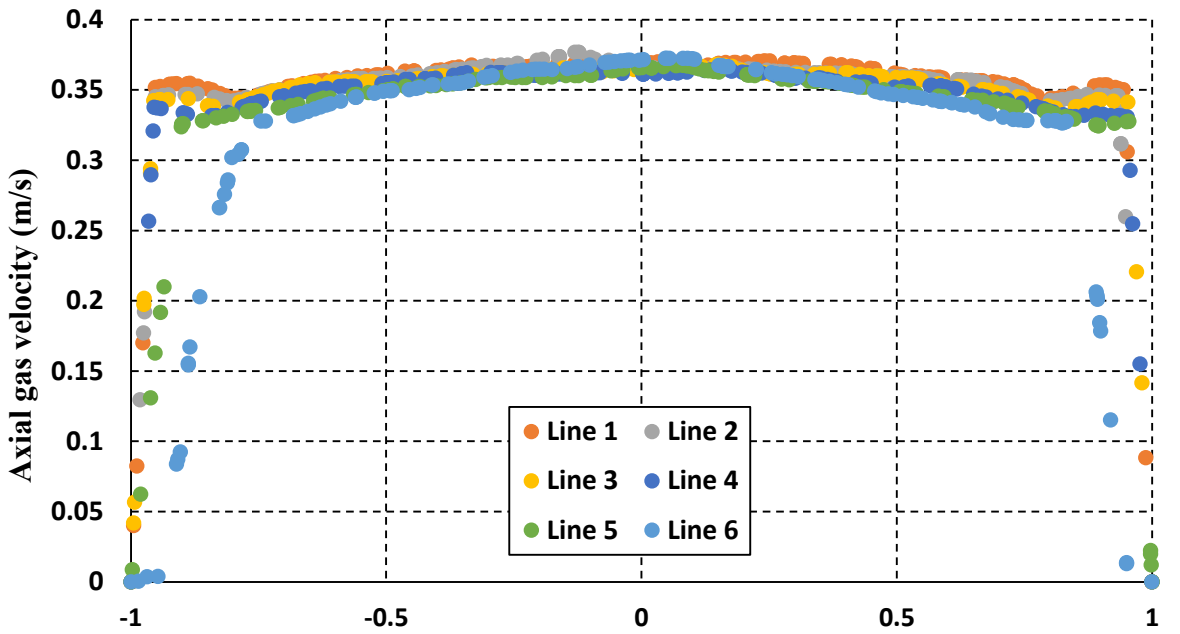
Continued

(b)



(c)

Non-dimensional radial position, r/R (-)



(c)

Non-dimensional radial position, r/R (-)

Continued

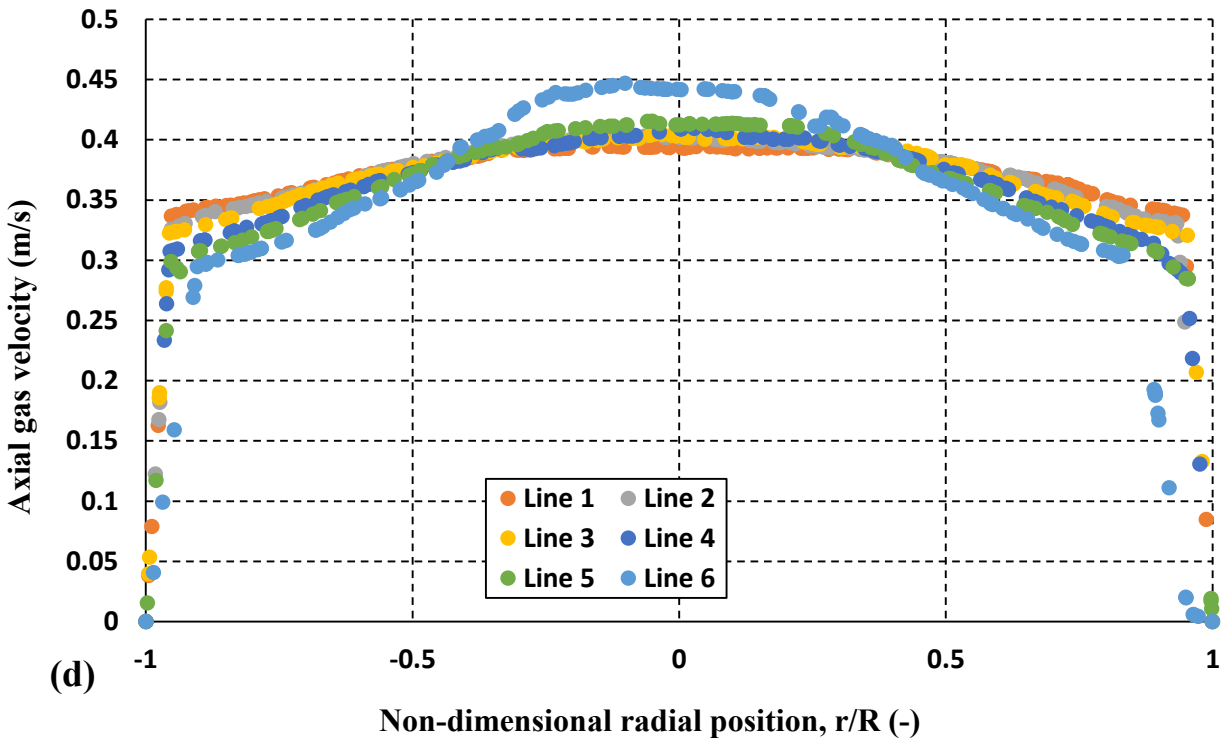


Figure 3.9: The radial distribution of air axial velocity (m/s) for star shape gas sparger superficial gas velocity of (a) 0.163, (b) 0.326, (c) 0.814, and (d) 1.14 cm/s.

Figure 3.10 shows contour plots of axial air velocity and schematic front views of air flow structures. As can be seen in this figure, the spreading angle increased 8 to 18 degree as the air velocity increased and consequently the air/activated sludge's contacts were enhanced. Therefore, by increasing the superficial gas velocity from 0.163 to 1.14 cm/s, the axial position of the column where the column cross section fully fill with the air bubbles were decreased from 0.366 to 0.143 from the bottom of the vessel.

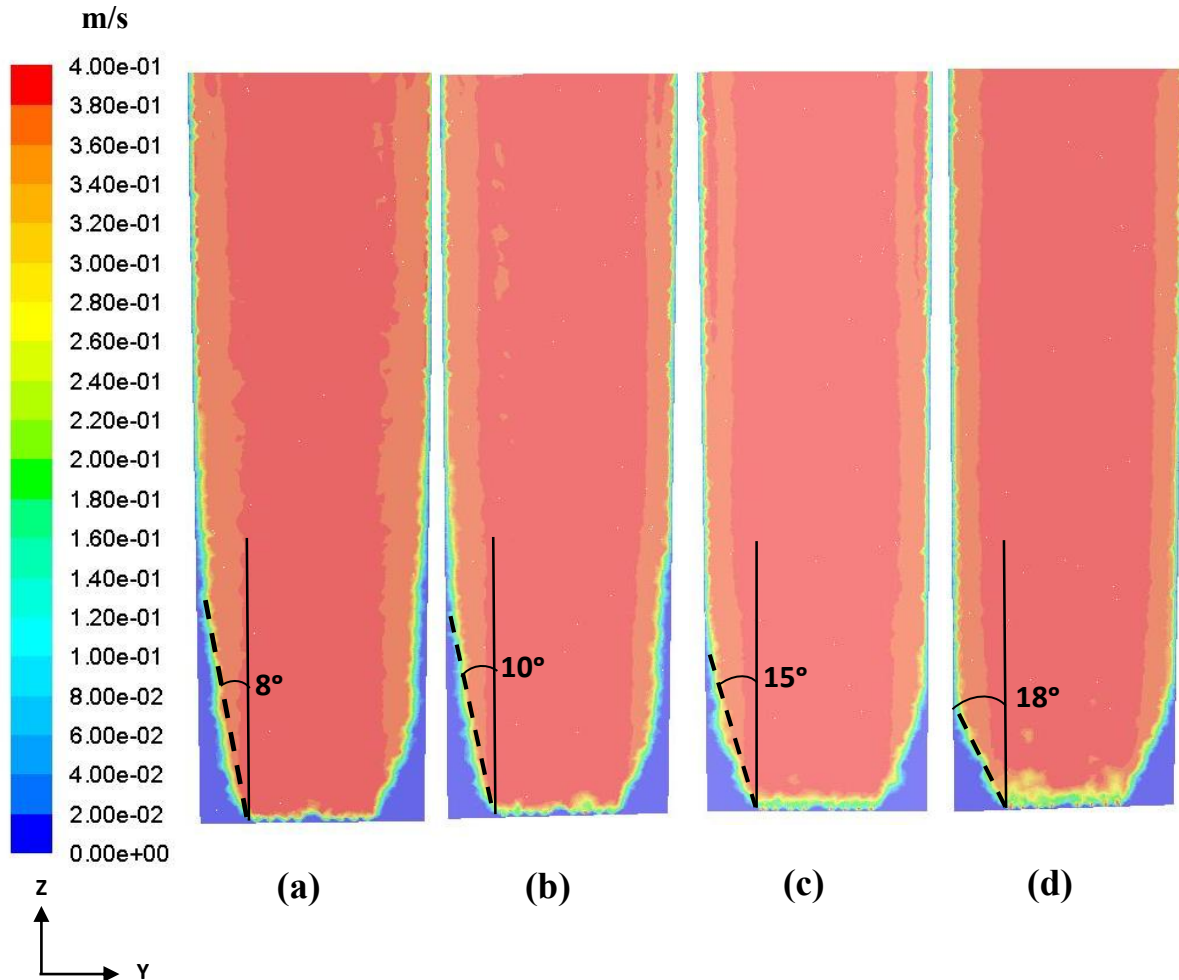


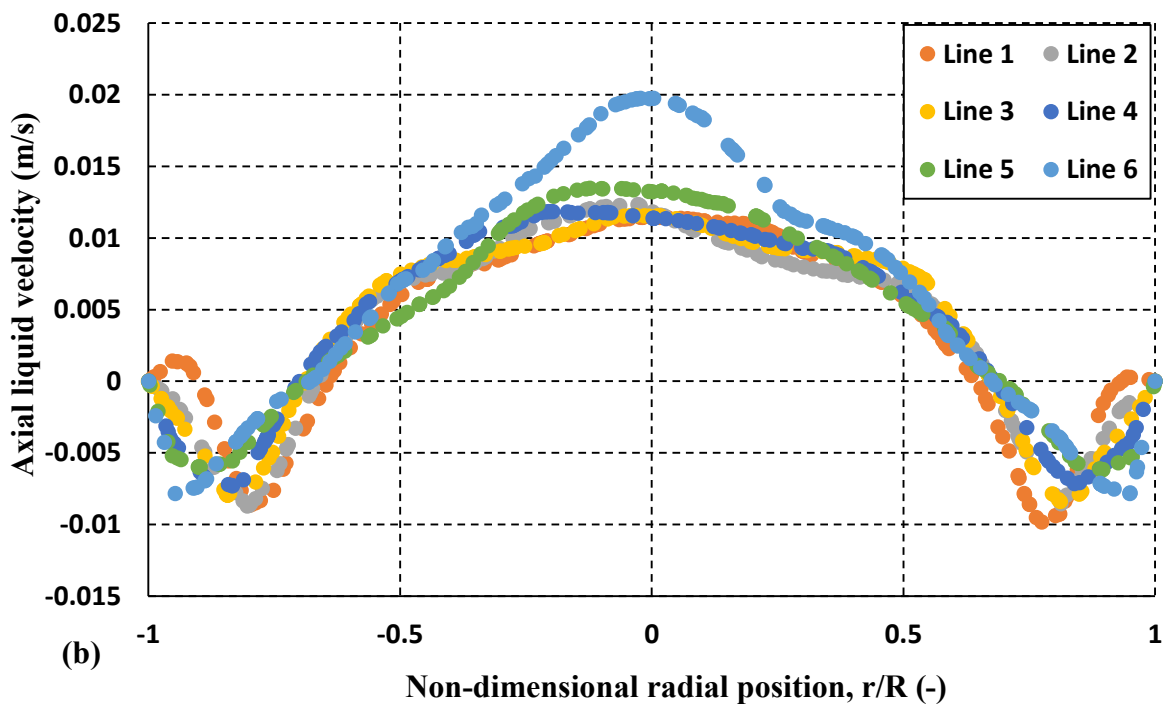
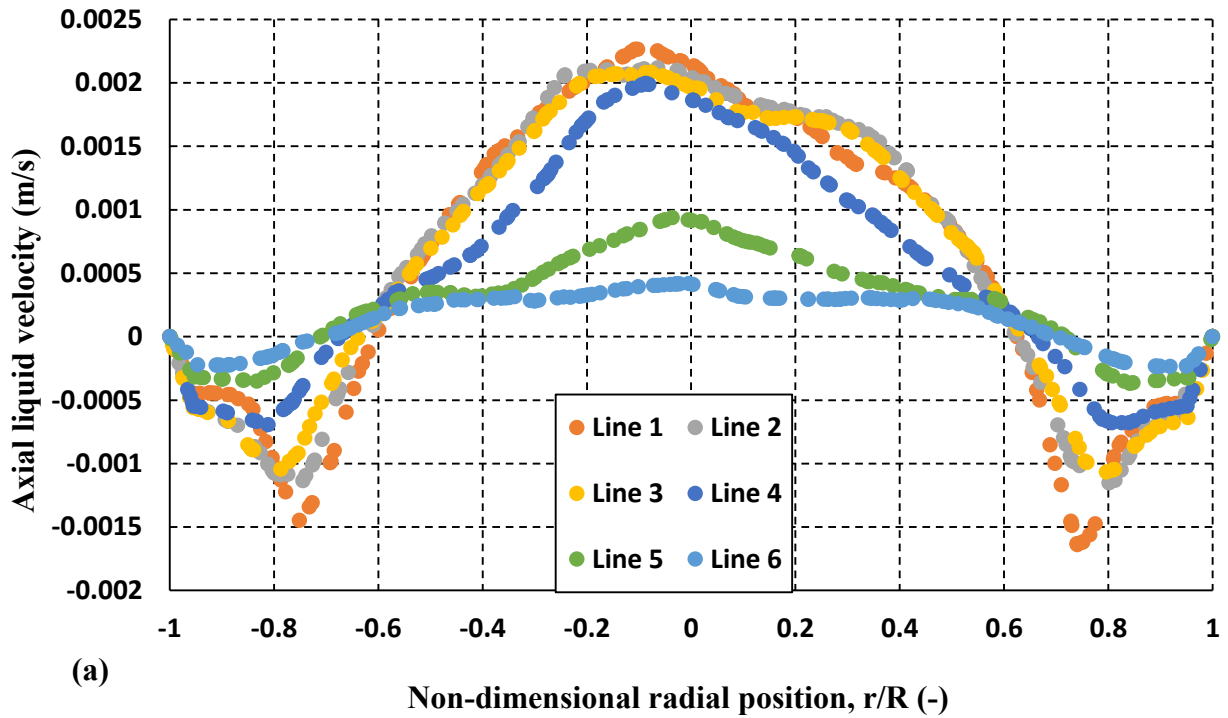
Figure 3.10: The contour plots of distribution of axial gas velocity (m/s) at vertical XZ plane for superficial gas velocity of: **(a)** 0.163 cm/s, **(b)** 0.326 cm/s, **(c)** 0.814 cm/s, and **(d)** 1.14 cm/s.

Figure 3.11 shows the axial liquid (activated sludge) velocity distribution on the radial position in middle of the tank for six axial positions from $z/H=0.143$ to $z/H=0.713$ when superficial gas velocities varied between 0.163 to 1.14 cm/s. As **Figure 3.11** represented, the axial velocity distribution of the liquid phase at the middle of tank was upward same as axial air velocity observed in **Figure 3.9** while it was downward with the lower magnitude close the column's wall. This confirms again the circulation pattern in liquid phase as mentioned earlier which is in line with the results of several literatures for liquid flow pattern (Li et al., 2016; Pflieger and Becker, 2001; Borchers et al., 1999; Pflieger et al., 1999). However an equal trend was not identified in all

cases indicating the importance of the effect of the superficial gas velocity on the bubble column performance. **Figure 3.11 (a)** shows that the liquid velocity goes towards its maximum in middle of the tank which was reduced for plane closer to the sparger. However such different trend can be observed in **Figures 3.11 (b), (c), and (d)** where the superficial gas velocity set as 0.326cm/s, 0.814, and 1.14 cm/s, respectively. These figures show the axial liquid velocity reached maximum positive value in middle of tank through axial position. However, the maximum value reduced as the axial position increased. This phenomena illustrated that the gas holdup in case of 0.163 cm/s is lower than others which could not produce enough shear rate to decrease the apparent viscosity same as other cases.

Figure 3.11 also shows the effect of superficial gas velocity on the flow pattern of liquid phase. As observed in **Figures 3.8**, there is an axial circulation loop with upward flow in the middle of the tank surrounded with downward flow near the column wall. The value of downward flow for gas superficial velocity of 0.163 to 1.14 cm/s was varied from 0.0015 to 0.02 m/s, respectively. As can be seen in this figure, by increasing the distance from sparger (i.e. Line 6 to Line 1 as shown in **Figure 3.11**), the liquid phase velocity decreased. However in the downward liquid flow, different trend can be observed. For superficial gas velocity of 0.163 cm/s, “Line 1” showed the maximum downward liquid velocity then it decreased gradually to Line 6. On the other hand, the liquid velocity distribution for 0.326, 0.814, and 1.14 cm/s was different, “Line 1” presented the minimum downward velocity and increased to Lines 6. The reason of this behavior could be due to this fact that for the lower gas velocities, there is a lower gas holdup leading to a greater upward force (shear rate) which is concentrated at the middle of the column at the introduction point of gas to liquid and then spreads towards radial position and consequently the upward velocity of

liquid is decreased. Therefore by increasing the superficial gas velocity, the downward velocity at top of the column decreases.



Continued ...

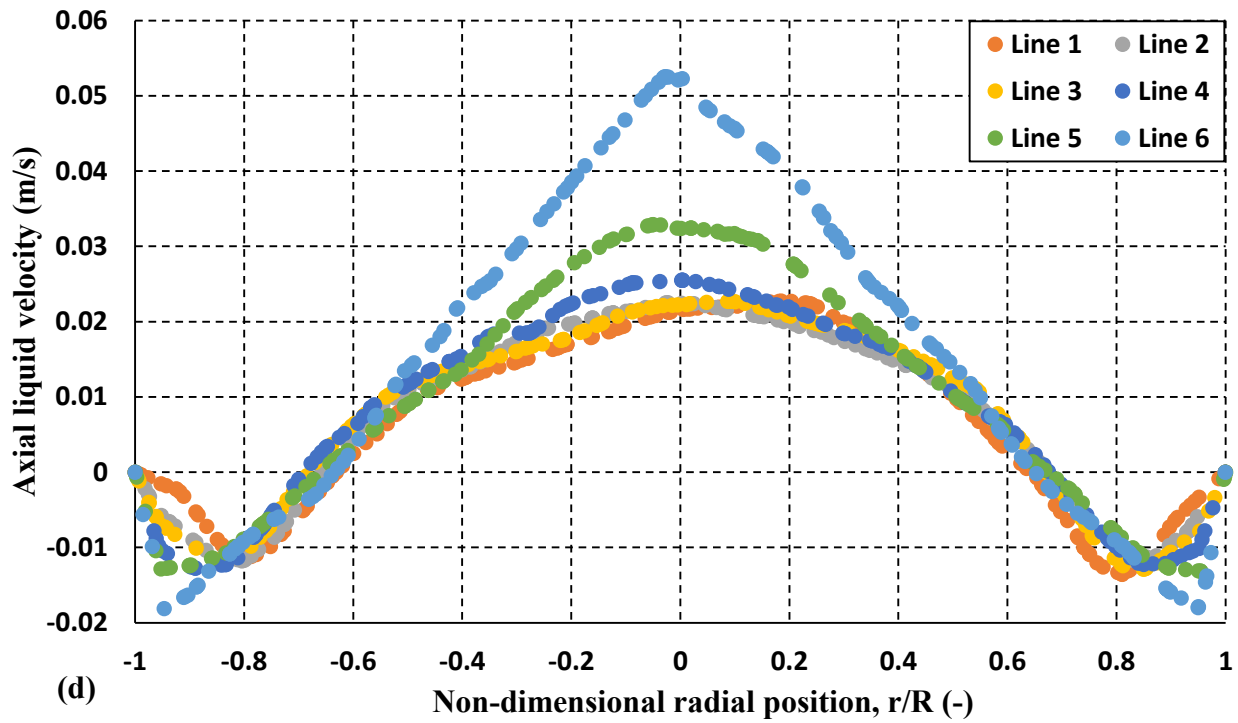
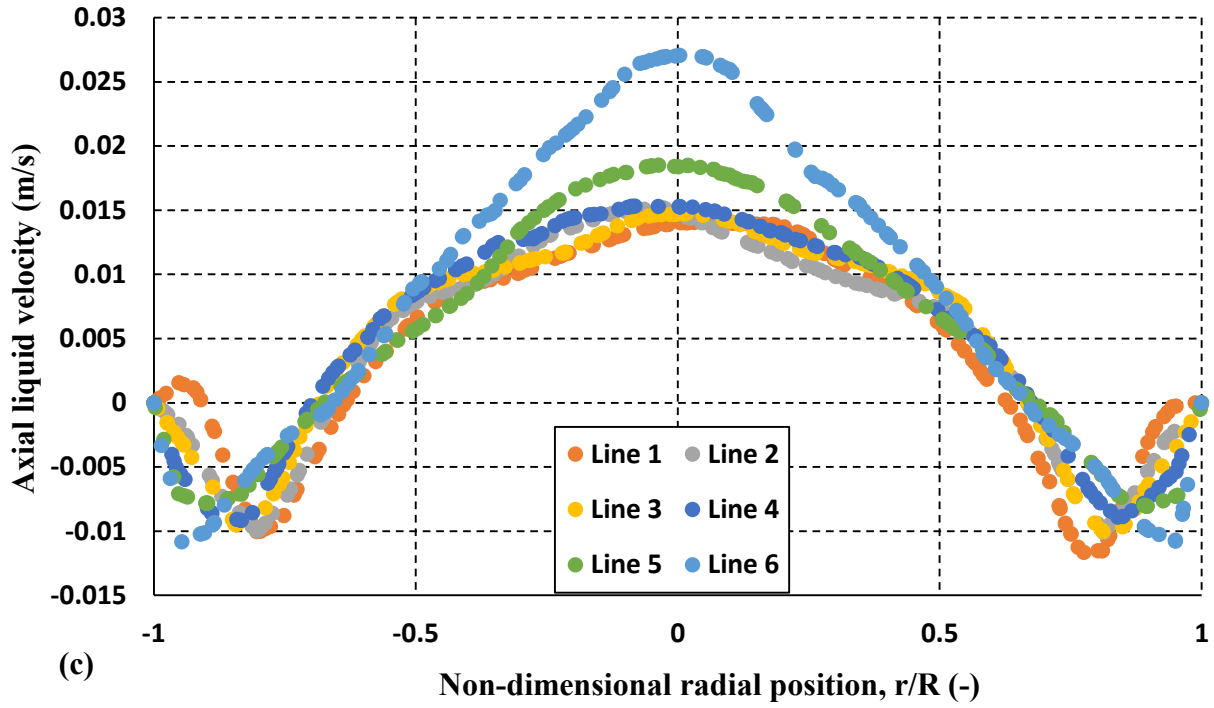
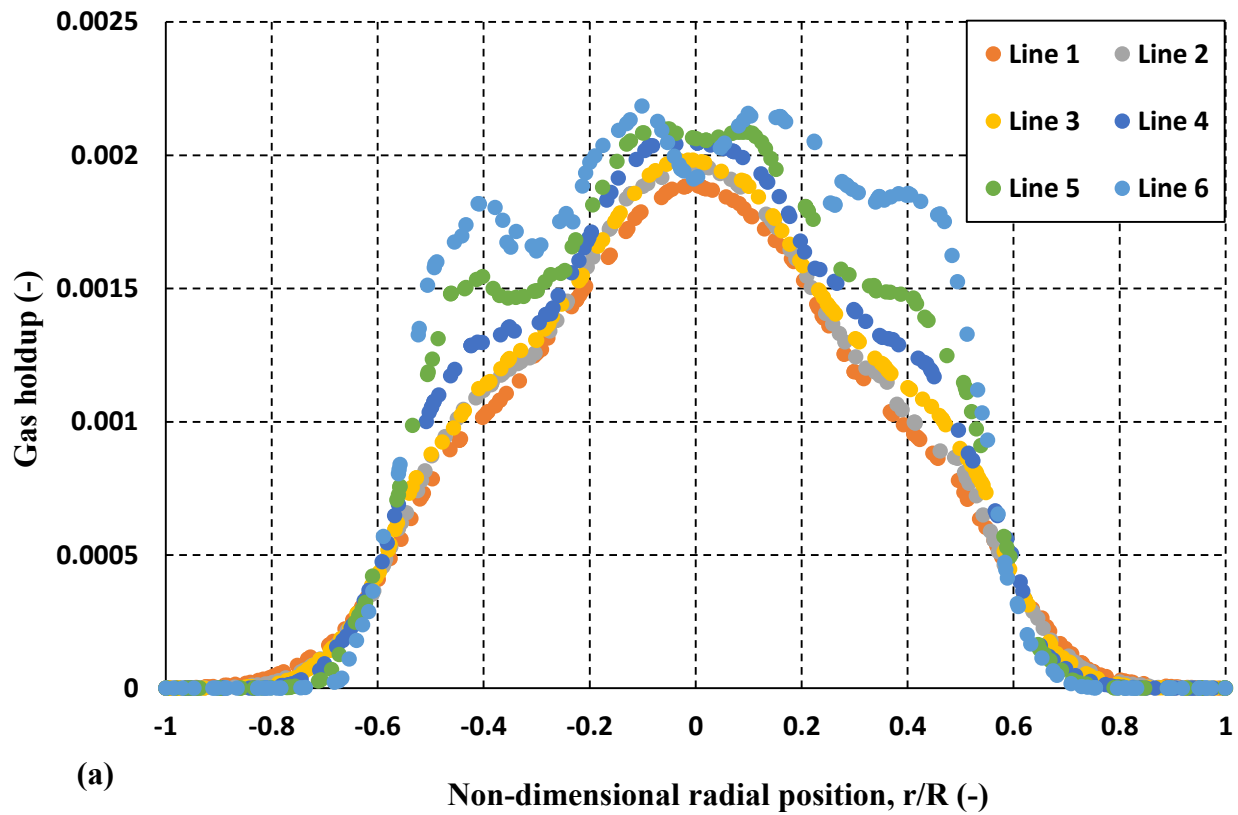
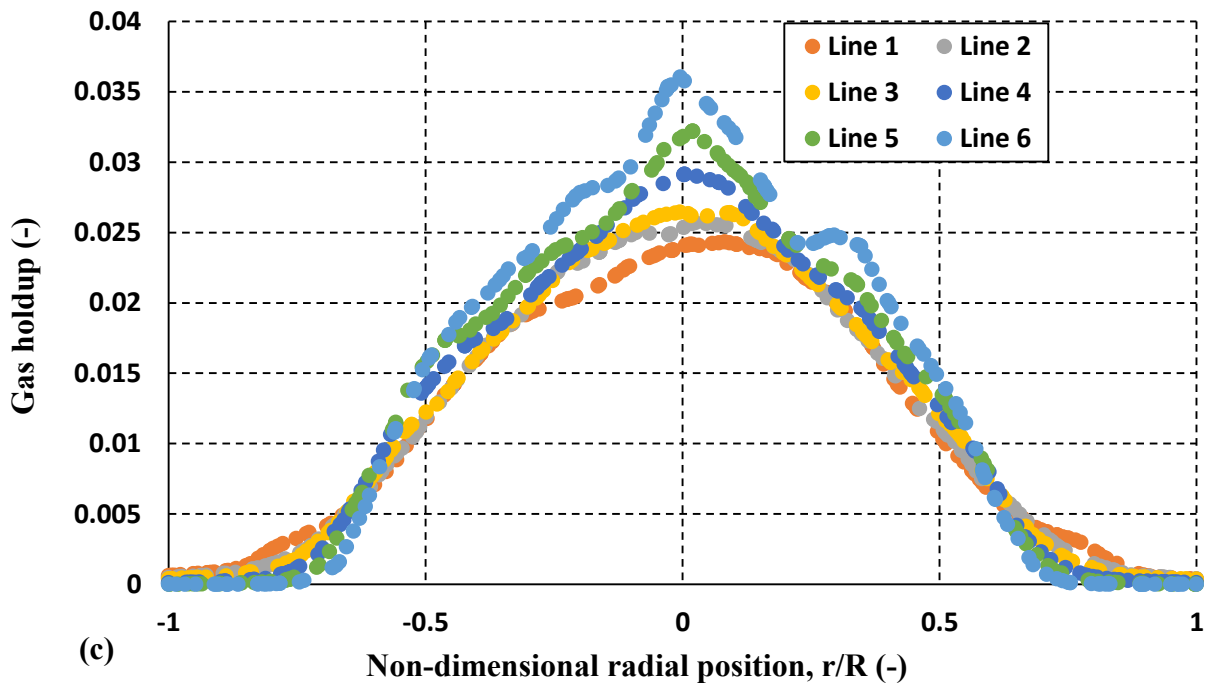
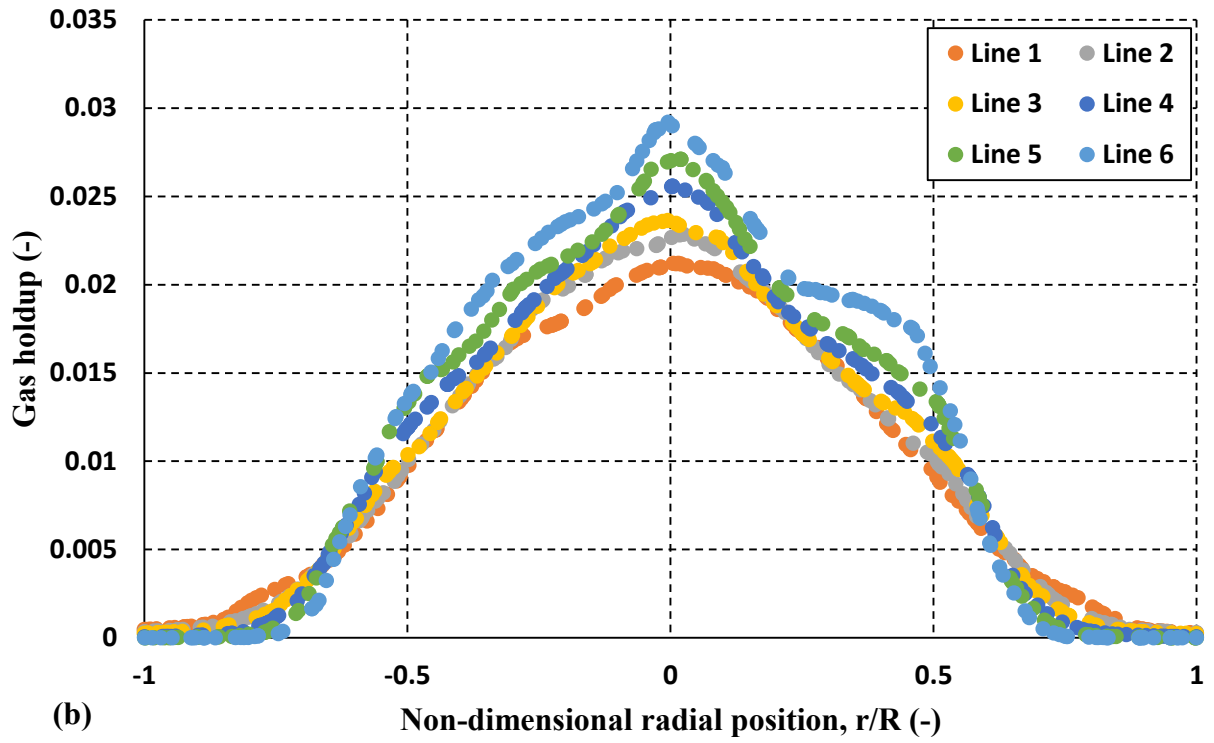


Figure 3.11: The radial distribution of the axial velocity (m/s) of the activated sludge for superficial gas velocity of (a) 0.163 cm/s, (b) 0.326 cm/s, (c) 0.814 cm/s, and (d) 1.14 cm/s.

Figure 3.12 shows the time average gas holdup of air in steady state mode at Lines 1 to 6. As can be observed in this figure, the air bubbles through the column was not distributed homogenously and the much volume of the bubble was concentrated at the middle of column and only a few amount of air bubbles spread in near wall area where liquid phase flew downward. Li et al. (2016) found the same gas holdup profiles which bubbles are concentrated at the middle of the column for 8 different air distributors. The superficial gas velocity is directly affected the gas holdup where by increasing the superficial gas velocity the value of gas holdup was increased and the bubbles spread wider in radial direction.



Continued ...



Continued ...

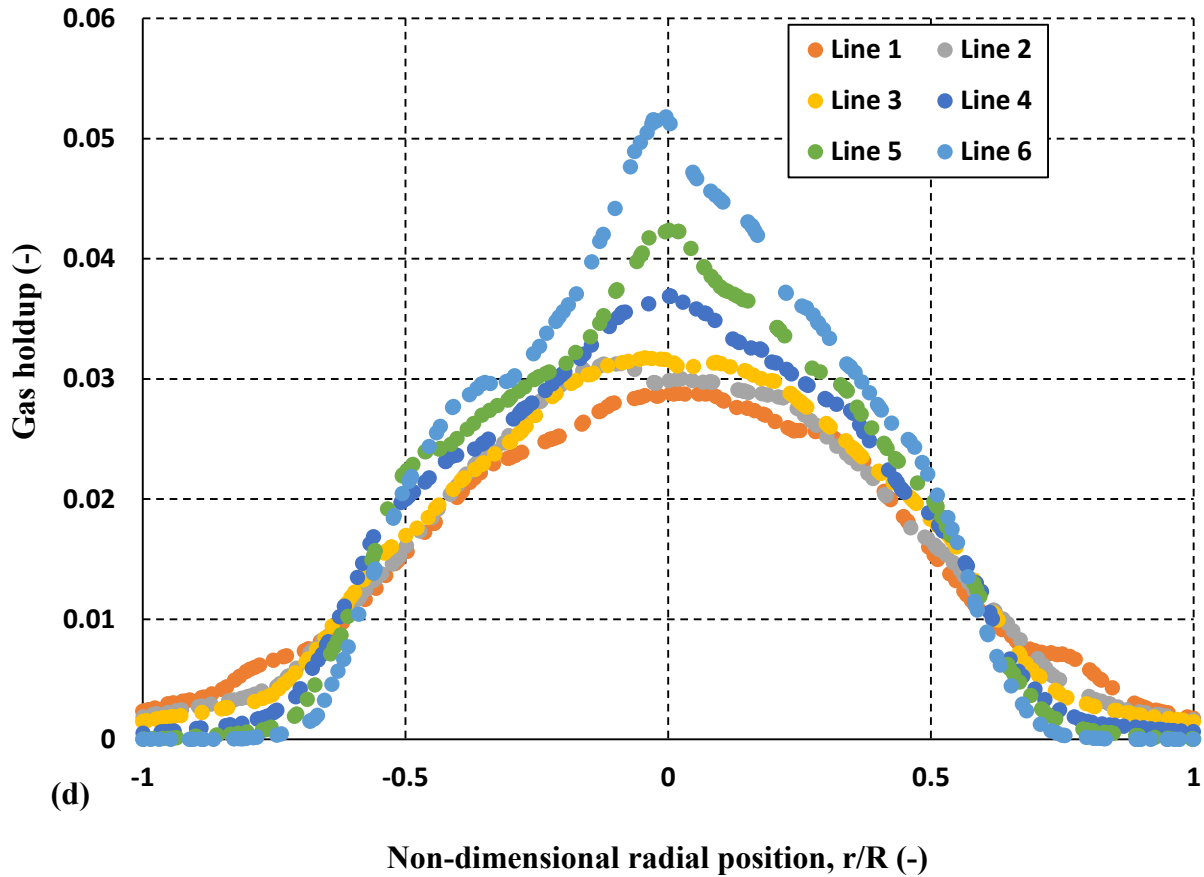
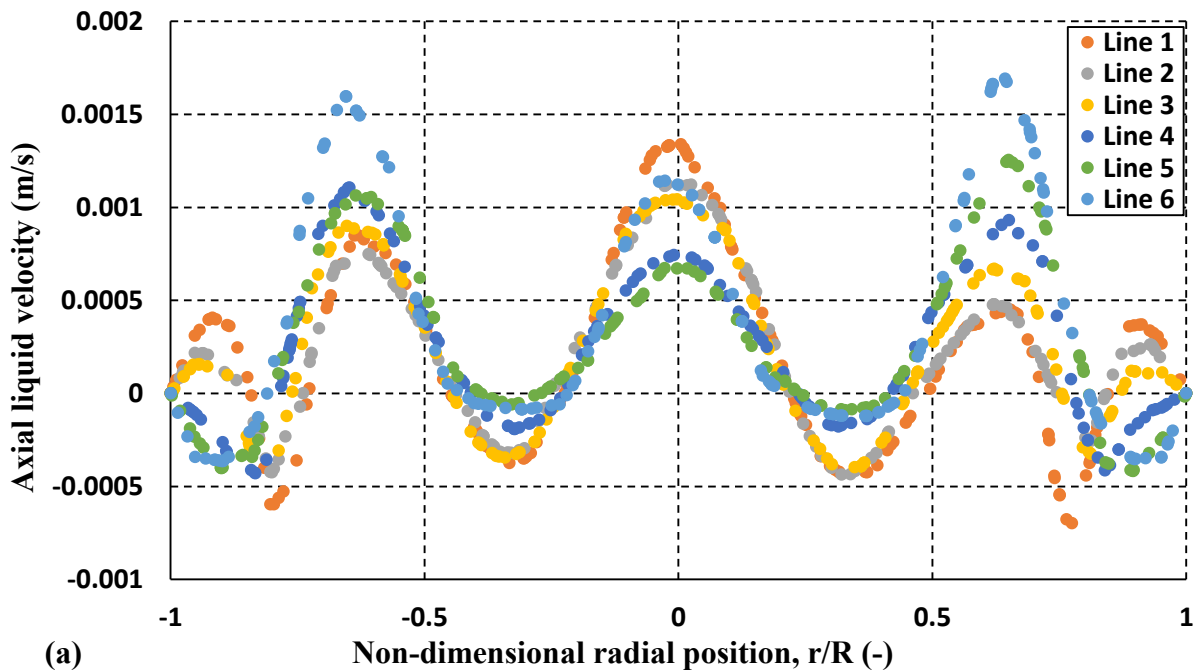


Figure 3.12: The radial distribution of secondary phase volume fraction for superficial gas velocity of (a) 0.163 cm/s, (b) 0.326 cm/s, (c) 0.814 cm/s, and (d) 1.14 cm/s.

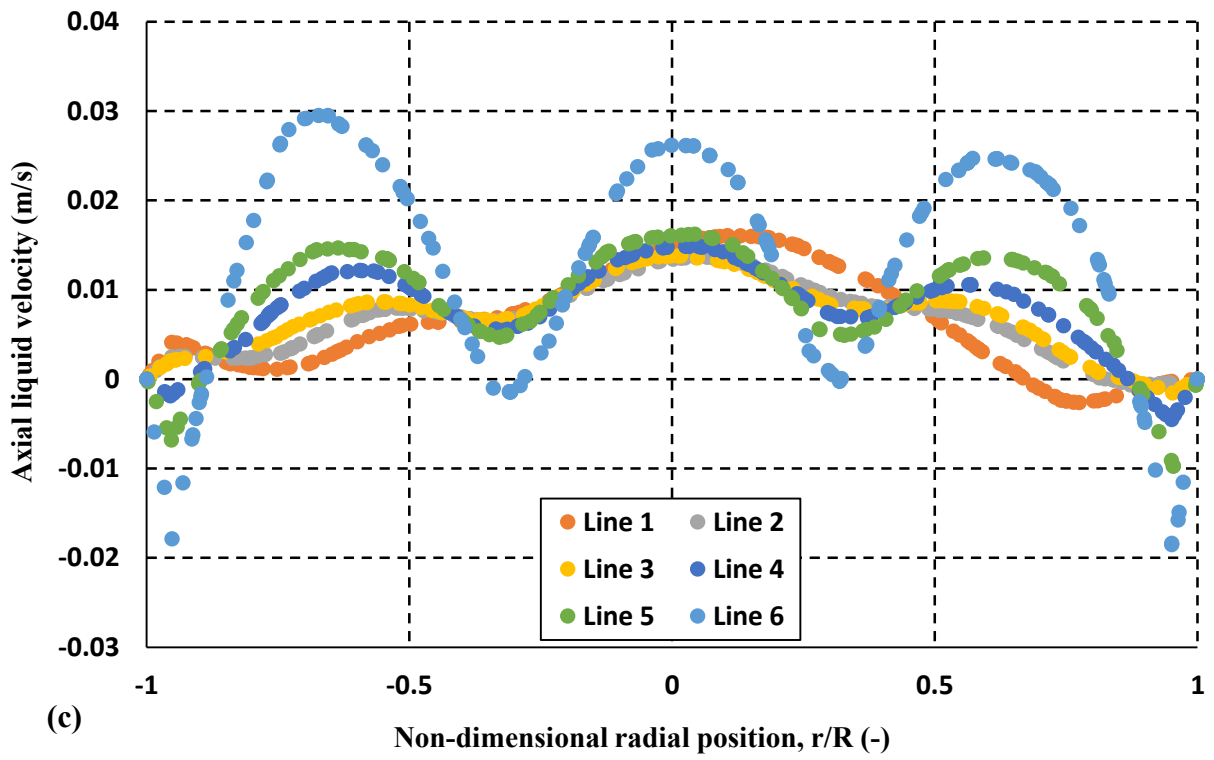
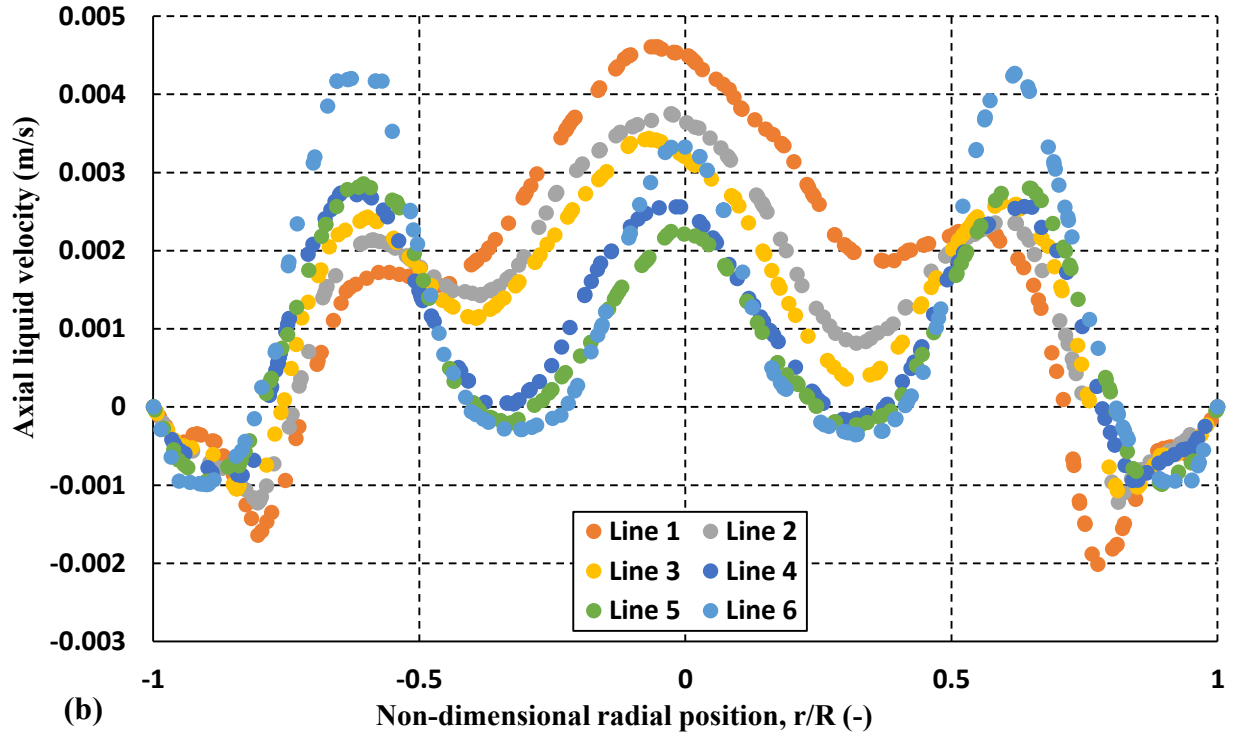
3.3.2 Modified Star Shape Gas Sparger

The flow field of the activated sludge and gas phase with new sparger was predicted by CFD for range of 0.163 to 1.14 cm/s of superficial gas velocity. The new sparger was provided completely different flow behaviour than the star shape sparger which was used by Babaei et al. (2015), particularly in axial velocity profile and gas holdup. As mentioned before, the new sparger's inflowing gas was exactly equal to the star shape sparger and the only difference was about position and surface area of holes. The new sparger with holes at the middle and end of the sparger's arms provided significantly wider distribution of bubbles through the column.

The liquid phase axial velocity profile for rate of superficial gas velocity of 0.163 to 1.14 cm/s is presented in **Figure 3.13**. **Figure 3.13 (a)** shows that the column flow was divided into seven parts including three upward and four downward flows. As can be seen in this figure the middle upward liquid flow was surrounded by a downward liquid flow which itself was surrounded by another upward flow domain. The latter upward flow was surrounded by a thin layer of downward flow near the wall. The aforementioned pattern has been changed by increasing superficial gas velocity in a way that the middle upward liquid flow was surrounded by downward liquid flow as shown for the star-shaped sparger. Therefore this figure illustrates that the modified sparger did not show a good performance at the low superficial gas velocity since there was not a unified powerful liquid flow. However by increasing the superficial gas velocity, this problem has been overcome and a dominant upward liquid velocity has been noticed in the column.



Continued ...



Continued ...

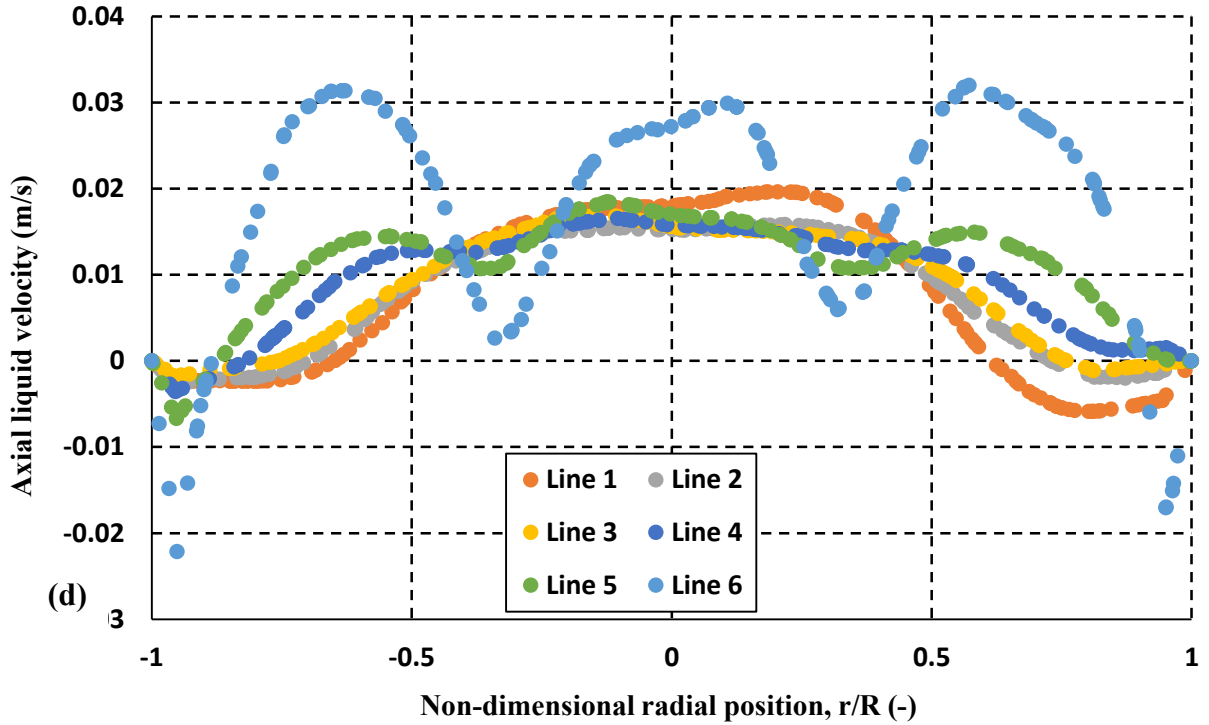
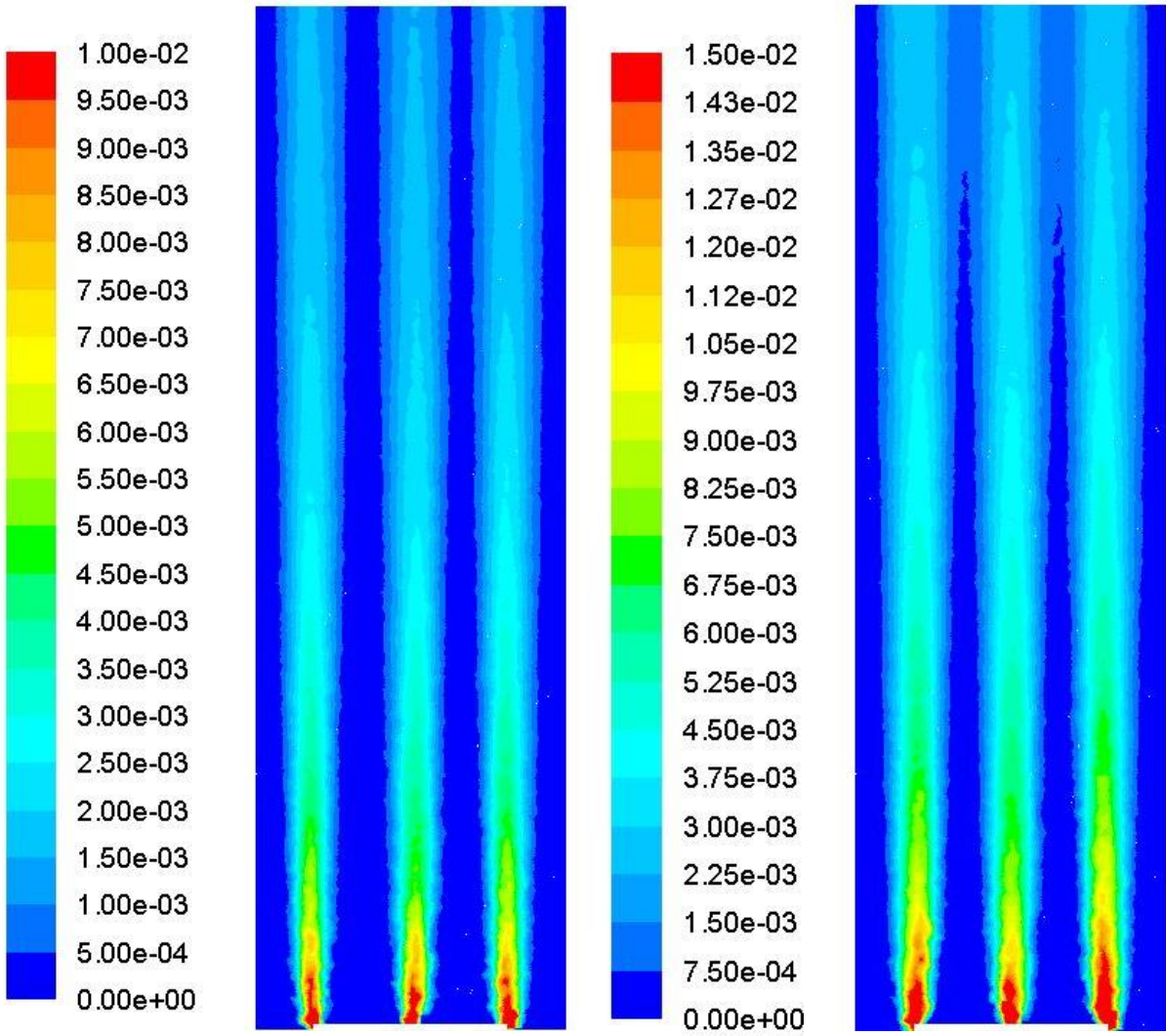


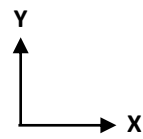
Figure 3.13: The radial distribution of the axial velocity (m/s) of the activated sludge for superficial gas velocity of (a) 0.163 cm/s, (b) 0.326 cm/s, (c) 0.814 cm/s, and (d) 1.14 cm/s.

Figure 3.14 illustrates the vertical contours for the bubble gas holdup for four different superficial gas velocities. As can be seen in this figure, for superficial gas velocity of 1.14 cm/s the bubbles were covered the entire column area above the sparger. In order to have a comparison between two spargers modeled in this study **Figure 3.15** shows the radial gas holdup distribution for superficial gas velocity of 0.163 cm/s. This figure illustrates the development of the radial gas holdup at lines 1 and 3 of modified gas sparger. As can be seen the presence of bubbles in vessel cross section was significantly increased which can optimize the interaction of bubbles and sludge respectively. In fact, the increase of radial dispersion in bubble column bioreactors can improve the rate of reaction and purification process.



(a)

(b)



Continued ...

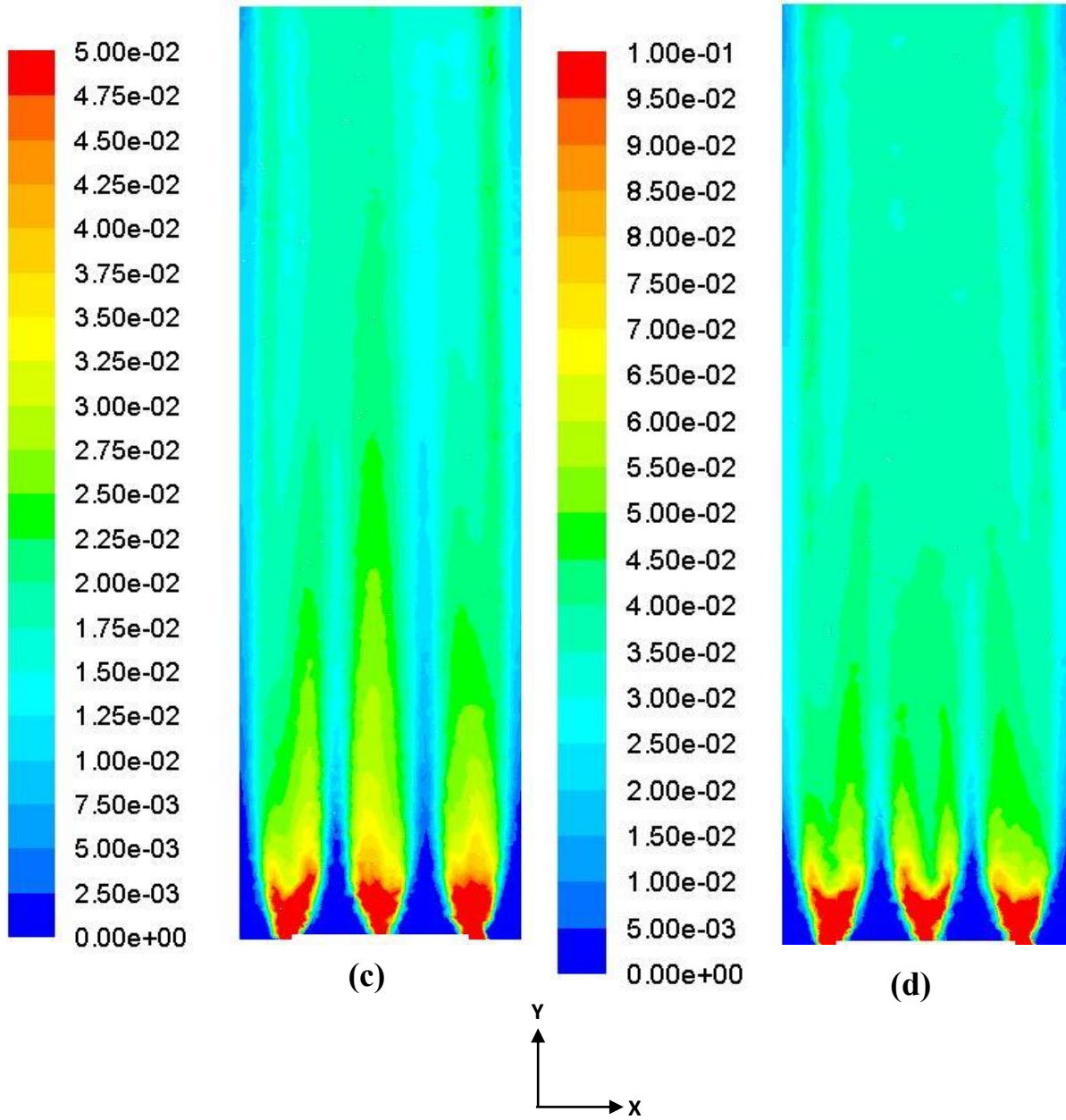


Figure 3.14: The contours of volume fraction of the modified star shape sparger XZ vertical plane for superficial gas velocities of: **(a)** 0.163 cm/s, **(b)** 0.326 cm/s, **(c)** 0.814 cm/s, and **(d)** 1.14 cm/s.

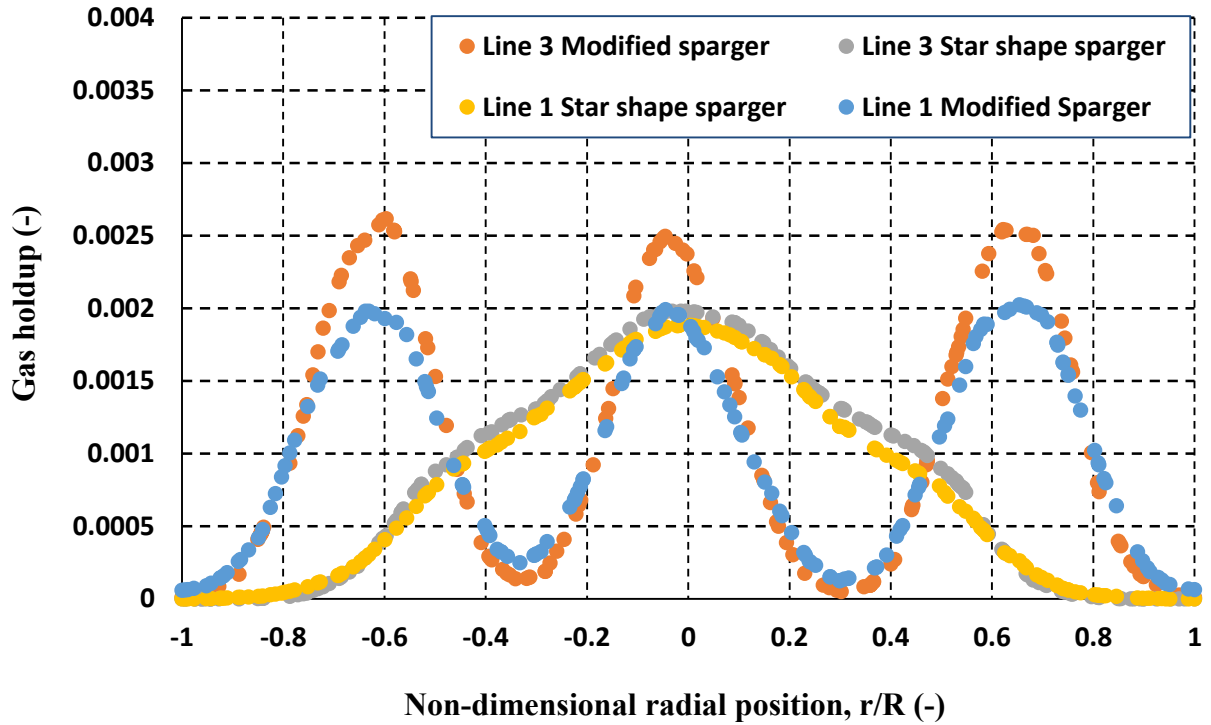


Figure 3.15: The comparison of the radial distribution of the gas holdup for the star shape sparger and the modified star shape at lines 1 and 3 for superficial gas velocity of 0.163 cm/s.

The time-averaged radial gas holdup for six axial positions of the bubble column for two superficial gas velocities is presented in **Figure 3.16**. As observed in this figure, the gas holdup was affected by the value of superficial gas velocity. Obviously, by increasing the superficial gas velocity the population of bubbles at the middle of the column was increased. According to **Figure 3.16 (a)** for superficial velocity of 0.163 cm/s, there were 3 peaks for the gas holdup in the radial trend instead of one peak in middle of the tank as obtained for the star shape sparger. However by increasing the gas velocity (as can be seen in **Figure 3.16 (b)**), the peaks were unified and moved towards the middle of the tank as the axial position from sparger increased. This figure also shows that the modified sparger for the superficial gas velocity of 0.814 cm/s distributed the bubbles nearly in the entire column providing a good interaction among the activated sludge and the bubbles.

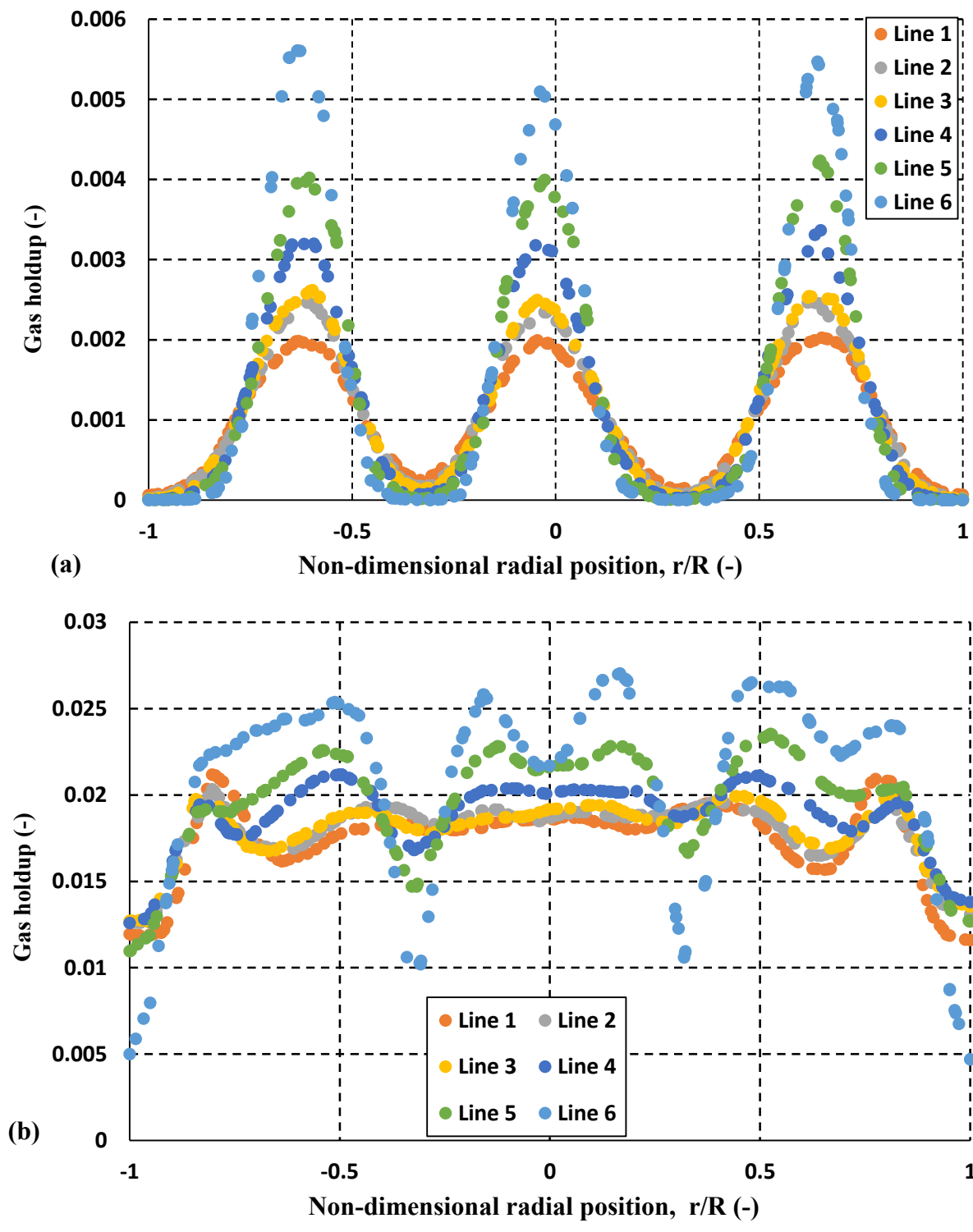


Figure 3.16: The radial distribution of gas holdup for superficial gas velocity of (a) 0.163 cm/s and (b) 0.814 cm/s.

Therefore in compared with the star shape gas sparger, the modified one provided more gas holdup and wider range of gas phase distribution in the column. **Figure 3.17** illustrates the differences of overall gas holdup in both spargers with range of superficial gas velocity of 0.163 to 1.14 cm/s. The overall gas holdup for the novel designed sparger was 1.45 to 2 times higher than star shape gas sparger.

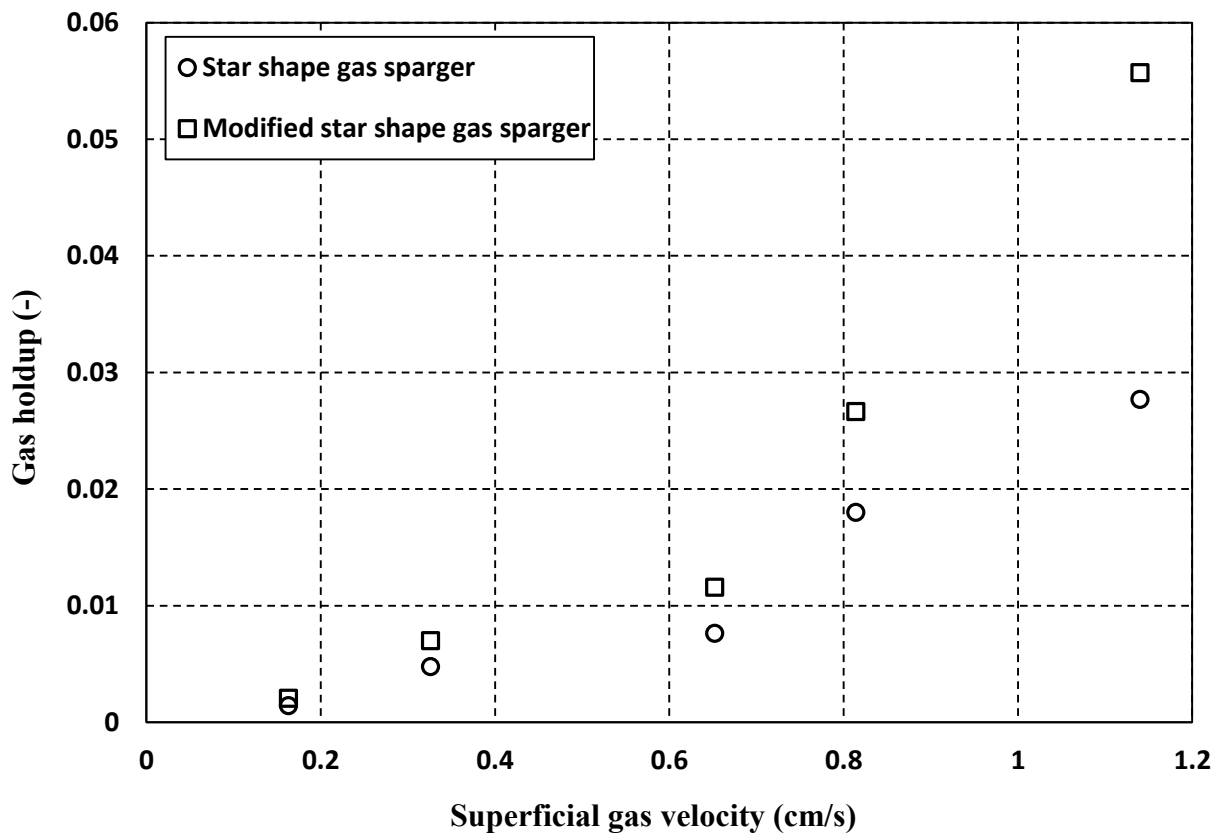


Figure 3.17: The comparison of the star shape and the modified star shape gas sparger.

3.4 Conclusions

1. In case of the model with the star shape gas sparger, the value of liquid velocity and gas holdup was increased by increasing the superficial gas velocity.

2. The mixing time in case of bubble column with star shape gas sparger was decreased by increasing the superficial gas velocity and was proportional to $12.117v_{S, \text{gas}}^{-0.426}$ until it reached almost a plateau.
3. The location of the tracer injection has been affected the mixing time significantly. In both cases, by releasing the tracer right at the middle of the column the best mixing time was achieved. Moreover, the tracer location of bottom and corner of the column gained the longest mixing time.
4. In case of the model with star shape gas sparger, the gas holdup distribution was not spreading wide enough in width of the column and only concentrated at the middle of the column.
5. The rise of the superficial gas holdup was increased the value of gas hold up in both models and also provided wider distribution of gas holdup along the vessel.
6. The gas phase velocity profile was changed by rate of superficial gas velocity in case of model with star shape gas sparger. The degree of the trend of bubble dispersion from introduction point to whole of the column was increased from 8 to 18 degree for superficial gas velocity of 0.163 to 1.14 cm/s.
7. The model with modified gas sparger was provided much wider range of the radial gas distribution in compare with the star shape gas sparger. The value of overall gas holdup for the modified model was 1.45 to 2 times more than first model.

3.5 Notations

The following symbols are used in this chapter:

ASP = activated sludge process

C_D = drag force coefficient

$C_{\varepsilon 1}, G_{\varepsilon 2}$ = constants in k- ε model

CFD = computational fluid dynamics

D = diameter, m

g = gravity, m/s^2

G = generation of turbulent kinetic energy, $J/m^3 \cdot s$

K = turbulent kinetic energy, m^2/s^2

K = consistency coefficient, $Pa \cdot s^n$

M = interfacial momentum exchange term, N/m^3

M_D = drag force, N/m^3

M_L = lift force, N/m^3

M_{VM} = virtual mass force, N/m^3

n = power-law index

T = temperature, K or $^{\circ}C$

u = velocity, m/s

$v_{s,gas}$ = gas velocity, m/s

$v_{s,liquid}$ = liquid velocity, m/s

Re = Reynolds number, dimensionless

W = local mass fraction of the tracer, dimensionless

Greek letters

α = volume fraction, dimensionless

ε = turbulent energy dissipation rate, m^2/s^3

μ = turbulent viscosity, $Pa \cdot s$

ρ = density, $kg \cdot m^{-3}$

$\sigma_k, \sigma_{\varepsilon}$ = constants in k- ε model

τ = shear stress tensor

η = apparent viscosity, $Pa \cdot s$

$\dot{\gamma}$ = shear rate, 1/s

Indices

k = phase index

G = gas phase

L = liquid phase

S = solid phase

b = bubble

Chapter 4: Evaluation of the Effect of Sparger Type, Superficial Gas Velocity, and Tracer Injection Location on the Non-Newtonian Activated Sludge Bioreactor Mixing Performance

4.1 Introduction

The mixing and aeration processes of non-Newtonian fluids are essentially important in such industries as biochemical, food, cosmetic, pharmaceutical, and wastewater treatment. It is a challenging task to predict the mixing performance in a multiphase flow in non-Newtonian fluid. The Activated Sludge Process (ASP) is a well-known process since through this process, an activated mass of microorganisms which was able to stabilizing a waste aerobically is produced. Generally, in the ASP, the wastewater is agitated and aerated simultaneously in order to remove the waste biologically from sludge. The main drawbacks in designing of the current wastewater treatment systems are the assumptions considered for the mixing process and the gas and liquid behavior. These assumptions are applied to design bubble column and aeration system.

Generally, the most important multiphase chemical reactors are divided into three categories as **(a)** the trickle bed reactor (fixed or packed bed), **(b)** fluidized bed reactor, and **(c)** the bubble column reactor (Datsevich and Mukhortov, 2007; Manish and Majumder, 2009). Generally in the bubble column reactor, the gas phase injects from the bottom of the vessel. The injected gas phase rises up the vessel in the form of the bubbles due to the effect of phase interactions i.e. virtual mass, drag, and lift forces (Kulkarni and Joshi, 2005). The liquid phase circulations have effects on the gas holdup, heat and mass transfer, and the mixing process significantly (Chisti et al., 1988; Basheer and Subramaniam, 2012). One of the most important factors in the bubble columns is the

superficial gas velocity where the change of this parameter impacts the distribution of size and shapes of bubbles in the column (Karpinska Portela, 2013).

The bubble column consists of simple geometry and aeration system and the operation of this kind of reactor is not much energy consuming process. In general, the performance of the bubble column reactor operation depends on different factors such as height of filled liquid inside the column, the diameter of bubble column, the rate of superficial gas velocity, and the design of gas distributor. As mentioned in the last chapter, the design of distributor has a significant effect on gas holdup and bubbles distribution pattern. Therefore, the fundamental knowledge is a crucial need to optimize the performance of a bubble column reactor (Li et al., 2016; Ranade and Tayalia, 2001).

Mixing time is a time that a process reaches a particular degree of homogeneity. Usually to measure the mixing time value, a small amount of tracer is released among the process vessel and the concentration of tracer is monitored during the operation. The rate and quality of chemical reactions in semi-batch bioreactors depend on the performance of mixing process. Generally, the liquid mixing process becomes more important in cases that the rate of chemical reaction or mass transfer is faster than the rate of liquid mixing (Rao and Joshi, 1998). Despite of the high demand of efficient mixing in industrial operations, it is still not understood completely and usually the industrial designs are based on assumptions about liquid behavior during mixing process.

There are several studies in the field of investigation the process of mixing (Babaei et al., 2015; Sanchez Miron et al., 2004; Gondo et al., 1973). The effect of large bubbles on liquid mixing process in bubble column was studied by Gondo et al. (1973), their study showed that among the factors as the column diameter, height, and phases interaction modes (i.e. co-current or counter-

current), the former has the highest impact on the mixing time. Most of the studies on the mixing time measurements in the bubble column have been concentrated on the gas phase hydrodynamics rather than mixing process (Li et al., 2016). The fundamental studies on the understanding of the mixing process and the optimization process especially in the presence of the non-Newtonian fluids are found challenging and also valuable from industrial view of point.

Recently, Babaei et al. (2015) studied the mixing process and performance of aeration of an activated sludge bioreactor. They worked on the dynamic gas disengagement (DGD) technique which is a method that investigates the gas phase characteristics and mixing process of the column after shutting off the gas flow. They also studied the effect of superficial gas velocity and fluid mixed liquor suspended solid (MLSS) on the flow field, the average bubble rise velocity, diameter of bubbles, and mixing time measurements. There are some important parameters that they did not present any evidence about them such as the liquid and gas velocity profile, effect of tracer injection location on mixing time, and local gas holdup profiles.

In the field of wastewater treatment simulations, the CFD applications especially in design of screens, grit chambers and activated sludge tanks has been experienced a significant improvement (Karspinka and Bridgeman, 2016). In fact the most important ability of the CFD simulations is in modeling the activated sludge bubble column multiphase flow and predicting the flow field and gas-liquid behavior with high level of accuracy. So, the use of CFD modeling in bubble column design could replace the old methods of multiphase modeling that is based on the assumptions especially in case of wastewater treatment optimization process. In this study, CFD enables to precisely simulate the inside physical phenomena of gas-liquid interactions and mixing process. The simulated model predicted the bubble column flow field, mixing time and effects of different parameters on performance of operation.

There are several variables such as type of gas sparger, superficial gas velocity, tracer injection location, and fluid rheology that have effects on the mixing performance and consequently on the measured mixing time. The full factorial design is a method that can design all possible experiments including two or more factors and each factor could have discrete possible values or levels (Capetillo and Ibarra, 2017). The factorial design method is used to predict the effect of each variable and all possible interactions among variables to achieve more accurate response (Gottipati and Mishra, 2010; Capetillo and Ibarra, 2017; Arbizu and Pérez, 2003; Pavan et al., 2007).

Despite of the importance of the mixing process in activated sludge bubble column systems, there is not enough studies in this field with the design of experiment methods. Using CFD modeling, in this chapter, the effects of the superficial gas velocity, sparger type, and tracer injection location on the mixing time through full factorial design method will be presented. The activated sludge rheology with the MLSS concentration of 0.712 g/L was modeled using power-law rheological model. The CFD results were validated by experimental data available in literature (Babaei et al., 2015).

In this Chapter, first CFD model development will be briefly presented and then results will be shown with the adequate discussion. Through section of results and discussion, the experimental design will be explained. Finally the concluding remarks from this study will be presented.

4.2 CFD Model Development

Computational Fluid Dynamics (CFD) is one of the most powerful tools to simulate the complex flows such as multiphase flow in the activated sludge bubble column. As can be seen in **Figure 4.1 (a)**, the geometry consists of a cylindrical tank with diameter of 0.248 m and height of 1.000

m. The bubble column was equipped with a sparger at the bottom of the vessel. According to **Figure 4.1 (b)**, the cross shaped gas sparger consisted of six arms of 0.078 m long with 24 holes of 1 mm diameter on each arm. For optimizing the aeration process and gas holdup in bubble column, the new gas sparger was designed with exactly the same dimensions as the first sparger (star shape gas sparger). As can be seen in **Figure 4.1 (c)**, the new sparger contained 7 holes with diameter of 1.8516 mm that 6 of them located at the end of each arms and one of them was at the middle of the sparger.

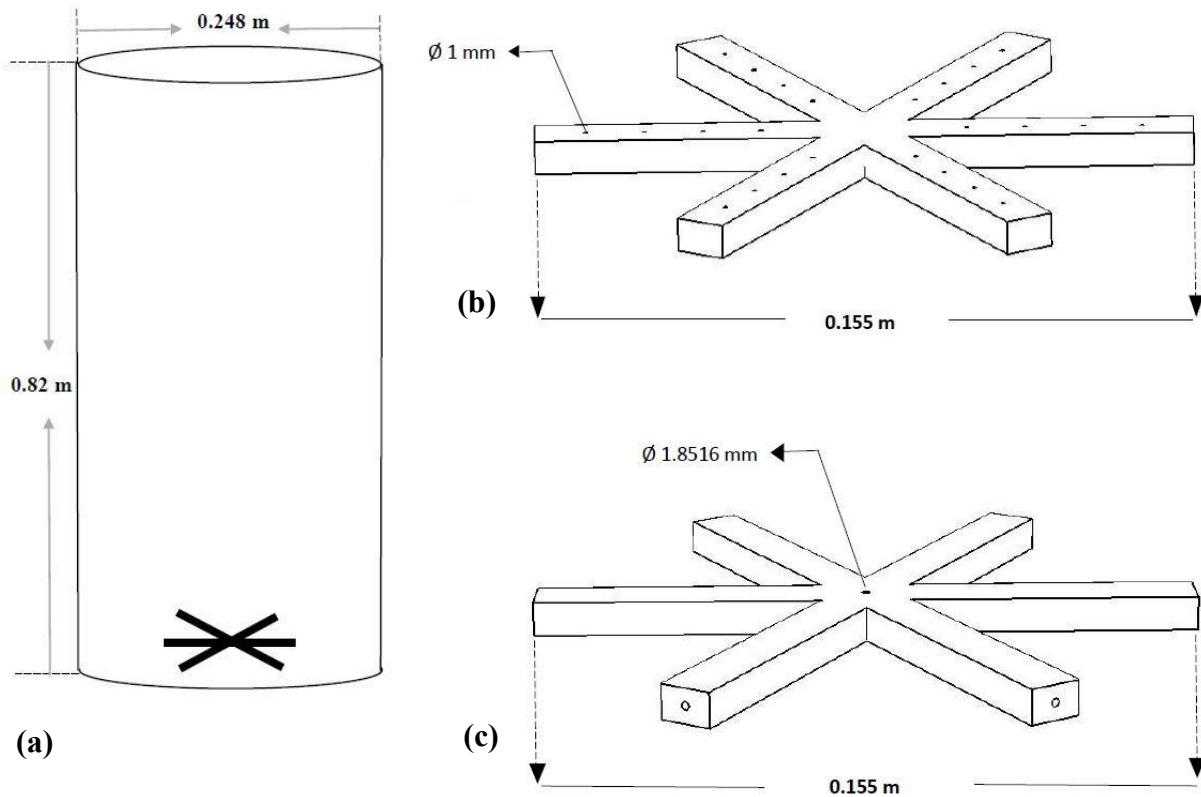


Figure 4.1: (a) the geometry of bubble column, (b) the isometric view of the star shape sparger, and (c) the isometric view of the modified sparger.

ANSYS Design Modeller (Version 17.1) platform was employed to discretize the 3D computational domain with three unstructured tetrahedral mesh network. For optimizing the accuracy of results especially at the middle of the column, a size function was employed to generate very refined mesh in the central area of the vessel and three mesh networks consisting of

414923, 749125, and 1544130 cells were generated. **Figure 4.2** shows the radial distribution of gas holdup in case of the superficial gas velocity of 0.814 cm/s at line 3. As can be seen, the medium and fine grid provided a nearly the same radial gas holdup profile. The coarse grid presented different profile in compare with the medium and fine grids. The grid discrepancy has been analyzed in terms of root-mean-square (RMS) deviation method with following equation:

$$RMS = \frac{\left[\frac{1}{n} \sum_1^n (\epsilon_1 - \epsilon_2)^2 \right]^{1/2}}{\left[\frac{1}{n} \sum_1^n (\epsilon_2)^2 \right]^{1/2}} \quad (4.1)$$

where n is the number of nodes in the flow field. The RMS values between coarse grid and medium grid was 5.86 and for medium and fine grid was 4.1. Since, the RMS value for medium and fine grid was about 4 percent, therefore the mesh network consisting 749125 cells was used for all simulations in this study. Once the mesh file has been produced, it was exported to the ANSYS/Fluent package (version 17.1) which was applied for calculating the 3D flow field generated by the aeration process. The CFD model predicted the flow behaviour by using the standard k-ε model which is the most applicable model for simulating turbulence in the gas-liquid multiphase flows (Ekambara et al., 2005). The non-Newtonian fluid was described using the power-law rheological model with $k=0.00528 \text{ Pa.s}^n$ and $n = 0.6887$ (Babaei et al. 2015).

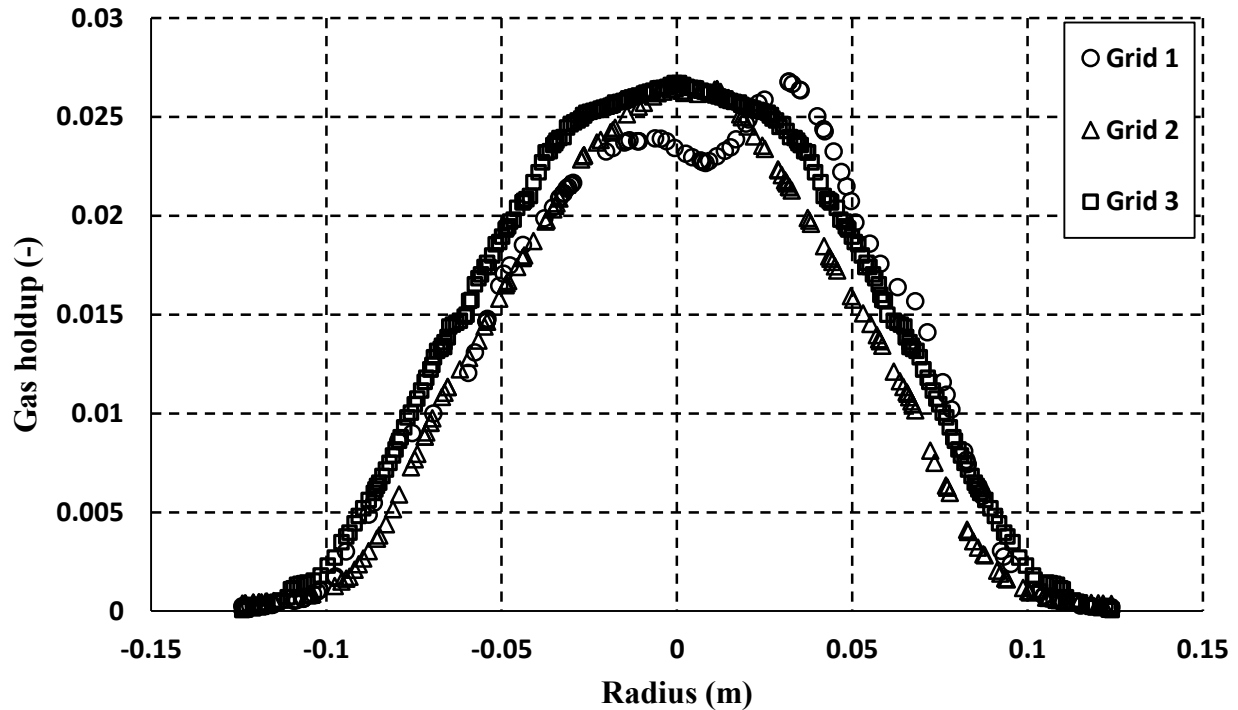


Figure 4.2: Effect of the grid numbers on radial gas holdup in case of superficial gas velocity of 0.814 cm/s at line 3.

In this study, superficial gas velocity was changed from 0.081 to 1.14 cm/s corresponding to the experimental values selected by Babaie et al. (2015). The equations were solved during the process simultaneously in unsteady state mode with the time step of 0.01s. The convergence of calculations was checked by monitoring the residuals of all numerical equations. The convergence of the simulations were achieved when the scaled residuals dropped below 10^{-5} . Supercomputing facilities of HPCVL (High Performance Computing Virtual Laboratory) was employed to predict bubble column behavior. The operation system for calculating numerical model was run in parallel mode with 24 dual cores Dell PowerEdge R410 Server with 2 sockets with a 6-core Intel® Xeon® processor (Intel x5675) running at 3.1 GHz. In case of calculations of present study, the grid was

partitioned to 24 parts then one CPU was used to calculate each partition equations. Depending on case, the convergence for each unsteady state model was held after about 72 hours.

After completion of all the flow field calculations, the transient simulations switched to calculations for the tracer homogenization were provided by using the Species and Transport Model, as presented in **Equation (3.15)**. During mixing time measurements, the value of the tracer mass fraction during all of the simulations was set to 1. In order to find the exact mixing time, the tracer mass fraction in the vessel was recorded. The tracer fluid properties were set same as bulk fluid (activated sludge with MLSS of 0.712). Moreover, the effects of injection location of tracer have been studied in this work. The locations of tracer injection were set to four different locations in the vessel **Figure 4.3**.

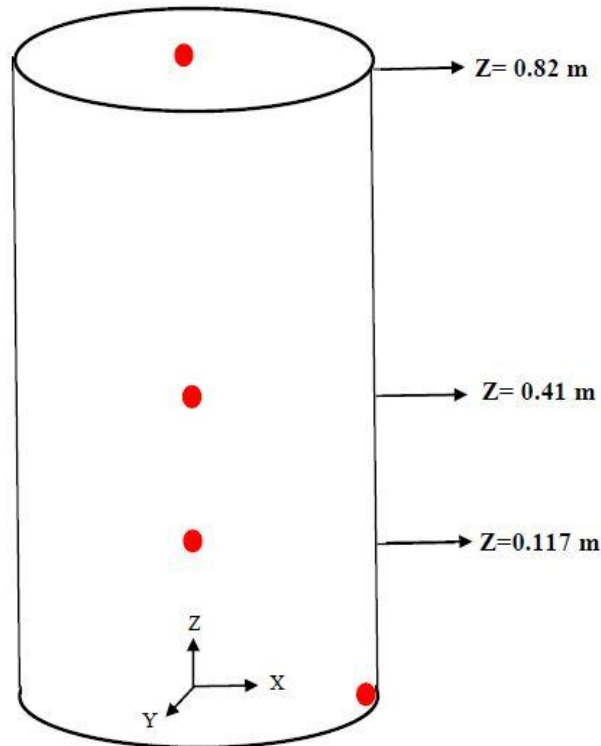


Figure 4.3: The locations of tracer injection.

To validate the CFD model, the results of the CFD simulations for the mixing time and gas holdup were compared to the experimental data presented by Babaei et al. (2015) as shown in **Figure 3.4**. McClure et al. (2015) studied the effect of superficial gas velocity and location of tracer injection on the tap water bubble column experimentally and numerically. They suggested that in the range of 0.07 to 0.29 m/s of superficial velocity, there is no significant change has been seen in mixing time, however other parameters such as the location of the tracer injection and measurement points had significant effects on the mixing time. Their achievements transmuted to a new concept for measuring mixing time in the bubble column reactors by injecting tracers in several locations.

4.3 Results and Discussion

There are many different applications of full factorial design method in statistical analysis (Capetillo and Ibarra, 2017; Arrowsmith et al., 2006; Vicente et al., 1998). The statistical design of experiments is a method decreasing the number of experiments to be performed, finding the interaction among the variables and optimizing the process variables. The full factorial design is one of the comprehensive statistical methods that covers all of the possible experiments. In this case, we had 3 variables of superficial gas velocity (X_1), tracer injection location (X_2), and gas sparger type (X_3). The number of the levels of each variable was different where there were 5 levels for superficial gas velocity from 0.163 cm/s to 1.14 cm/s, four levels of tracer injection locations from 1 to 4 that each one presents a specific location in the vessel as mentioned above and 2 levels for the type of the gas sparger including the typical star shape sparger and the modified star shape sparger. As can be seen, **Table 4.1** illustrates the experimental range and levels of the variables.

Table 4.1: Experimental range and levels of the independent variables.

Variables	Symbol	Level	Level	Level	Level	Level
		1	2	3	4	5
Superficial gas velocity (cm/s)	X ₁	0.163	0.326	0.57	0.814	1.14
Tracer injection location (-)	X ₂	1	2	3	4	–
Sparger type (-)	X ₃	Typical star shape	Modified star shape	–	–	–

Table 4.2 presents experimental results for the mixing time (s) using full factorial approach. The provided data by full factorial design can be analyzed by the fitting the second-order polynomial model (quadratic function) using the trial version of JMP software from SAS.

Table 4.2: Design matrix in coded units and the experimental responses.

Run	Variables			Response
	X ₁	X ₂	X ₃	t _m (s)
1	1.14	3	Typical star shape	10.12
2	0.163	3	Modified star shape	24.84
3	0.163	4	Modified star shape	26.08
4	0.326	1	Typical star shape	16.68

Continued

Run	Variables			Response
	X ₁	X ₂	X ₃	t _m (s)
7	0.814	1	Typical star shape	9.23
8	0.57	1	Modified star shape	12.67
9	0.163	4	Typical star shape	26.64
10	1.14	2	Modified star shape	2.92
11	0.163	3	Typical star shape	25.37
12	0.57	4	Typical star shape	15.24
13	0.163	2	Modified star shape	18.87
14	0.163	2	Typical star shape	19.24
15	0.57	3	Typical star shape	14.38
16	0.814	1	Modified star shape	8.96

Continued

Run	Variables			Response
	X ₁	X ₂	X ₃	t _m (s)
17	0.814	3	Typical star shape	11.85
18	0.326	2	Typical star shape	11.89
19	1.14	1	Typical star shape	7.52
20	0.814	2	Modified star shape	4.91
21	1.14	3	Modified star shape	10.04
22	1.14	1	Modified star shape	7.45
23	0.814	3	Modified star shape	11.66
24	0.163	1	Typical star shape	23.4
25	0.814	2	Typical star shape	5.13
26	1.14	4	Typical star shape	11.72

Continued

Run	Variables			Response
	X ₁	X ₂	X ₃	t _m (s)
27	0.57	3	Modified star shape	13.91
28	0.326	3	Modified star shape	17.87
29	0.57	2	Typical star shape	7.93
30	0.326	4	Typical star shape	19.43
31	0.326	2	Modified star shape	11.46
32	0.326	4	Modified star shape	18.95
33	0.57	4	Modified star shape	14.84
34	1.14	4	Modified star shape	11.63
35	0.57	2	Modified star shape	7.48
36	0.814	4	Modified star shape	12.67
37	0.326	1	Modified star shape	16.17

Continued

Run	Variables			Response
	X ₁	X ₂	X ₃	t _m (s)
38	1.14	2	Typical star shape	2.97
39	0.57	1	Typical star shape	13.09
40	0.163	1	Modified star shape	22.96

The regression analysis was performed to fit the response function (Y) with the quadratic equation as follows:

$$\begin{aligned}
 Y = & 33.1545 - 40.7388X_1 - 5.8247X_2 - 0.2862X_3 + 0.5014X_1X_2 \\
 & + 0.2177X_1X_3 - 0.0062X_2X_3 + 19.0704X_1^2 + 1.428X_2^2
 \end{aligned}
 \tag{4.2}$$

The capability of the equation was estimated by the Fisher's F-test to analysis of variance (ANOVA). **Table 4.3** shows the results of the ANOVA analysis of quadratic regression equation for mixing time. As can be seen in this table, the F-value of 33.5239 illustrates the model's capability of simulating the mixing time. In ANOVA method, the value of the (Prob > F) < 0.0500 shows that the simulated model is significant, however the values >0.1000 illustrate the insignificant model. According to Table 3, the value of Prob > F-values for the mixing time is less than 0.05 which is the evidence of the significant model.

Figure 4.4 shows the main effect plots for the mixing time of the superficial gas velocity, tracer injection location and sparger type which is provided by the statistical design. The mentioned plots illustrate the contribution of each variable and mixing time. As can be seen in this figure, the effect

of superficial gas velocity was positive on decreasing the mixing time where the increase of this parameter decreased the mixing time. The slope of each plot shows the level of efficiency on minimizing the mixing time. The superficial velocity plot shows that the effect of this parameter was more significant than other variables. Moreover, the slope of sparger type illustrates the insignificant effect of this variable on decreasing the mixing time. The other obvious point is that by changing the tracer injection location from 4 to 1 and increasing the gas velocity, the lower mixing time will be reached. Also the plots show that the tracer injection location 2 has the lowest mixing time.

Figure 4.5 presents a series of vertical cross-section planes showing the dispersion of the tracer at superficial gas velocity of 0.163 cm/s for four injection points applied in this study. As can be seen in Figure 3.5(b), when tracer was released in injection point (2), i.e. in middle of the column, it was dispersed through both upward and downward directions leading to the lower mixing times however for other injections points there was only one direction either upward or downward depending on the locations. This figure also depicts the pathline of the liquid phase showing one dominant axial circulation loop consisting of some small secondary recirculation zones. One of the important parameters which should be assessed is the mixing flow pattern existing in the bubble column. The mixing flow pattern depends on the bubble column size, superficial gas velocity, liquid physical properties, and sparger geometry. Out of the aforementioned parameters effective on the mixing flow pattern, superficial gas velocity and sparger geometry have been chosen in this study to be evaluated. The investigation of flow pattern in the bubble column was generally categorized into study of liquid phase and gas phase behavior.

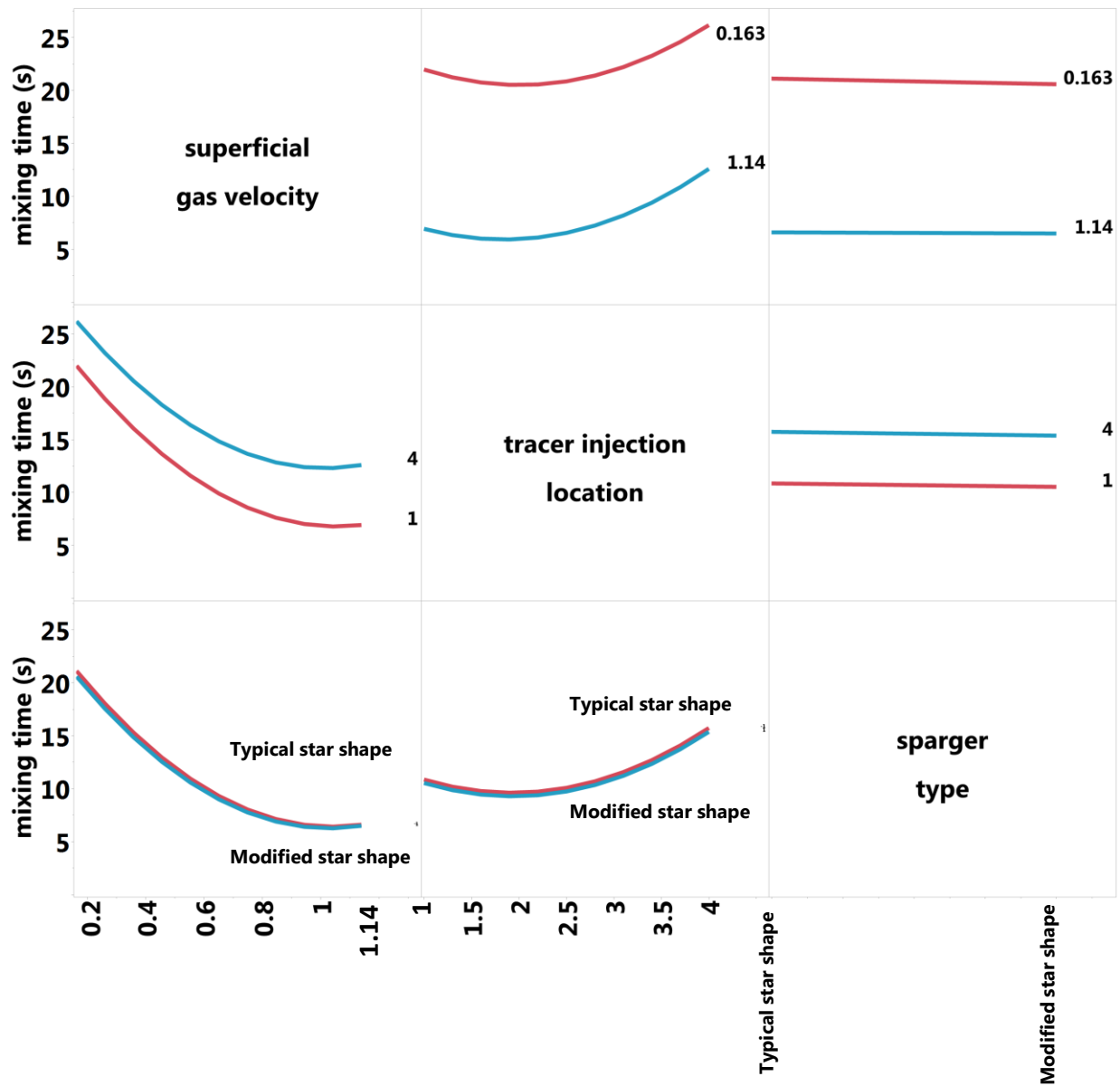
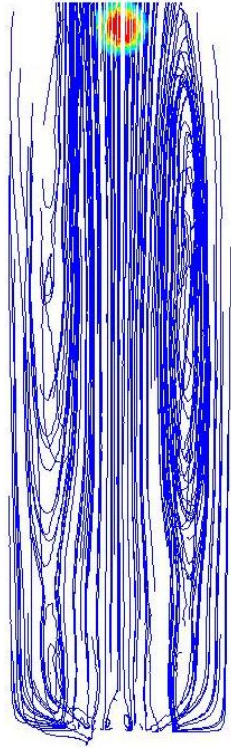
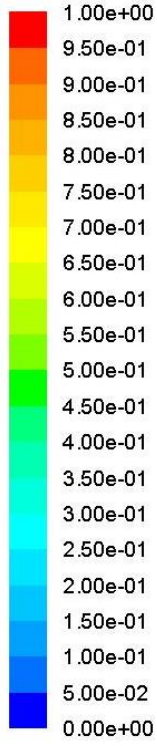
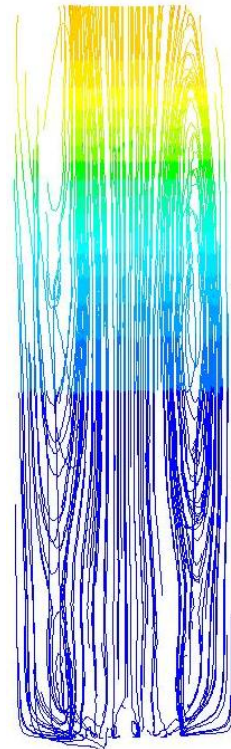
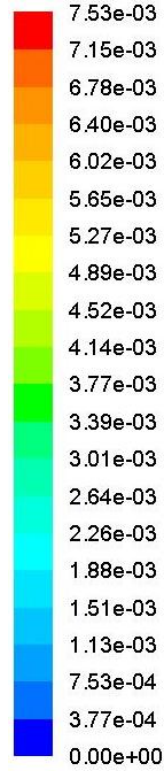


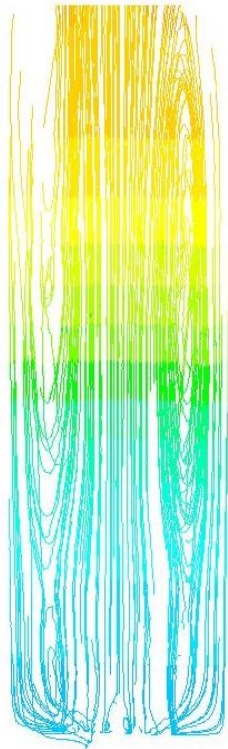
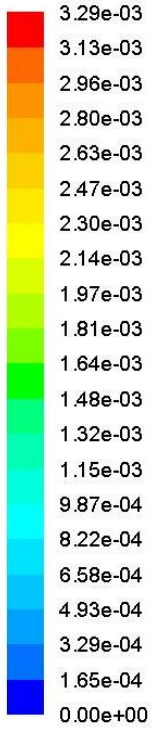
Figure 4.4: Main effect plots for mixing time (s) for all 3 variables.



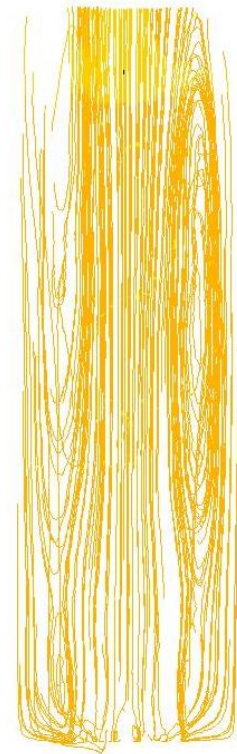
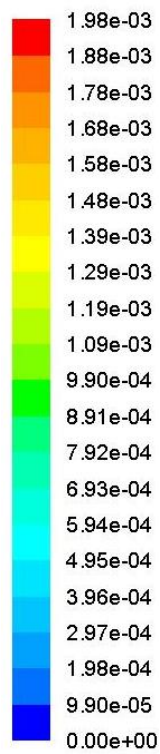
0 s



5 s

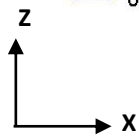


10 s

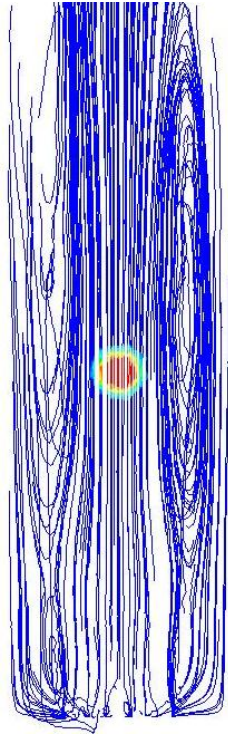
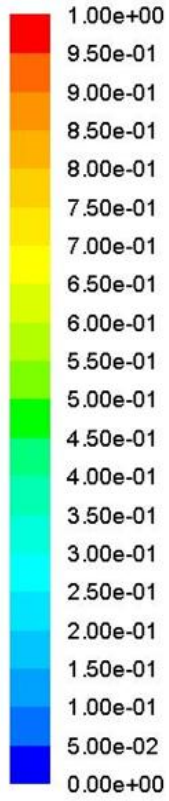


23.4 s

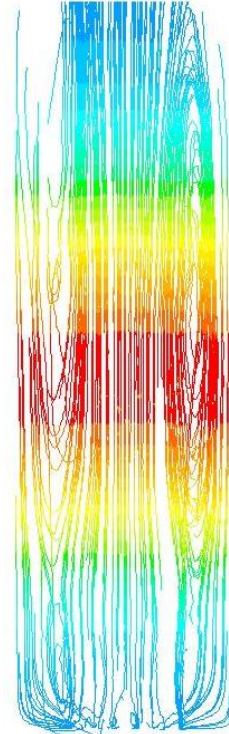
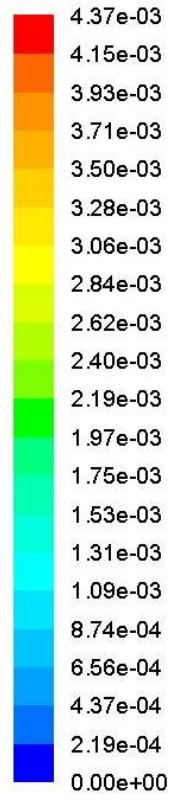
(a) Injection point 1



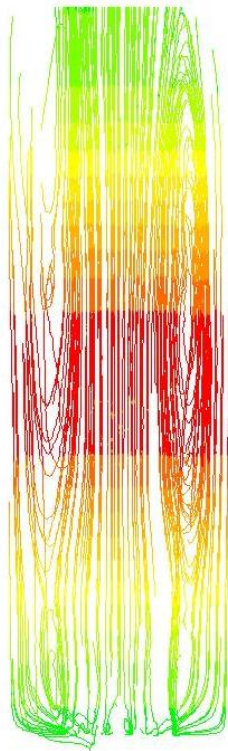
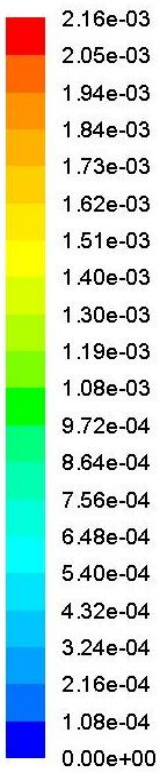
(Continued)



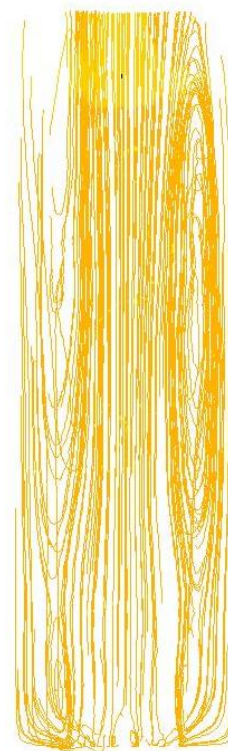
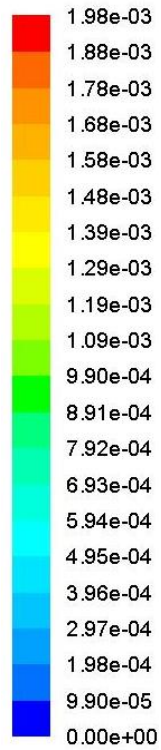
0 s



5 s



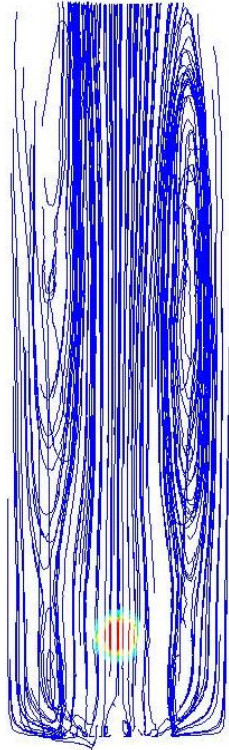
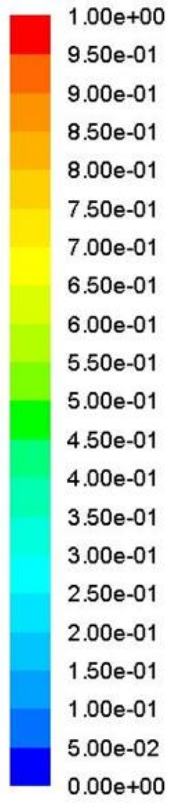
10 s



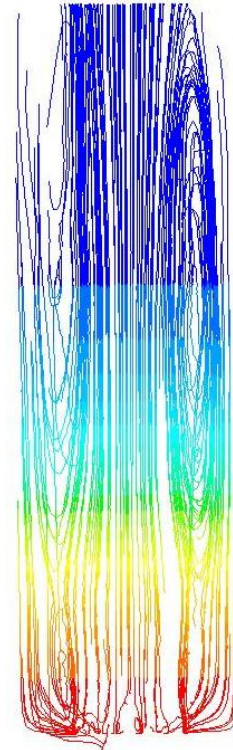
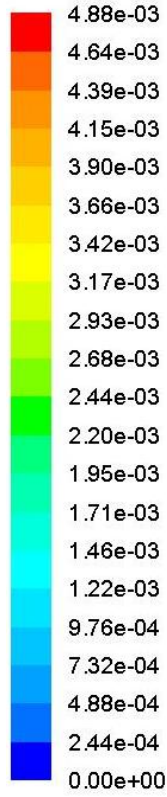
19.24 s

(b) Injection point 2

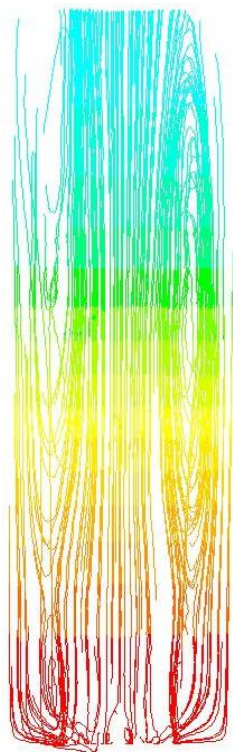
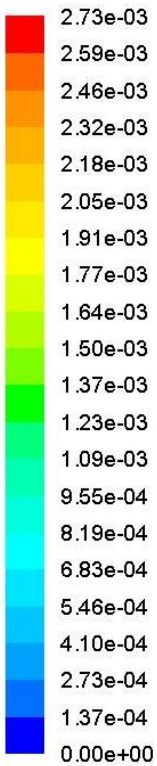
Continued



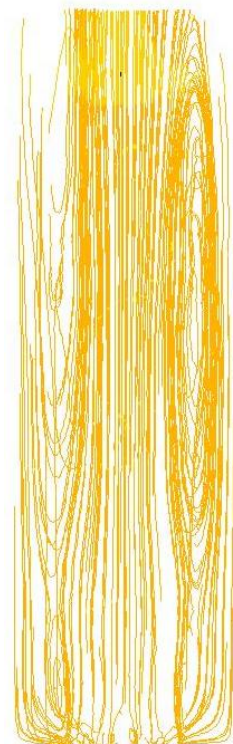
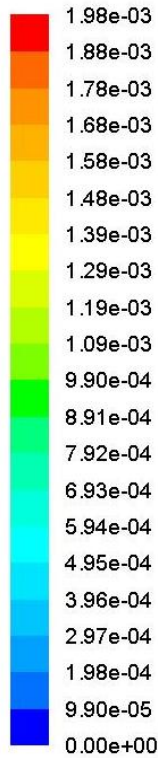
0 s



5 s



10 s



25.37 s

(c) Injection point 3

Continued

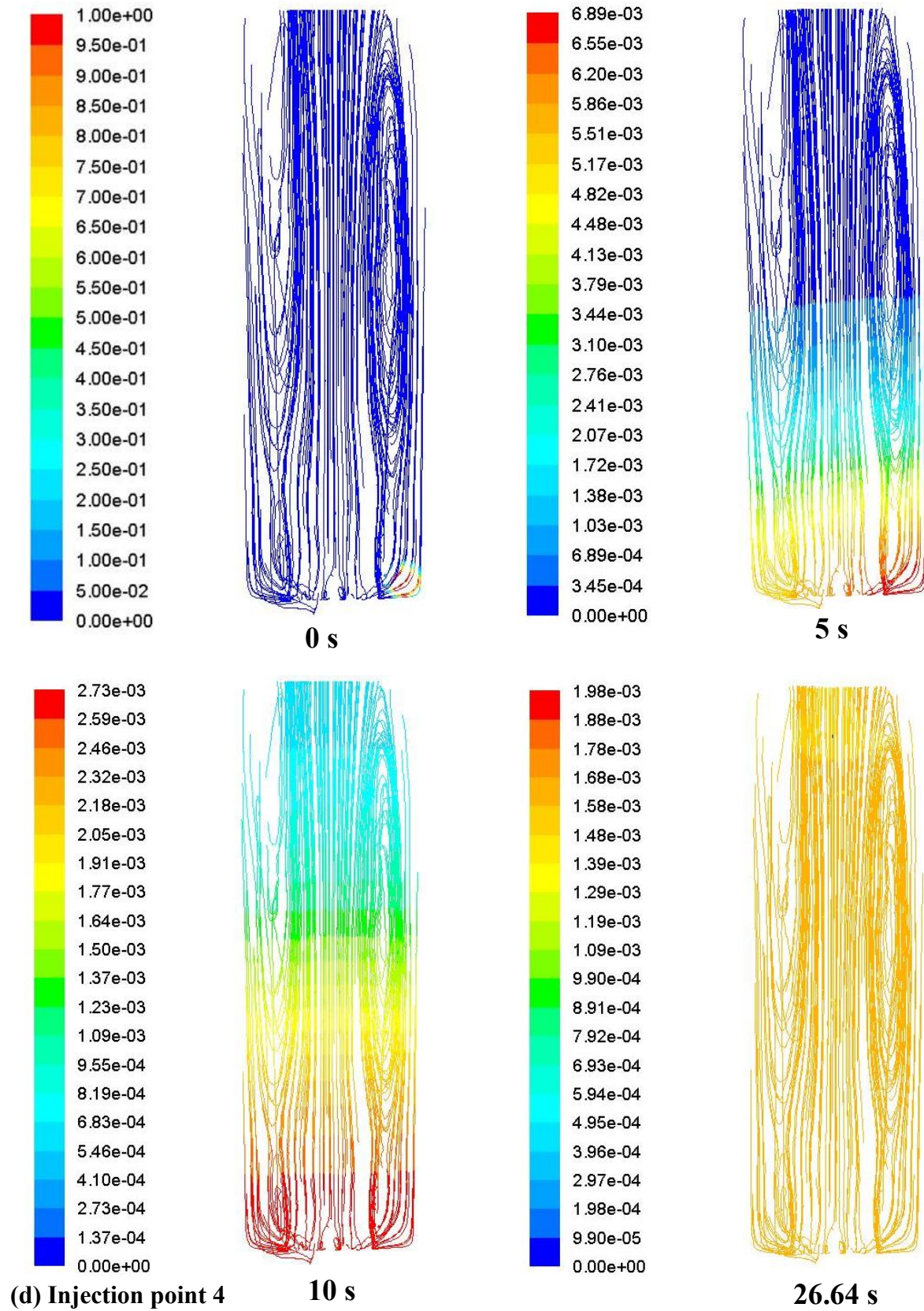


Figure 4.5: The contours of species mass fraction XZ vertical plane for all location: **(a)** location 1, **(b)** location 2, **(c)** location 3, and **(d)** location 4 with superficial gas velocity of 0.163 cm/s.

The regression coefficient of the fit model (R^2) was 0.9 that shows the high quality of the presented model. It illustrates that only 10% of mixing time variability was not described by the equations, however for a model with this wide range of variability is a fair value. **Figure 4.6** presents the good agreement between predicted mixing time values from equation (4.2) and mixing time which was provided by CFD analysis.

Table 4.3: ANOVA test for response function (mixing time (s)).

Source	Sum of Squares	DF	Mean square	F Ratio	Prob > F
Model	1398.8631	8	174.8578875	33.5239	<.0001
X_1	1182.3039	1	1182.3039	226.6723	<.0001
X_1^2	145.1845	1	145.1845	27.8349	<.0001
X_2	130.7991	1	130.7991	25.0769	<.0001
X_2^2	81.5674	1	81.5674	15.6382	0.0004
X_3	1.1628	1	1.1628	0.2229	0.6401
X_3^2	0.0000	0	0.0000	.	.
X_1X_2	1.5192	1	1.5192	0.2913	0.5933
X_1X_3	0.2291	1	0.2291	0.0439	0.8354
X_2X_3	0.0019	1	0.0019	0.0004	0.9848

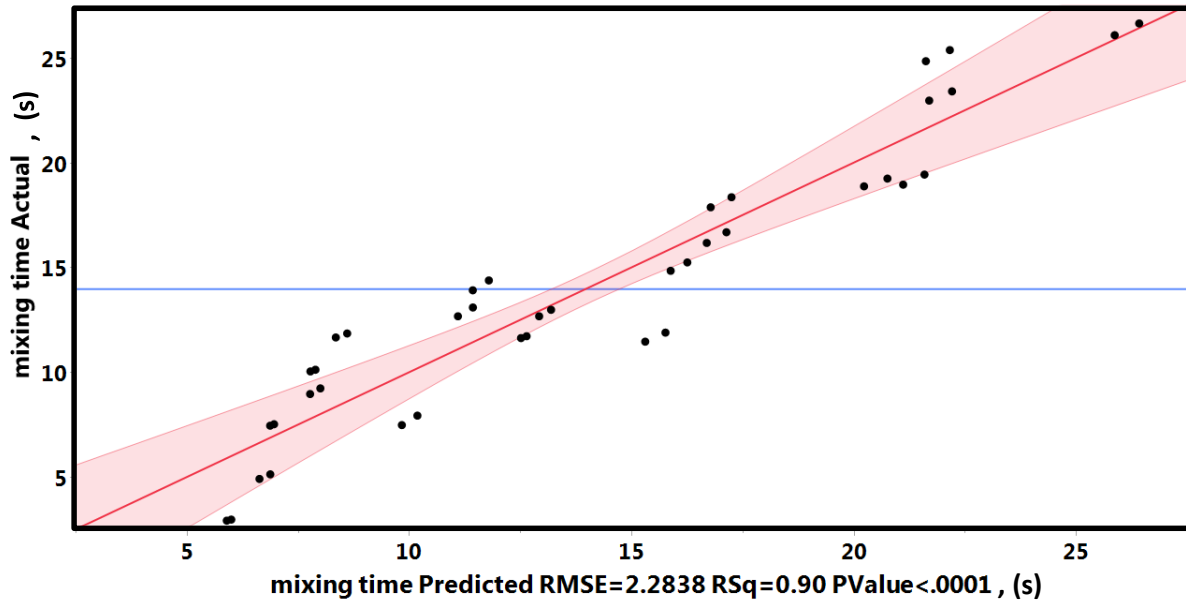
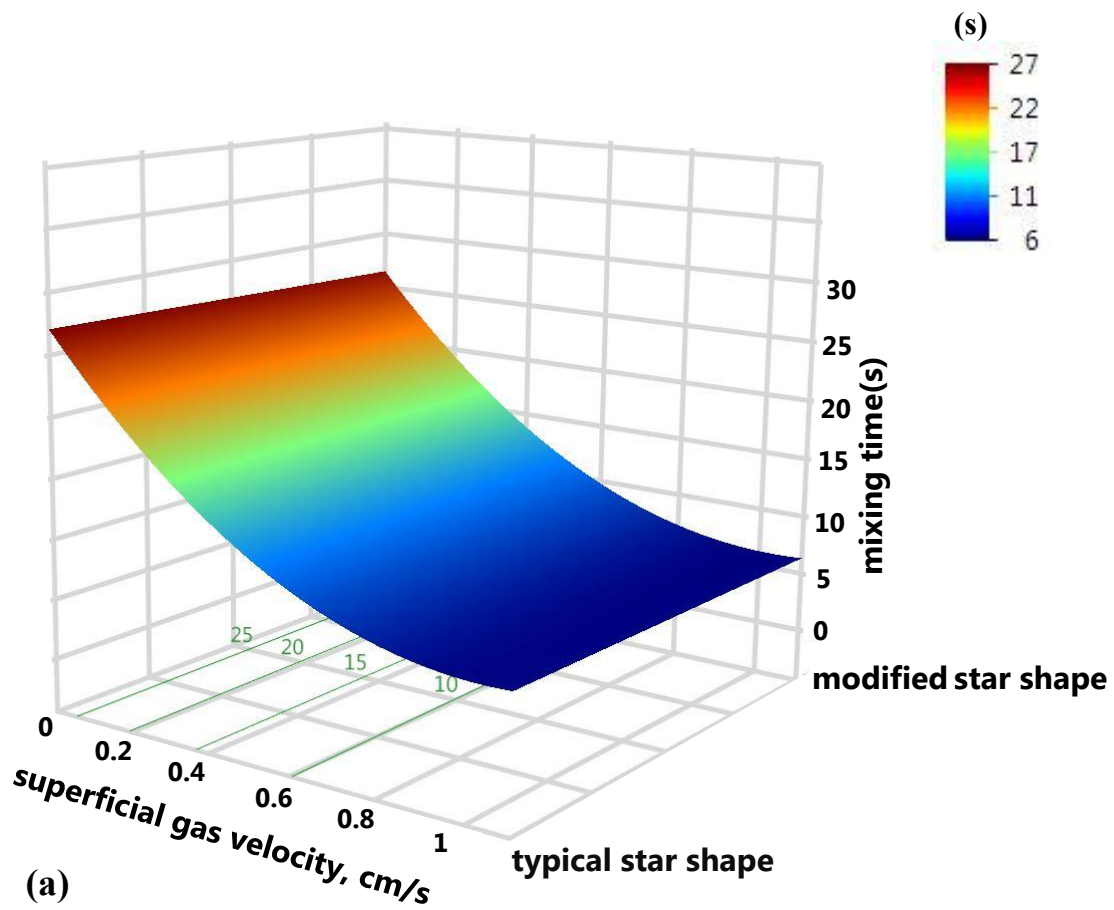
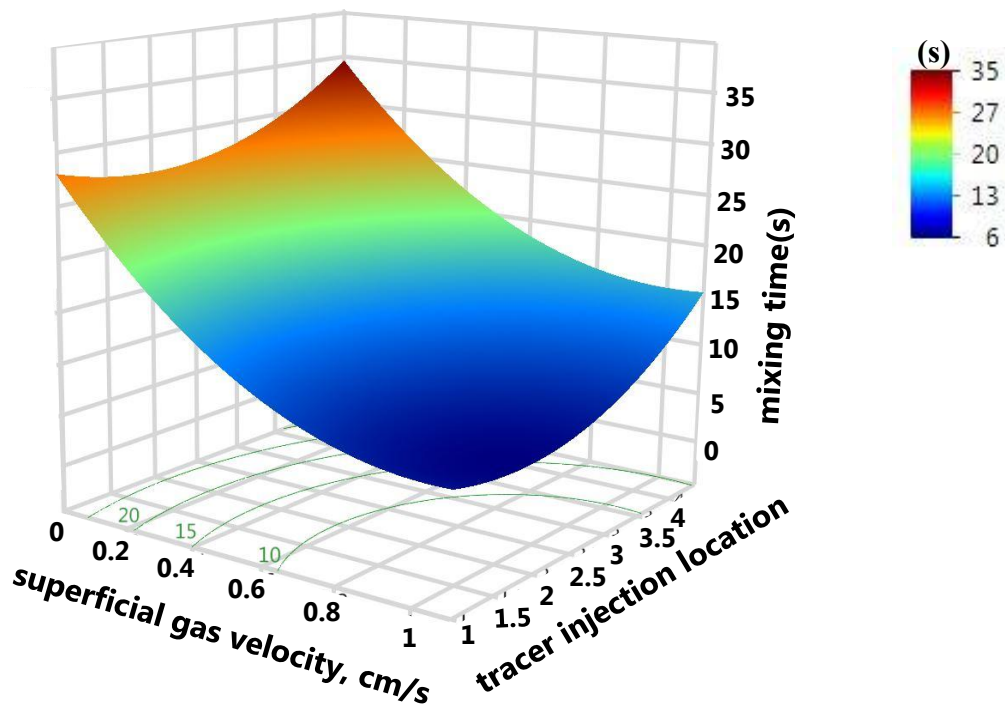


Figure 4.6: Predicted values for mixing time (s) versus their experimental values

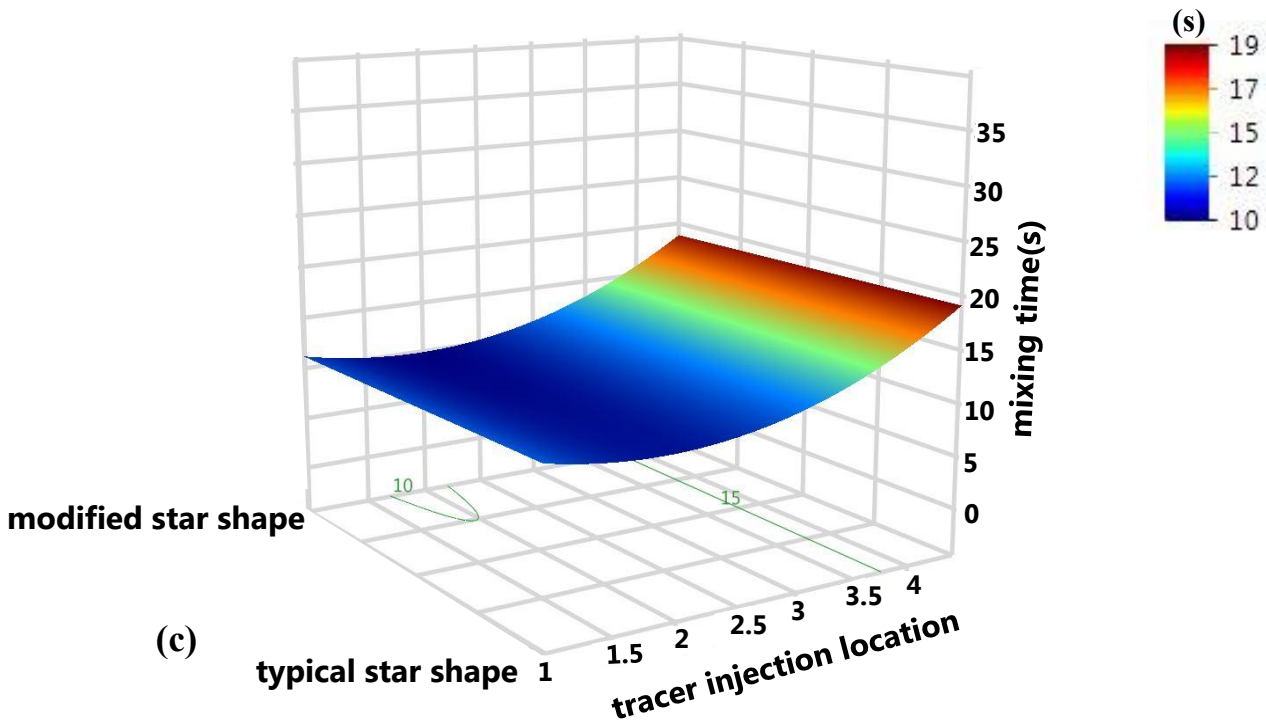
The Three dimensional (3D) figures of response surfaces and two dimensional (2D) contour plots as a function of two variables at a same time are presented, while the other variable was maintained at a constant value. These 3D figures are provided based on the quadratic prediction (equation 4.2). **Figure 4.7** shows the effect of the 3 variables and provided interactions on the mixing time in the 3D format response surface plot. **Figure 4.7(a)** illustrates that by increasing the superficial gas velocity, the mixing time in both types of gas sparger will be decreased about 20 seconds. Since, the comparison of the change rate in sparger types is not significant, there is less than 1 second difference in mixing time and the new designed sparger achieved lower value. The next 3D response surface plot shows the effects of superficial gas velocity and tracer injection location on the mixing time. According to **Figure 4.7(b)**, location 2 and velocity of 1.14 cm/s are providing the lowest mixing time among the levels of these two variables. **Figure 4.7(c)** is presented to investigate the effect of interaction of tracer injection location and gas sparger type. As can be seen in this Figure, the curvature evidenced that location 2 has a lowest mixing time while using the

new designed sparger simultaneously and again the difference between the types of the gas sparger is not significant.





(b)



(c)

Figure 4.7: The response surface is showing the mixing time as a function of two independent variables (the other variables were assumed at respective average level): (a) superficial gas velocity (X_1) and gas sparger type (X_3), (b) superficial gas velocity (X_1) and tracer injection location (X_2), and (c) tracer injection location (X_2) and gas sparger type (X_3).

In compare with other variables, the effect of the superficial gas velocity on the mixing time was higher and the sparger type has the lowest effect. According to presented results, the type of sparger did not provide any significant development for mixing time, so in this case there is no specific difference between the star shape and new designed sparger. The tracer injection location was shown same behaviour for both gas spargers. It was found out that the tracer injection location can develop mixing process without any significant cost and operation. By injecting the tracer at the middle of the vessel, the mixing time experienced a dramatic decrease. Due to this research, the location 4 is not a good choice for injecting tracer into the vessel.

For optimizing the process of mixing time, the first step is considering the preferred objective for each variable and response. To describe the optimum setup of this study, the **Equation 4.2** was minimized. To find the best local minimum value for mixing time, all variables were unified in a general function by JMP software. To reach the lowest mixing time (2.92 s), the optimization process modeling recommended the configuration of optimum values as follows: the superficial gas velocity of 1.14 cm/s, the tracer injection location 2, and the new designed sparger type. **Figure 4.8** illustrated the relationship among superficial gas velocity, tracer injection location and mixing time. As can be seen, it is justified again that the location 2 achieved the lowest value of mixing time at superficial gas velocity of 1.14 cm/s. The mixing time value is decreasing gradually proportional to $11.889v_{s,gas}^{-0.424}$ until it reached a plateau.

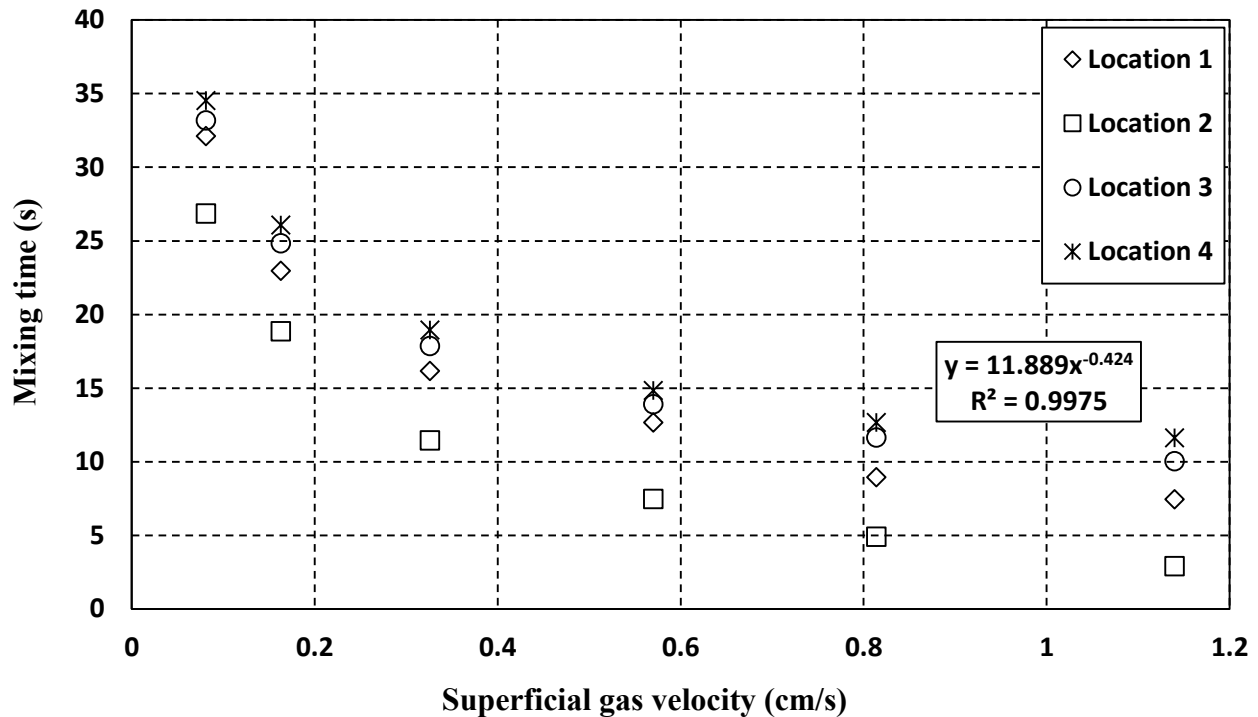


Figure 4.8: Mixing time as function of superficial gas velocity (cm/s) and tracer injection locations for modified star shape sparger.

Although the outcome of this study illustrated that the sparger type could not improve the value of mixing time significantly, each sparger type owes a unique mixing process in compare to other type. In this regard, the velocity vectors of two different velocities are presented in **Figure 4.9** to investigate the trends of mixing in each case. As can be seen in **Figure 4.9(a)**, in case of superficial gas velocity of 1.14 cm/s the liquid velocity vectors shows that there are upward and downward flows at the center of the column and near walls and some circulations at the bottom of the vessel near the sparger area. **Figure 4.9(b)** shows the same flow pattern, while the distribution of upward liquid flow is wider and the circulations at the bottom of the vessel are stronger than typical sparger model.

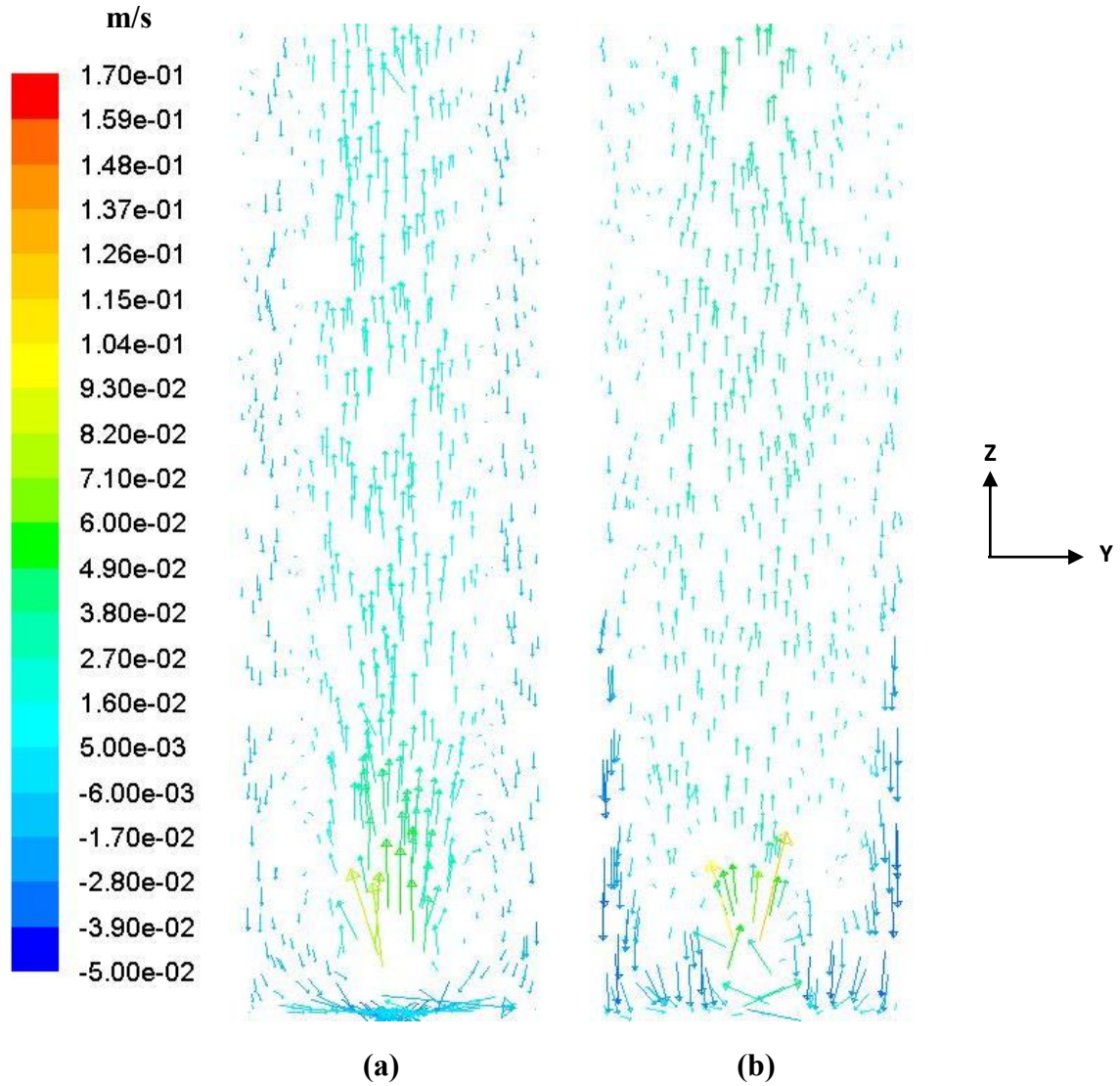


Figure 4.9: Liquid velocity (m/s) vector plots at vertical YZ plane in case of superficial gas velocity of 1.14 cm/s for models with **(a)** typical gas sparger and **(b)** modified gas sparger.

Figure 4.10 presents the pathlines of models with typical and modified gas sparger for superficial gas velocity of 1.14 cm/s with color of gas holdup. As can be seen in this figure, the distribution of bubbles is much wider for case of modified gas sparger in compare with the typical one. In fact, the wider distribution of bubbles in case of modified gas sparger reduced a number of circulations along the vessel (**Figure 4.10 b**). **Figure 4.10(a)** shows that the concentration of bubbles at the

center of the column causes different circulation flows in vessel which can decrease the mixing performance of the bubble column. On the other hand in case of activated sludge bubble column bioreactors, the wider distribution of bubbles provide more interaction between two phases and the rate of reactions can be increased significantly.

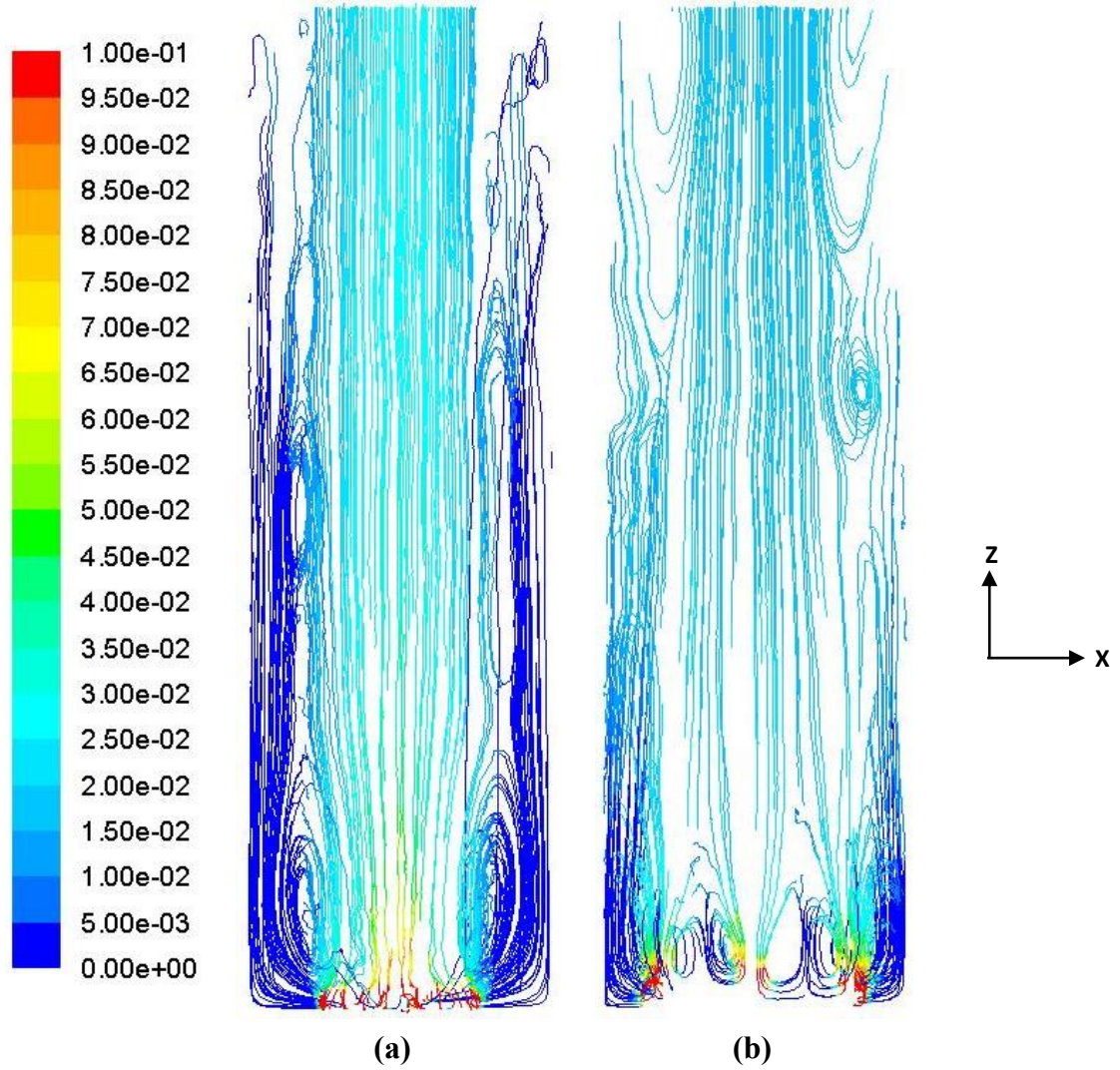


Figure 4.10: The contours of liquid pathline with color of gas holdup at XZ vertical plane in case of superficial gas velocity of 1.14 cm/s for models with (a) typical gas sparger and (b) modified gas sparger.

As mentioned before, the non-Newtonian sludge with a shear thinning behavior used in simulations of this study. The apparent viscosity of shear thinning fluid decreases with rise of shear rate. As can be seen in **Figure 4.11**, the apparent viscosity of typical and modified gas sparger for superficial gas velocity of 1.14 cm/s is compared. In case of typical gas sparger, the value of apparent viscosity at the bottom of the vessel near sparger is lower because of the concentration of bubbles near sparger area and then by increasing distance from sparger it is increased due to radial dispersion of bubbles. On the other hand, the apparent viscosity for case of modified gas sparger is more homogenous in the entire vessel due to better radial distribution of bubbles.

Figure 4.12 illustrated the outcome of the homogenous apparent viscosity for modified sparger in compare with typical sparge. As can be seen the axial liquid velocity in case of typical sparger is concentrated at the center of the column and surrounded by some circulations and in case of modified gas sparger the amount of liquid circulations is much lower.

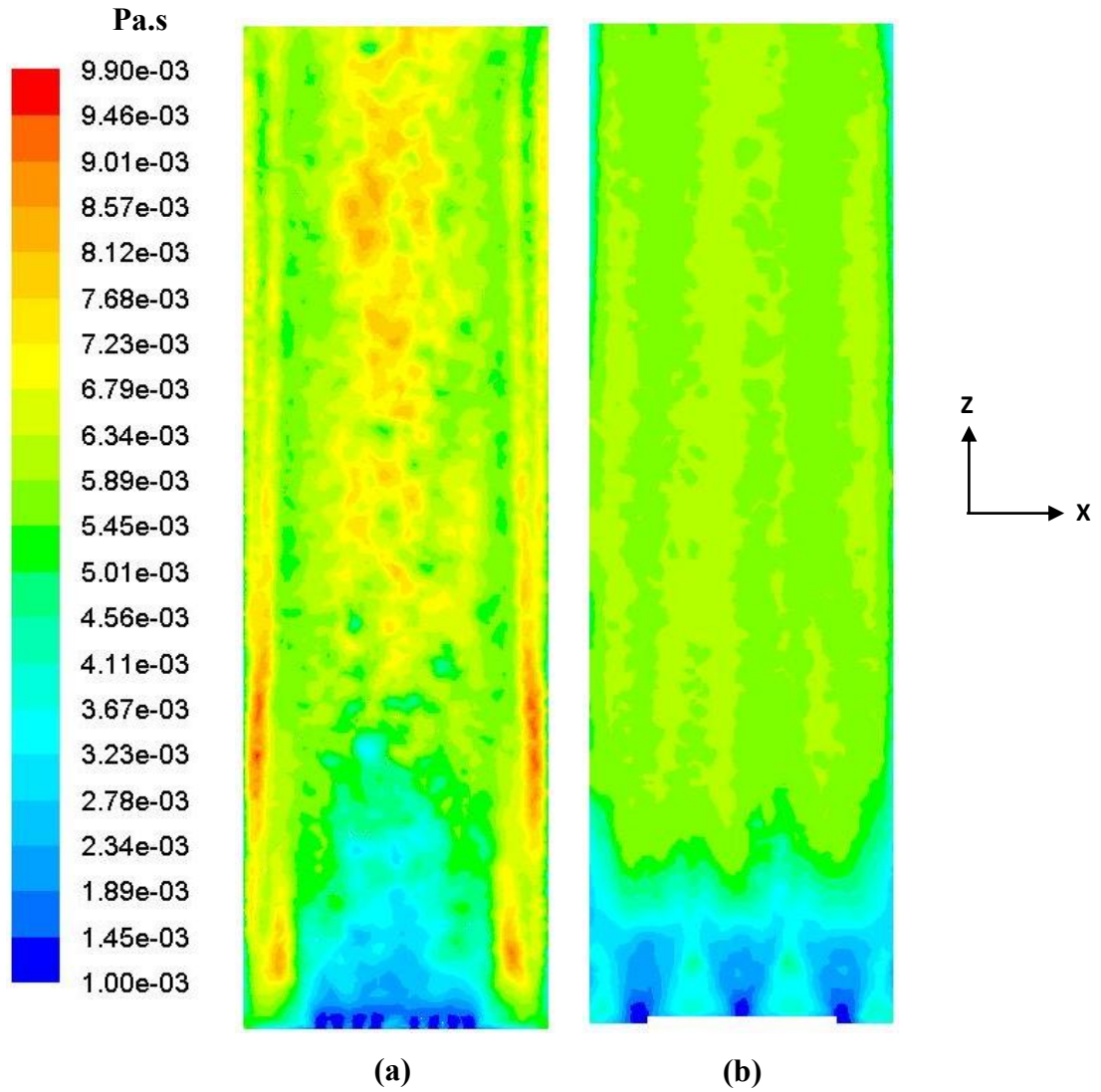


Figure 4.11: The vertical contour (XZ plane) of apparent viscosity (Pa.s) at superficial gas velocity of 1.14 cm/s for models with **(a)** typical gas sparger and **(b)** modified gas sparger.

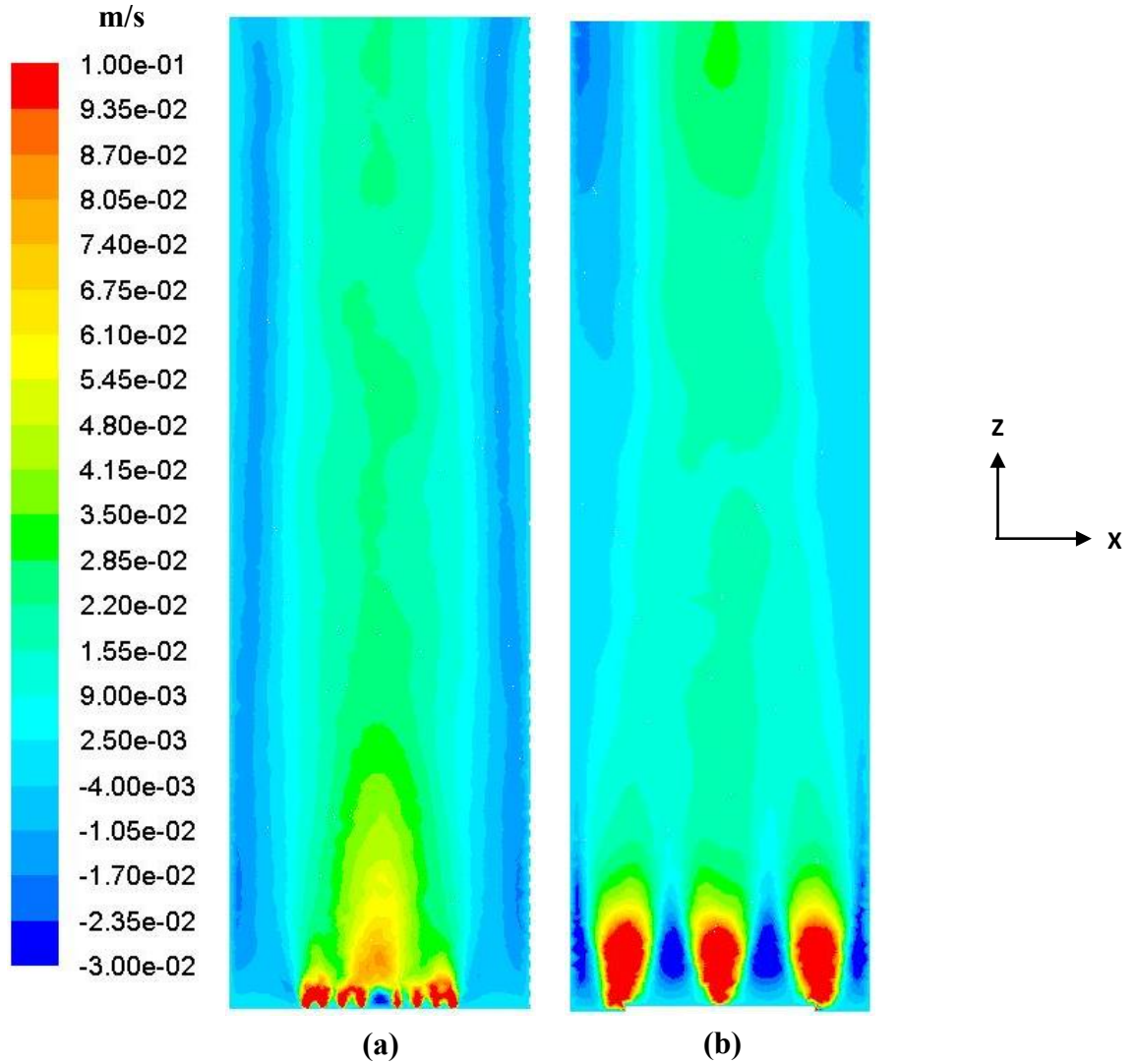


Figure 4.12: The vertical contour (XZ plane) of liquid viscosity (m/s) at superficial gas velocity of 1.14 cm/s for models with (a) typical gas sparger and (b) modified gas sparger.

4.4 Conclusions

The main claim of this study was to optimize the mixing process of the activated sludge bubble column by minimizing the value of the mixing time through CFD. The statistical method of full factorial design was used for estimating the effects of different variables (i.e. superficial gas velocity, tracer injection location and sparger type) individually and the influence of the

interactions between variables on the system. As a result, a quadratic polynomial model was provided with regression coefficient of 90%. It was illustrated that the most effective variable on the system was superficial gas velocity, however the type of the sparger did not show any significant effect on mixing time. In order to achieve the lowest mixing time in this type of bubble column, the tracer must be injected at the middle of the column. Through the interaction effects, the interaction between superficial gas velocity and tracer injection location had more influence on the mixing time process.

Moreover, the trends of mixing for both models at superficial gas velocity of 1.14 cm/s (which is a best rate of velocity due to achieve lower mixing time) were investigated. The radial distribution of bubbles causes the upward flow of liquid phase and the liquid circulations was occurred between the central upward flow and downward flow of sludge near wall. In case of the model with modified gas sparger, the amount of liquid circulations along the vessel was smaller because of the wider radial distribution of bubbles. Totally, there was no significant difference among two models mixing time, but the trend of mixing was completely different.

4.5 Notations

The following symbols are used in this chapter:

ASP = activated sludge process

CFD = computational fluid dynamics

K = turbulent kinetic energy, m^2/s^2

K = consistency coefficient, $Pa \cdot s^n$

n = power-law index

RMS = root-mean-square

Greek letter

ε = gas holdup, non-dimensional

Chapter 5: Overall Conclusions and Recommendations for Future Research

5.1 Conclusions

In this study, the Computational Fluid Dynamic (CFD) technique was employed to provide a complete investigation about the activated sludge bioreactors.

In Chapter 3 the effect of rate of superficial gas velocity, tracer injection location, and sparger type on bubble column flow field was presented to predict flow behavior during operation. In this regard, the liquid axial velocity profile, the radial and vertical distribution of gas holdup, and the radial distribution of axial gas velocity for case of typical gas sparger was investigated. The liquid flow pattern illustrated the presence of the amount of liquid circulations along the process vessel. Moreover, the radial distribution of gas holdup showed that the bubbles were concentrated at the middle of the column. In order to provide a wider distribution of gas holdup and decrease the amount of liquid circulations, the modified gas sparger was presented. The results of this chapter could obtain in some industries such as wastewater treatment to design and optimize the bubble column bioreactor systems. In this CFD investigation the following results were found:

The CFD model with star shape gas sparger:

- The value of gas holdup and liquid axial velocity was risen with the increase of superficial gas velocity.
- The axial liquid velocity profile predicted as a parabolic shape that the maximum value was located at the center axis of the column and showed a downward flow near wall.

- The parabolic shape gas holdup profile illustrated that the bubbles concentrated at the middle of the column.
- In case of lower superficial gas velocities a long liquid circulation was created between the center upward flow and the near wall downward flow. However, the increase of superficial gas velocity was reduced the amount of liquid circulations along the vessel.
- The mixing time value was decreased due to growth of superficial gas velocity and was proportional to $12.117v_{s, \text{gas}}^{-0.426}$ until it reached almost a plateau.
- The tracer injection location parameter showed a significant effect on the value of the mixing time.
- Tracer injection location 2 (which is located at the middle of the column) achieved lowest mixing time value among all four locations.
- Tracer injection location 4 (which is located at the bottom and corner of the vessel) achieved the worst mixing time.

The CFD model with star shape gas sparger:

- The increase of superficial gas velocity was improved the rate of gas holdup and liquid axial velocity.
- The radial distribution of gas hold up was significantly wider than the model with star shape sparger and also the vertical distribution of bubbles was improved significantly.
- The gas holdup profile was not concentrated at the middle of the column in this case, and the bubbles combined together at the center of the column in higher axial positions than sparger.
- The rise of superficial gas velocity decreased the value of the mixing time.
- The tracer injection location showed a significant effect on the mixing time value.

- The tracer injection location 2 provided the lowest mixing time and location 4 provided the highest value.
- The value of overall gas holdup experienced a great increase in this case especially for higher rates of superficial gas velocities.
- In this case the value of overall gas holdup was 1.45 to 2 times more than model with the typical star shape gas sparger.

In chapter 4, the evaluation of the mixing performance of non-Newtonian activated sludge in activated sludge bioreactor was investigated. In this regard, the effect of superficial gas velocity, sparger type, tracer injection location, and the interaction of these parameters studied by full factorial design statistical method. Moreover, the trends of mixing in each models was discussed to explore the mixing process. The statistical analysis and investigations on mixing process provided following results:

- The full factorial design statistical method provided a quadratic polynomial model with the regression coefficient of 0.9.
- The model variables consisted of superficial gas velocity, tracer injection location, and sparger type and the response factor was as mixing time.
- The analysis showed that the superficial gas velocity had stronger effect on the mixing time value among the other variables.
- According to statistical model, the tracer injection location and sparger type had lower effects on the mixing time.
- The provided velocity vector plots by CFD simulations illustrated that there is a higher liquid axial velocity value at axial locations near sparger in both models.

- In case of model with modified gas sparger, the upward liquid axial velocity was much wider than the case of model with the typical star shape gas sparger and also the amount of liquid circulations was lower.
- The investigation of sludge flow pathlines and the gas holdup distribution showed that the higher rate of radial bubble dispersion reduces the amount of liquid circulations in vessel.
- The increase of superficial gas velocity provides more flow rate of gas phase that can produce more shear rate among the liquid phase in mixing vessel and improve the mixing performance of the bubble column bioreactor.

5.2 Recommendations for Future Research

Since the importance of the bubble column in industries, further research could improve our current research. The first possible applied research topic can be simulate a CFD model with the sludge contains another rheological properties to investigate the effect of MLSS on the mixing process and hydrodynamics. In the other interesting case, the effect of rotational motion of the gas sparger on the flow behavior can be discussed. This study illustrated the effect of tracer injection location on mixing time which can be other valuable topic. The CFD has ability to simulate the shear thickening materials, the effect of superficial gas velocity on the flow behavior of this kind of fluids can be investigated in further researches.

References

- Abusam, A, Keesman, K.J., Spanjers, H., Straten, G van, Meinema, K., 2002. A procedure for benchmarking specific full-scale activated sludge plants used for carbon and nitrogen. IFAC Proceedings Volumes Volume 35, Issue 1, Pages 29-34.
- Aguilera-Alvarado, A. F., Pérez-Alonso, R., Irene Cano-Rodríguez, M., Uribe-Ramírez, A. R., Enrique Aguilar-Pérez, G., and Lugo-Martínez, J. R., 2013. CFD Study of the Weeping and Flooding Effects in a Nonsymmetrical Sparger in a Stirred Tank. *Industrial Engineering Chemistry Resources*, Volume 52, Issue 5, Pages 2141–215.
- Al-Oufi, F.M., Rielly, C.D., Cumming, I.W., 2011. An experimental study of gas void fraction in dilute alcohol solutions in annular gap bubble columns using a four-point conductivity probe. *Chemical Engineering Science* Volume 66, Issue 23, Pages 5739–5748.
- Amoudry, L. O., 2014. Extension of $k-\omega$ turbulence closure to two-phase sediment transport modelling: Application to oscillatory sheet flows. *Advances in Water Resources*, Volume 27, Pages 110-121.
- Arbizu, P.I., Luis Pérez, C., J., 2003. Surface roughness prediction by factorial design of experiments in turning processes. *Journal of Materials Processing Technology*, Volumes 143–144, Pages 390–396.
- Arcuri, E., Slaff, G., and Greasham, R., 1986. Continuous production of thicnamcin in immobilized cell systems. *Biotechnology BioEngineering*, Volume 28, Pages 842-849.
- Ardern, E., Lockett, W., T., 1914. Experiments on the oxidation of sewage without the aid of filters. *Journal of Chemical technology and biotechnology*, Volume 33, Issue 10, Pages 523.
- Arrowsmith, D., Bott, A., Bush, P., 2006. Development of a compact urea-SCR + CRTTM system for heavy-duty diesel using a design of experiments approach reprinted from diesel exhaust. . SAE Technical Paper, Volume 1, Pages 6-36.

Babaei, R., Bonakdarpour, B., Ein-Mozaffari, F., 2015. Analysis of gas phase characteristics and mixing performance in an activated sludge bioreactor using electrical resistance tomography. *Chemical Engineering Journal*, Volume (279), Pages 874-884.

Baron, G., V., Willaert, R., G., De Backer, L., 1996. Immobilised cell reactors: In *Immobilised Living Cell Systems: Modelling and Experimental Methods*. Edited by R.G. Wilaert, G.V. Baron and L. De backer, John Wiley and Sons Ltd.

Basheer, A., A., Subramaniam, P., 2012. Hydrodynamics, mixing and selectivity in a partitioned bubble column. *Chemical Engineering Journal*, Volume 187, Pages 261-274.

Baker, J.L.L., 1965. Flow regime transitions at elevated pressures in vertical two-phase flow. Argonne National Laboratory Report No. ANL-7093.

Bennett, A.W., Hewitt, G.F., Karsey, H.A., Keeys, R.K.F., Lacey, P.N.C., 1965. Flow visualisation studies of boiling at high pressure. *Proceeding of the Institution of Mechanical Engineers*, Volume 180, Issue 3, Pages 1-11.

Blazek, J., 2005. *Computational Fluid Dynamics: Principles and Applications*. 2nd edition. Amsterdam: Elsevier Inc.

Bolton.G.T., Hooper.K.W., Mann.R., Stitt.E.H.,2004. Flow distribution and velocity measurement in a radial flow fixed bed reactor using electrical resistance tomography. *Chemical Engineering science* Volume 59, Issue 10, Pages 1989–1997.

Bombardelli, F.A., Buscaglia, G., Rehmann, C C.R., Rincón, L.E., García, M.H., 2007. Modeling and scaling of aeration bubble plumes: A two-phase flow analysis. *Journal of Hydraulic Research*, Volume 45, Issue 5.

Borchers, O., Busch, C., Sokolichin, A., Eigenberger, G., 1999. Applicability of the standard $k-\epsilon$ turbulence model to the dynamic simulation of bubble columns Part II: Comparison of detailed experiments and flow simulation. *Chemical Engineering Science*, Volume 54, Pages 5927–5935.

Bove, s., Solberg, T., Hjertager, B., H., 2005. A novel algorithm for solving population balance equations: the parallel parent and daughter classes. Derivation, analysis and testing. *Chemical Engineering Science*, Volume 60, Issue 5, Pages 1449–1464.

Bunner, B., Tryggvason, G., 1998. Direct numerical simulation of large three-dimensional bubble systems. In: Proceedings of the 1998 ASME Fluids Engineering Division Summer Meeting, Washington, June.

Bunner, B., Tryggvason, G., 1999. Direct numerical simulations of three dimensional bubbly flows. *Physics of Fluids*, Volume 11, Pages 1967–1969.

Buwa, V.V., V.V., Ranade., 2002. Dynamics of gas–liquid flow in a rectangular bubble column: experiments and single/multi-group CFD simulations. *Chemical Engineering Science* Volume 57, Issues 22–23, Pages 4715–4736.

Brannock, M., Wang, Y., Leslie, G., 2010. Mixing characterization of full-scale membrane bioreactors: CFD modeling with experimental validation. *Water Res*, Volume 44, Issue:10, Pages 3181-3191.

Braak, E., Alliet, M., Schetritea, S., Albasia, C., 2011. Aeration and hydrodynamics in submerged membrane bioreactors. *Journal of Membrane Science*, Volume 379, Issues 1–2, Pages 1–18.

Capetillo, A., Ibarra, F., 2017. Multiphase injector modelling for automotive SCR systems: A full factorial design of experiment and optimization. *Computers and Mathematics with Applications*, In Press, Corrected Proof-Note to users.

Chakraborty, D., Guha, M., Banerjee, P., K., 2009. CFD simulation on influence of superficial gas velocity, column size, sparger arrangement, and taper angle on hydrodynamics of the column flotation cell. *Chemical Engineering Communications*, Volume 196, Issue 9, Pages 1102-1116.

Chen W, Hasegawa T, Tsutsumi A, Otawara K, Shigaki Y., 2003. Generalized dynamic modeling of local heat transfer in bubble columns. *Chemical Engineering Journal*, Volume 96, Pages 37–44.

Chisti, M.,Y., Halard, B., Moo-Young, M., 1988. Liquid circulation in airlift reactors. *Journal of Chemical Engineering Science*, Volume 43, Issue 3, Pages 451-457.

Cockx, A., Do-Quang, Z., Audic, J.M., Line, A., Roustan, M., 2001. Global and local mass transfer coefficients in waste water treatment process by computational fluid dynamics. *Chemical Engineering Process*, Volume 40, Issue 2, Pages 187-194.

Corneliussen, S., Couput, J.P., Dahl, E., Dykesteen, E., Frøysa, K.E., Malde, E., Moestue, H., Moksnes, P.O., Scheers, L., Tunheim, H., 2005. Handbook of multiphase flow metering. Nor. Soc. Oil Gas Meas.

Clayton T. Crowe, Clayton T. Crowe, 2005. Multiphase Flow Handbook.

Davis ML, Cornwell DA (1991). Introduction to Environmental Engineering, 2nd Edition. McGraw-Hill, Inc. USA.

Datsevich, L., B., Mukhortov, D., A., 2007. Pre-saturation in multiphase fixed-bed reactors as a method for process intensification/reactor minimization. Journal of Catalysis Today, Volume 120, Issue 1, Pages 71–77.

Daly, J., G., Patel, S., A., Bukur, D., B., 1992. Measurement of Gas Holdups and Sauter Mean Bubble Diameters in Bubble Column Reactors by Dynamic Gas Disengagement Method. Chemical Engineering Science, Volume 47(13-14), Pages 3647-3654.

Deckwer WD, Louisi Y, Zaidi A, Ralek M., 1980. Hydrodynamic properties of the Fisher–Tropsch slurry process. Ind Eng Chem Process, Volume 19, Pages 699–708.

Deen, N.G., Solberg, T., Hjertager, B.H., 2001. Large eddy simulation of gas–liquid flow in a square cross-sectioned bubble column. Chemical Engineering Science, Volume 56, Pages 6341–6349.

Degaleesan S, Dudukovic M, Pan Y., 2001. Experimental study of gas-induced liquid-flow structures in bubble columns. AIChE Journal, Volume 47, Pages 1913–31.

Degre'mont, 1990. Water treatment handbook. Sixth edition, Degre'mont, France.

Delnoij, E., Lammers, F., Kuipers, J., van Swaaij, W., 1997. Dynamic simulation of dispersed gas–liquid two-phase flow using a discrete bubble model. Chemical Engineering Science, Volume 52, Pages 1429–1458.

Delnoij, E., Kuipers, J.A.M., van Swaaij, W.P.M., 1999. A three-dimensional CFD model for gas–liquid bubble columns. Chemical Engineering Science Volume 54, Issues 13–14, Pages 2217-2226.

Dhotre, M.T., Joshi, J.B., 2004. Two-dimensional CFD model for prediction of pressure drop, heat transfer coefficient in bubble column reactors. *Chemical Engineering Research and Design*, Volume 82, Pages 689–707.

Dhotre, M.T., Niceno, B., Smith, B.L., 2008. Large eddy simulation of a bubble column using dynamic sub-grid scale model. *Journal of Chemical Engineering*, Volume 136, pages 337–348.

Ekambara, K., Dhotre, M.T., Joshi, J.B., 2005. CFD simulations of bubble column reactors: 1D, 2D and 3D approach. *Chemical Engineering Science*, Volume 60, Pages 6733 – 6746.

Ekambara, K., Joshi, J.B., 2003a. CFD simulation of mixing and dispersion in bubble column reactors. *Chemical Engineering Research and Design*, Volume 81. Pages 987–1002.

Ekambara, K., Joshi, J.B., 2003b. CFD simulations of residence time distribution and mixing in bubble column reactors. *Canadian Journal of Chemical Engineering*, Volume 81, Pages 669–676.

Esmaeeli, A., Tryggvason, G., 1998. Direct numerical simulations of bubbly flows. Part I. Low Reynolds number arrays. *Journal of Fluid Mechanics*, Volume 377, Pages 313–345.

Esmaeeli, A., Tryggvason, G., 1999. Direct numerical simulations of bubbly flows. Part II. Moderate Reynolds number arrays. *Journal of Fluid Mechanics*, Volume 385. Pages 325–358.

Essemiani, K., Vermande, S., Marsal, S., Phan, L. and Meinhold, J., 2004. Optimisation of WWTP units using CFD – A tool grown for real scale application, Prague.

Essemiani, K., De Traversay, C., Gallot, J., C., 2004. Computational-fluid-dynamics (CFD) modelling of an industrial crystallizer: application to the forced-circulation reactor. *Biotechnology and Applied Biochemistry*, Volume 40, Pages 235–241.

Fathi Roudsari, S., Turcotte., G., Dhib, R., Ein-Mozaffari, F., 2012. CFD modeling of the mixing of water in oil emulsions. *Computers and Chemical Engineering*, Volume 45, Pages 124-136.

Fayolle, Y., Cockx, A., Gillot, S., Roustan, M., Heduit, A., 2007. Oxygen transfer prediction in aeration tanks using CFD. *Chemical Engineering Science*, Volume 62, Issue 24. Pages 7163-7171.

Fletcher, D., F., McClure, D., D., Kavanagh, J., M., Barton, G., W., 2016. CFD simulation of industrial bubble columns: Numerical challenges and model validation successes. *Applied Mathematical Modelling*, Volume 44, Pages 25–42.

Fluent Corporation, 2006. *Fluent 6.3 User's Guide*, Lebanon, NH, USA. Gillot, S., Heduit, A., 2008. Prediction of alpha factor values for fine pore aeration systems. *Water Sci. Technol*, Volume 57 (8). Pages 1265-1269.

Fan, L.S., 1989. *Gas liquid-solid fluidization engineering*. Butterworth publishers.

Fransolet, E., Crine, M., Marchot, P., Toye, D., 2005. Analysis of gas holdup in bubble columns with non-Newtonian fluid using electrical resistance tomography and dynamic gas disengagement technique. *Chemical Engineering Science*, Volume 60, Issue 22, Pages 6118–6123.

Ghasemi, S., Sohrabi, M., Rahmani, M., 2009. A comparison between two kinds of hydrodynamic models in bubble column slurry reactor during Fischer-Tropsch synthesis: Single-bubble class and two-bubble class. *Chemical Engineering Research & Design*, Volume 87, Pages 1582-1588.

Ghajar, A., J., 2005. Non-boiling heat transfer in gas-liquid flow in pipes – a tutorial. *Journal of the Brazilian Society of Mechanical Sciences and Engineering*, volume 27, no. 1.

Gheni, S., Abdulaziz, Y., A., Al-Dahhan, M., H., 2016. Effect of L/D Ratio on Phase Holdup and Bubble Dynamics in Slurry Bubble Column using Optical Fiber Probe Measurements. *International Journal of Chemical Reactor Engineering*, Volume 14, Issue 2, Pages 124-146

Glover, G.C., Printemps, C., Essemiani, K., Meinhold, J., 2006. Modelling of wastewater treatment plants – how far shall we go with sophisticated modelling tools? *Water Science and Technology*, Volume 53, Issue 3. Pages 79–89.

Godbole, S. P., M. F. Honath, and Y. T. Shah., 1982 “Gas Holdup Structure in Highly Viscous Newtonian and Non-Newtonian Liquids in Bubble Columns,” *Chemical Engineering Commun*, Volume 18, Page 119.

Govan, A.H., 1990. *Modelling of Vertical Annular and Dispersed Two-Phase Flows*, Ph.D. thesis, Imperial College, London.

Gouricha, B., Vialb, Ch., El Azhera, N., Belhaj Soulamic, M., Ziyadd, M., 2008. Influence of hydrodynamics and probe response on oxygen mass transfer measurements in a high aspect ratio bubble column reactor: Effect of the coalescence behaviour of the liquid phase". *Biochemical Engineering Journal*, Volume 39, Issue 1, Pages 1–14.

Gottipati, R., Mishra, S., 2010. Process optimization of adsorption of Cr (VI) on activated carbons prepared from plant precursors by a two-level full factorial design. *Chemical Engineering Journal*, Volume 160, Pages 99–107.

Gresch, M., Armbruster, M., Braun, D., Gujer, W., 2011. Effects of aeration patterns on the flow field in wastewater aeration tanks. *Water Res*, Volume 45, Issue 2, Pages 810-818.

Grevskott, S., Sannæs, B.H., Duduković, M.P., Hjarbo, K.W., Svendsen, H.F. 1996. Liquid circulation, bubble size distributions, and solids movement in two- and three-phase bubble columns. *Chemical Engineering Science* Volume 51, Issue 10, Pages 1703-1713.

Haque, M.W., Nigam, K.D.P., Joshi, J.B., 1986. Optimum gas sparger design for bubble columns with a low height to diameter ratio. *Chemical Engineering Journal*, Volume 33, Pages 63–69.

Han, R., Ding, D., Xu, Y., Zou, W., Wang, Y., Li, Y., Zou, L., 2008. Use of rice husk for the adsorption of congo red from aqueous solution in column mode. *Bioresour. Technol*, Volume 99. Pages 2938–2946.

Hawkesa, N.J., Lawrenceb, C.J., Hewitt, G.F., 2000. Studies of wispy-annular flow using transient pressure gradient and optical measurements. *International Journal of Multiphase Flow*, Volume 26. Pages 1565-1582.

Hills, J., 1974. "Radial Non-uniformity of Velocity and Voidage in a Bubble Column", *Trans. Instn. Chemical Engineering*, Volume 52. Pages 1–9.

Hooshyar, N., Fatemi, S., Rahmani, M., 2009. Mathematical modeling of isochloroacetic acid synthesis in an industrial slurry bubble column. *International Journal of Chemical Reactor Engineering*, Volume 7, Page 25.

Hugmark, G., A., 1967. Holdup and mass transfer in bubble columns. *Industrial Engineering and Chemical Process Design and Development*, Volume 6, Pages 218-220.

Hunt, J.C.R., Auton, T.R., Sene, K., Thomas, N.H., Kowe, R., 1987. ICHMT International seminar on transient phenomena in multiphase flow, Dubrovnik, Yugoslavia, Pages 103–125.

Hyndman, G. L., Larachi, F., Guy, C., 1997. Understanding gas-phase hydrodynamics in bubble columns: a convective model based on kinetic theory. *Chemical Engineering science*, Volume 52. Pages 63-77.

Ishii, M., Zuber, N., 1979. Drag coefficient and relative velocity in bubbly, droplet or particulate flows. *AIChE Journal*, Volume 25, Issue 5, Pages 843–855.

Jiang, X., Yang, N., Zhu, J., Yang, B., 2015. On the single and two-bubble class models for bubble column reactors. *Chemical Engineering Science*, Volume 123, Pages 514–526.

Jin, B., Lant, P., 2004. Flow regime, hydrodynamics, floc size distribution and sludge properties in activated sludge bubble column, air-lift and aerated stirred reactors. *Chemical Engineering Science*, Volume 59. Pages 2379–2388.

Joshi, J.B., 2001. Computational flow modeling and design of bubble column reactors. *Chemical Engineering Science*, Volume 56. Pages 5893–5933.

Joshi, J., B., Sharma, M., M., 1979. A circulation cell model for bubble columns. *Transaction Institute of Chemical Engineering*, Volume 57, Pages 244-251.

Kantarci, N., Borak, F., Ulgen, K. O., 2005. Bubble column reactors. *Process Biochemistry*, Volume 40. Pages 2263–2283.

Karpinska, M. A., Bridgeman, J., 2016. CFD-aided modelling of activated sludge systems - A critical review. *Water Research*, Volume 88. Pages 861-879.

Karpinska Portela, A.M., 2013. New Design Tools for Activated Sludge Process (PhD thesis). FEUP, University of Porto, Porto, Portugal.

Kawagoe, K., T. Inoue, K. Nakao, and T. Otake., 1976 “Flow Patterns and Gas Holdup Conditions in Gas-Sparged Contactors”, *International Chemical Engineering*, Volume 16, Pages 176- 183.

Kawase, Y., Moo-Young, M., 1987. Heat transfer in bubble column reactors with Newtonian and non-Newtonian fluids. *Chemical Engineering Research and Design*, Volume 65, Pages 121-126.

Kojima, H., Anjyo, H., Mochizuki, Y., 1986. Axial Mixing in Bubble Column with Suspended Solid Particles. *Journal of Chemical Engineering of Japan*, Volume 19, Issue 3, Pages 232-234.

Krishna, R., Urseanu, M.I., van Baten, J.M., Ellenberger, J., 1999. Influence of scale on the hydrodynamics of bubble columns operating in the churn-turbulent regime: experiments vs. Eulerian simulations. *Chemical Engineering Science*, Volume 54, Pages 4903–4911.

Krishna, R., Urseanu, M.I., van Baten, J.M., Ellenberger, J., 2000. Liquid phase dispersion in bubble columns operating in the churn-turbulent flow regime. *Chemical Engineering Journal*, Volume 78, Pages 43–51.

Krishna, R., Van Baten, J.M., 2001. Scaling up bubble column reactors with the aid of CFD. *Transactions of the Institute of Chemical Engineers*, Volume 79, Pages 283–309.

Krishna, R., Van Baten, J.M., 2003. Mass transfer in bubble columns. *Catalytic Today*, Volume 79–80, Pages 67–75.

Kulkarni, A.A., Ekambara, K., Joshi, J.B., 2007. On the development of flow pattern in a bubble column reactor: experiments and CFD. *Journal of Chemical Engineering*, Volume 62, Pages 1049–1061.

Kulkarni, V.A., Badgandi, V. S., Joshi, J.B., 2009. Design of ring and spider type spargers for bubble column reactor: Experimental measurements and CFD simulation of flow and weeping. *Chemical Engineering Research and Design*, Volume 87, Pages 1612–1630.

Kulkarni, A.V., 2010. Design of pipe/ring type of sparger for bubble column reactor. *Chemical Engineering Technology*, Volume 33 Issue 6, Pages 1015–1022.

Laborde-Boutet, C., Larachi, F., Dromard, N., Delsart, O., Schweich, D., 2009. CFD simulation of bubble column flows: Investigations on turbulence models in RANS approach. *Chemical Engineering Science* Volume 64, Issue 21, Pages 4399–4413.

Lain, S., Broder, D., Sommerfeld, M., 1999. Experimental and numerical studies of the hydrodynamics in a bubble column using the Euler–Lagrange approach. *Chemical Engineering Science*, Volume 54, Pages 4913.

Lain, S., Broder, D., Sommerfeld, M., Goz, M.F., 2002. Modelling hydrodynamics and turbulence in a bubble column using the Euler–Lagrange procedure. *International Journal of Multiphase Flows* Volume 28, Pages 1381–1407.

Lakehal, D., Smith, L.B., Milelli, M., 2002. Large-eddy simulation of bubbly turbulent shear flows. *Journal of Turbulence*, Volume 3, Pages 1–21.

Lapin A, Paaschen T, Junghans K, Lübbert A., 2002. Bubble column fluid dynamics, flow structures in slender columns with large-diameter ring-spargers. *Chemical Engineering Science*, Volume 57, Pages 1419–24.

Larachi, F., Grandjeana, B., P., A., Chaouki, J., 2003. Mixing and circulation of solids in spouted beds: particle tracking and Monte Carlo emulation of the gross flow pattern. *Chemical Engineering Science*, Volume 58, Issue 8, Pages 1497–1507.

Launder, B.C., Reece, G.J. and Rodi, W. 1975 Progress in the development of a Reynolds stress turbulence closure. *Journal of Fluid Mechanics*, Volume 68, Pages 537-566.

Le Moullec, Y., Potier, O., Gentric, C., Pierre Leclerc, J., 2008. Flow field and residence time distribution simulation of a cross-flow gas-liquid wastewater treatment reactor using CFD. *Chemical Engineering Science*, Volume 63, Issue:9, Pages 2436-2449.

Le Moullec, Y., Potier, O., Gentric, C., Leclerc, J.P., 2011. Activated sludge pilot plant: comparison between experimental and predicted concentration profiles using three different modelling approaches. *Water Resources*, Volume 45, Issue 10, Pages 3085-3097.

Lei, L., Ni, J., 2014. Three-dimensional three-phase model for simulation of hydrodynamics, oxygen mass transfer, carbon oxidation, nitrification and denitrification in an oxidation ditch. *Water Resources*, Volume 53, Pages 200-214.

Li H, Prakash A., 2002. Analysis of flow patterns in bubble and slurry bubble columns based on local heat transfer measurements. *Chemical Engineering Journal*, Volume 86, Pages 269–76.

Lin, T.J., Reese, J., Hong, T., Fan, L.S., 1996. Quantitative analysis and computation of two-dimensional bubble columns. *American Institute of Chemical Engineers Journal*, Volume 42, Pages 301–318.

Lin TJ, Wang SP., 2001. Effects of macroscopic hydrodynamics on heat transfer in bubble columns. *Chemical Engineering Science*, Volume 56, Pages 1143–1149.

Loth, E., 2008. Drag of non-spherical solid particles of regular and irregular shape. *Powder Technology* Volume 182, Issue 3, Pages 342–353.

Maalej S, Benadda B, Otterbein M., 2003. Interfacial area and volumetric mass transfer coefficient in a bubble reactor at elevated pressures. *Chemical Engineering Science*, Volume 58, Pages 2365–2376.

Mann, R., Dickin, F., J., Wang, M., Dyakowski, T., Williams. R., A., Edwards, R., B., Forrest, A., E., Holden, P., J., 1997. Application of electrical resistance tomography to interrogate mixing process at plant scale. *Chemical Engineering Science*, Volume 52, Pages 2087-2097.

Manish, P., Majumder, S., B., 2009. Quality of mixing in a downflow bubble column based on information entropy theory. *Journal of Chemical Engineering Science*, volume 64, issue 8, pages 1798–1805.

Metcalf and Eddy Inc., 1995. *Wastewater Engineering: Treatment, disposal, and reuse*, 3rd edition. (G. Tchobanoglous and F. L. Burton, ed.) Tata McGraw-Hill Publishing Company Ltd, New Delhi.

Montantea, G., Moštkb, M., Jahodab, M., Magelli, F., 2005. CFD simulations and experimental validation of homogenisation curves and mixing time in stirred Newtonian and pseudoplastic liquids. *Chemical Engineering Science*, Volume 60, Issues 8–9, Pages 2427–2437.

Moustiri, S., Hebrard, G., Thakre, S., S., Roustan, M., 2001. A unified correlation for predicting liquid axial dispersion coefficient in bubble columns. *Chemical Engineering Science*, Volume 56, Pages 1041-1047.

McClure, D., D., Aboudha, N., Kavanagh, J., M., Fletcher, D., F., Barton G. W., 2015. Mixing in bubble column reactors: Experimental study and CFD modeling. *Chemical Engineering Journal*, Volume 264, Pages 291–301.

Mudde, R.F., Simonin, O., 1999. Two and three dimensional simulations of a bubble plume using a two fluid model. *Chemical Engineering Science*, Volume 54, Pages 5061–5069.

Mudde, R.F., Lee, D.J., Reese, J., Fan, L.S., 1997. Role of coherent structures on Reynolds stresses in a 2D bubble column. *American Institute of Chemical Engineers Journal*, Volume 43, Pages 913–926.

Naessens, W., Maere, T., Nopens, L., 2012. Critical review of membrane bioreactor models – Part 1: Biokinetic and filtration models. *Bioresource Technology* Volume 122, Pages 95–106.

Naessens, W., Maere, T., Ratkovich, N., Vedantam, S., Nopens, I., 2012. Critical review of membrane bioreactor models – Part 2: Hydrodynamic and integrated models. *Bioresource Technology* Volume 122, Pages 107–118.

Ndinis, N., V., Wiley, D., E., Fletcher, D., F., 2005. Computational Fluid Dynamics Simulations of Taylor Bubbles in Tubular Membranes: Model Validation and Application to Laminar Flow Systems. *Chemical Engineering Research and Design* Volume 83, Issue 1, Pages 40-49.

Ozturk SS, Schumpe A, Deckwer WD., 1987. Organic liquids in a bubble column: holdups and mass transfer coefficients. *AIChE Journal*, Volume: 33, Pages 1473–80.

Pakzad, L., 2007. Using electrical resistance tomography (ERT) and computational fluid dynamics (CFD) to study the mixing of pseudoplastic fluids with a SCABA 6SRGT impeller. Ryerson University, Toronto, Ontario, Canada.

Pakzad, L., Ein-Mozaffari, F., Upreti, S., R., Lohi, A., 2013. Evaluation of the mixing of non-Newtonian biopolymer solutions in the reactors equipped with the coaxial mixers through tomography and CFD. *Chemical Engineering Journal*, Volume 215–216, Pages 279–296.

Pan, Y., Dudukovic, M.P., Chang, M., 2000. Numerical investigations of gas-driven flow in two-dimensional bubble columns. *American Institution of Chemical Engineers Journal*, Volume 46, Issue:3, Pages 434–449.

Pan, Y., Dudukovic, M.P., Chang, M., 1999. Dynamic simulation of bubble flow in bubble columns. *Chemical Engineering Science*, Volume 54, Pages 2481–2489.

Pavan, F., A., Gushikem, Y., Mazzocato, A., C., Dias, S., L., P., Lima, E., C., 2007. Statistical design of experiments as a tool for optimizing the batch conditions to methylene blue biosorption

on yellow passion fruit and mandarin peels. *Dyes and Pigments*, Volume 72, Issue 2, Pages 256–266.

Papari, S., Kazemeini, M., Fattahi, M., 2012. Mathematical modeling of a slurry reactor for DME direct Synthesis from syngas. *Journal of Natural Gas Chemistry*, Volume 21, Pages 148-157.

Pfleger, D., Gomes, S., Gilbert, N., Wagner, H.G., 1999. Hydrodynamic simulations of laboratory scale bubble columns: fundamental studies of the Eulerian–Eulerian modelling approach. *Chemical Engineering Science*, Volume 54, Pages 5091–5099.

Pfleger, D., Becker, S., 2001. Modelling and simulation of the dynamic flow behaviour in a bubble column. *Chemical Engineering Science*, Volume 56, Pages 1737-1747.

Prakash, A., Margaritis, A., Li, H., Bergougnou, M.A., 2001. Hydrodynamics and local heat transfer measurements in a bubble column with suspension of yeast. *Biochemical Engineering Journal* Volume 9, Issue 2, Pages 155–163.

Puertas Arbizu, I., Luis Pérez, C., J., 2003. Surface roughness prediction by factorial design of experiments in turning processes. *Journal of Materials Processing Technology*, Volumes 143–144, Pages 390–396.

Ranade, V.V., Tayalia, Y., 2001. Modeling of fluid dynamics and mixing in shallow bubble column reactors: influence of sparger design. *Chemical Engineering Science*, Volume 56, Pages 1667–1675.

Rao, K.S.M.S.R., Joshi, J.B., 1998. “Liquid-phase mixing and power consumption in mechanically agitated solid-liquid contactors”, *Chemical Engineering Journal*, Volume 39, Issue:2, Pages 111-124.

Reilly, I. G., D. S. Scott, T. J. W. De Bruijin and J. Piskorz, 1986. A Correlation for Gas Holdup in Turbulent Coalescing Bubble Columns. *Canadian Journal of Chemical Engineering*, Volume 64, Issue: 5, Pages 705–717.

Rubio, F.C., Garcia, J.L., Molina, E., Chistic, Y., 2001. Axial inhomogeneities in steady-state dissolved oxygen in airlift bioreactors: predictive models. *Chemical Engineering Journal* Volume 84, Issue 1, Pages 43–55.

Sada, E., Katoh, S., Yoshil, H., 1984. Performance of the gas-liquid bubble column in molten salt systems. *Indian Engineering and Chemical Process Design and Development*, Volume 23, Pages 151-154.

Sahinkaya, E., Dilek, F.B., 2005. Biodegradation of 4-chlorophenol by acclimated and unacclimated activated sludge—Evaluation of biokinetic coefficients. *Environmental research* Volume 99, Issue 2, Pages 243–252.

Samstag, R.W., Wicklein, E., 2012. Application of CFD to activated sludge mixing analysis. In: *CFD Workshop- Presentation. 3rd IWA/WEF Wastewater Treatment Modelling Seminar-WWT mod 2012*, February 26e28 Mont-Sainte-Anne, QC, Canada.

Sánchez Mirón, A., Cerón García, M-C., García, Camacho, F, Molina Grima, E., Chisti, Y., 2004 *Mixing in Bubble Column and Airlift Reactors. Chemical Engineering Research and Design* Volume 82, Issue 10, Pages 1367-1374.

Sanyal, J., Vasquez, S., Roy, S., Dudukovic, M.P., 1999. Numerical simulation of gas–liquid dynamics in cylindrical bubble columns reactors. *Chemical Engineering Science*, Volume 54, Pages 5071–5083.

Schiller and Naumann, L. Schiller, Z. Naumann, 1933. *Über die grundlegenden Berechnungen bei der Schwefkraftaubereitung Zeitschrift des vereins deutscher ingenieure*, Volume 77, Issue:12, Pages 318–320

Shah, Y.T., Joseph, S., Smith, D.N., Ruether, J.A., 1985. Two-bubble class model for churn turbulent bubble-column reactor. *Industrial & Engineering Chemistry Process Design and Development*, Volume 24, Pages 1096-1104.

Shives, M., Crawford, C., 2016. Adapted two-equation turbulence closures for actuator disk RANS simulations of wind & tidal turbine wakes. *Renewable Energy*, Volume, Issue: 92, Pages 273-292.

Shamlou, P.A., Koutsakos, E., 1989. Solids suspension and distribution in liquids under turbulent agitation. *Chemical Engineering Science* Volume 44, Issue 3, Pages 529-542.

Sieblist, C., Jenzsch, M., Pohlscheidt M., Andreas Lübbert. 2011. 2.06 – Bioreactor Fluid Dynamics. Reference Module in Life Sciences Comprehensive Biotechnology (Second Edition), Pages 47–62.

Sokolichin, A., Eigenberger, G., 1999. Applicability of the standard turbulence model to the dynamic simulation of bubble columns: Part I. Detailed numerical simulations. Chemical Engineering Science, Volume 54, Pages 2273–2284.

Sokolichin, A., Eigenberger, G., Lapin, A., Lubbert, A., 1997. Dynamic numerical simulation of gas–liquid two-phase flows Euler/Euler versus Euler/Lagrange. Chemical Engineering Science, Volume 52, Issue: 4, Pages 611–626.

Stanley, S., J., Wabo, E., Mann, R., Primrose, K., 2001. Dual-Validation of Miscible Liquid mixing in a stirred vessel imaged by electrical resistance tomography. 2nd world Congress Process Tomography. Hanover, Germany, Pages 151-158.

Sun, Y., Furusaki, Sh., 1990. Continuous production of acetic acid using immobilized Acetobacter acetii in a three-phase fluidized bed bioreactor. Journal of Fermentation and Bioengineering Volume 69, Issue 5, Page ii.

Thorat BN, Joshi JB, 2004. Regime transition in bubble columns: experimental and predictions. Experimental Thermal and Fluid Science, Volume 28, Pages 423–30.

Tomiyaama, A., Celata, G.P., Hosokawa, S., Yoshida, S., 2002. Terminal velocity of single bubbles in surface tension force dominant regime International Journal of Multiphase Flow, Pages 1497–1519.

Vandu CO, Krishna R., 2004. Volumetric mass transfer coefficients in slurry bubble columns operating in churn-turbulent flow regime. Chemical Engineering Process, Volume 43, Pages 987–95.

Vermande, S. Simpson, K., Essemiani, K., Fonade, C., Meinhold, J., 2007. Impact of agitation and aeration on hydraulics and oxygen transfer in an aeration ditch: Local and global measurements. Chemical Engineering Science Volume 62, Issue 9, Pages 2545–2555.

Vicente, G., Coteron, A., Martinez, M., Aracil, J., 1998. Application of the factorial design of experiments and response surface methodology to optimize biodiesel production. *Industrial Crops and Products*, Volume 8, Pages 29–35.

Wallis, G.B., 1969. *One-Dimensional Two-Phase Flow*. McGraw-Hill, New York, 243.

Wang S, Arimatsu Y, Koumatsu K, Furumato K, Yoshimato M, Fukunaga K, et al. Gas holdup, liquid circulating velocity and mass transfer properties in a mini-scale external loop airlift bubble column. *Chemical Engineering Science*, Volume 58, Pages 3353–3360.

Wu, Z.C., Zhou, M.H., Huang, Z.W., Wang, D.H., 2002. Electrocatalysis method for wastewater treatment using a novel beta-lead dioxide anode. *Journal of Zhejiang University SCIENCE*, Volume 3, Issue: 2, Pages 194-198.

Wu, Y., Al-Dahhan, M.H., 2001. Prediction of axial liquid velocity profile in bubble columns. *Chemical Engineering Science* Volume 56, Issue 3, Pages 1127–1130.

Wu, B., Chen, S., 2008. CFD Simulation of Non-Newtonian Fluid Flow in Anaerobic Digesters. *Biotechnology and Bioengineering* Volume 99, Issue 3, Pages 700–711

Xie, Borchers H., Yang, J., Hu, Y., Zhang, H., Yang, Y., Zhang, K., Zhu, X., Li, Y., Yang, C., 2014. Simulation of flow field and sludge settling in a full-scale oxidation ditch by using a two-phase flow CFD model. *Chemical Engineering Science*, Volume 109 (0), Pages 296-305.

Yang, Y., Yang, J., Zuo, J., Li, Y., He, S., Yang, X., Zhang, K., 2011. Study on two operating conditions of a full-scale oxidation ditch for optimization of energy consumption and effluent quality by using CFD model. *Water Resources*, Volume 45 (11), Pages 3439-3452.

Yang, Y.P., Wu, X.Y., Xu, X.H., Wang, D.H., 2001. Treatment of dyeing wastewater by photo-assisted Fenton system. *Journal of Chemical Engineering of Chinese Universities*, Volume 15(3), Pages 242-247 (in Chinese).

Zou, R., Jiang X., Li, B., Zu, Y., Zhang, L, 1988. Studies on gas holdup in a bubble column operated at elevated temperatures. *Industrial Engineering and Chemical Research*, Volume 27, Pages 1910-1916.

